Linear Energy Transfer (LET) - Guided Optimization Incorporating Biological Effectiveness for Intensity-Modulated Proton Therapy

by

Xuemin Bai

A dissertation submitted to the Department of Industrial Engineering

Cullen College of Engineering

in partial fulfillment of the requirements for the degree of

Doctor of Philosopy

in Industrial Engineering

Chair of Committee: Gino Lim

Committee Member: Wenhua Cao

Committee Member: Taewoo Lee

Committee Member: Cunjiang Yu

Committee Member: Ying Lin

University of Houston

December 2019

ABSTRACT

Relative biological effectiveness (RBE) is used to measure the biological effect of treatment plans in Intensity modulated proton therapy (IMPT). However, this approach is challenging because of considerable model uncertainties for clinical tissues. Therefore, the primary goal of this dissertation research is to develop biological effectiveness incorporated optimization approaches to enhance understanding of the biological impact of IMPT in radiation therapy research.

First, our work considers LET as a physical surrogate of biological effect in treatment planning. By maximizing dose-averaged LET in the target and minimizing it on OARs, the method not only can produce satisfactory dose distributions but also achieve reduced LET distributions in critical structures as well as an increased LET in the target volume. Then, we develop a new mathematical model to increase the biological effect in radioresistant tumors in such a way that a robust biological effect distribution can be achieved. To accomplish this purpose, the sum of the differences between the highest and the lowest biological effect in each voxel, approximated by the product of dose and LET, is penalized. After that, we noticed that using LET as a surrogate will increase the model complexity and ignore the difference between dose and LET distribution, which is a more fundamental property. A study focuses on the potential benefits of LET keeps going up after the physical dose Bragg Peak is come up with to improve the biological effect performance. avoid high values of LET in critical structures located within or near the target and increase LET in the tumor area, without compromising the target coverage. In the final work, the impact of BAOpt on the biological effect in IMPT is investigated.

TABLE OF CONTENTS

LIST OF TABLES

LIST OF FIGURES

Chapter 1
Introduction of radiation therapy

1.1 Background

In 2018, an estimated 1,735,350 new cases of cancer were diagnosed in the United States and 609,640 people diedh from the disease. Cancer remains the second most common cause of death in the United States, exceeded only by heart disease, accounting for nearly one in every four deaths [1].

There are many types of cancer treatment. The types of treatment that patients receive will depend on the type of cancer and patients' health condition. Usually, surgery, radiation therapy, chemotherapy, immunotherapy, targeted therapy, hormone therapy, stem cell transplant, and targeted medicines are the main current treatment methods. Among these methods, more than half of cancer patients will receive radiotherapy in addition to surgery or chemotherapy. For some particular types of cancer, i.e. early head and neck cancer, it may be used alone [2], [3].

Radiation therapy (also called radiotherapy) is the use of high-energy radiation to damage tumor cells' DNA and cause double strand break. Meanwhile, health cells' DNA also receive double strand break. But, the normal cells are less sensitive to the radiation compared to the tumor cells, which means the normal cells can heal better than the tumor cells. Radiation therapy does not kill cancer cells right away. It takes days or weeks of treatment before DNA is damaged enough for cancer cells to die. Then, cancer cells keep dying for weeks or months after radiation therapy ends. Since radiation can damage both cancer cells and healthy cells, the aim of radiation therapy

is to maximize tumor cell kill while minimizing toxic effects on surrounding healthy tissues. Radiation therapy can be used alone or in combination with other treatment methods. And it most often uses X-rays, but protons, carbon ion or other types of energy also can be used.

There are two main types of radiation therapy, internal radiation therapy and external beam radiation therapy. Internal radiation therapy is a treatment in which a source of radiation is put inside the patient's body. The radiation source can be solid or liquid. External beam radiation therapy comes from a machine that aims radiation at patient's cancer. The machine is large and may be noisy. It does not touch patient's body, but can move around, sending radiation to a part of body from many directions. There are different systems that can produce different types of radiation for external beam therapy, such as x-ray machines, Cobalt-60 machines, linear accelerators, proton beam machines, and neutron beam machines. External beam therapy is the most widely used radiation therapy treatment in the world.

Before the beginning of radiation treatment, radiation therapy team consisting of radiation oncologists, radiation therapists, medical physicists, and medical dosimetrists need carefully plan patient's treatment. At the beginning period, the patient body structure will be simulated into a cube with three-dimensions. The simulation allows the radiation oncologist to define the exact location and configuration of the treatment for your cancer or tumor. In order to accomplish this, CT images will be taken in the radiation oncology department. Sometimes, the other image techniques such as magnetic resonance imaging (MRI) and positron emission tomography (PET) are also used to get more precise images to identify the structures. Those diagnostic images

then help physicians determine the geometry information, such as organ locations, organ sizes, and isocenter. Along with the contour of these structures, the physician will also prescribe objective doses to the target volumes and constraints to OARs, which is defined as treatment "protocol". Next, optimization techniques are utilized to determine, intensity profiles from each treatment beam angles and required parameters of treatment delivery machines, to generate a treatment plan for the patient.

Generally, to help the normal cells' recover, the total prescribed dose of radiation is divided into many small doses and given in multiple treatment sessions, which is known as "fractionation". The total dose is fractionated (spread out over time) for several important reasons. Tumor cells are generally less efficient in repair between fractions than normal cells, so fractionation gives health tissues more time to recover which means reduce the damage. Fractionation also avoids tumor cells were in a relatively radio-resistant phase of the cell cycle during the treatment and allow them to cycle into a sensitive phase of the cycle [4].

The more formal optimization process is typically referred to as forward planning and inverse planning. In forward planning, the required decisions include how many radiation beams to use, which angles each will be delivered from, whether attenuating wedges be used and which multi-leaf collimators configuration will be used to shape the radiation from each beam. Forward planning is usually applied in three-dimensional conformal radiation therapy (3DCRT) and passive scattering proton therapy (PSPT). However, the quality of inverse planning highly depends on the experience of planners. To make the therapy delivery modalities more flexible and

precise, new technology such as Intensity-modulated radiation therapy (IMRT) and Intensity-modulated proton therapy (IMPT) were come up with. These types of treatment planning are called inverse planning. In these radiation treatment plans, planner specifies the desired requirement, such as prescribed dose of the tumor voxels, max tolerance of OARs into the model, the optimization algorithms will try to determine all the parameters to achieve the requirements as good as possible. In this thesis, we focus on IMPT treatment planning.

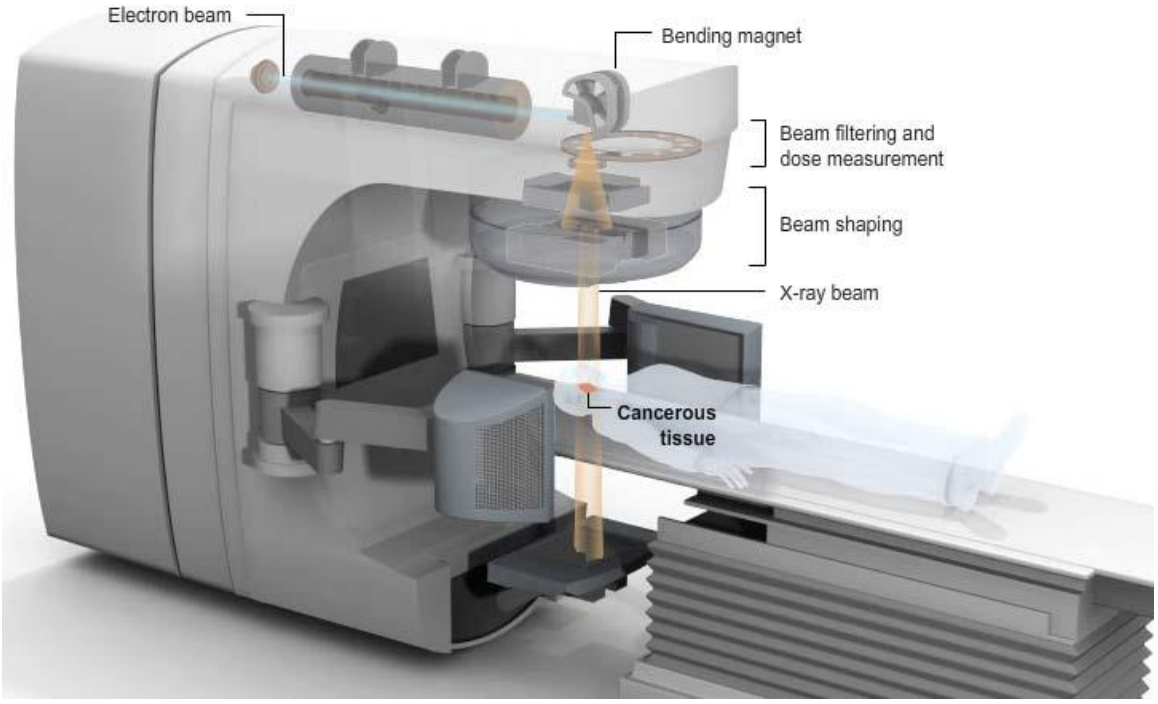

Figure 1.1: Intensity-modulated radiation therapy (IMRT).

1.2 Intensity Modulated Proton Therapy (IMPT)

Proton beams have the ability to deposit dose over a confined distance at the end of the beam range, namely the Bragg peak, and almost no dose is released beyond the peak. This characteristic of proton beams provides an accurate localization of dose in

three dimensions compared with intensity-modulated radiation therapy (IMRT) and passive scattering proton therapy (PSPT). As a result, intensity-modulated proton therapy (IMPT) delivered by pencil-beam scanning can generate highly conformal and homogeneous doses to target volumes with complex shapes while minimizing the undesired dose to adjacent organs at risk (OARs) [5]. A new study from researchers at The University of Texas MD Anderson Proton Therapy Center found that the use of feeding tubes in oropharyngeal carcinoma (OPC) cancer patients treated with intensity modulated proton therapy (IMPT) decreased by more than 50 percent compared to patients treated with intensity modulated radiation therapy (IMRT). This suggests that proton therapy may offer vital quality of life benefits for patients with tumors occurring at the back of the throat (MD Anderson News, 2013).

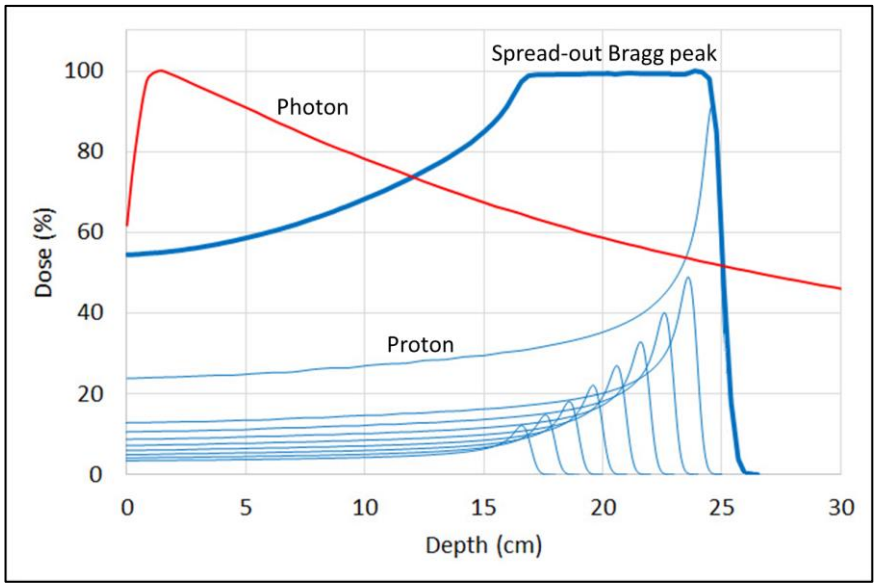

Figure 1.2: Depth-dose curves of a photon beam (red), a proton spread-out Bragg peak (blue, thick), and the proton pencil beams constituting the spread-out Bragg peak (blue, thin).

There are mainly two strategies have been proposed to generate IMPT plans when multiple beam angles are used to deliver IMPT: (1) the signal-field optimization (SFO-IMPT), in which of each beam is optimized individually to deliver the uniform prescribed dose to the target while respecting the dose tolerance of normal tissues [6]; (2) the multi-field optimization (MFO-IMPT), in which all spots from all fields are optimized simultaneously to generate a homogeneous total dose distribution [7]. MFO-IMPT allows for superior dose distributions compared with either PSPT or SFO-IMPT. Due to the increase of the degree of freedom in the optimization process, MFO-IMPT has the greatest flexibility to produce optimum dose distribution patterns, especially for complex anatomic geometries. Our research is focused on the MFO-IMPT. For brevity, we will use the term IMPT to refer to MFO-IMPT in the remainder of the document unless otherwise necessary for clarity.

1.3 Uncertainties in Radiation Therapy

Optimization problems are typically considered with precisely specified parameters. The solutions to such problems may be highly sensitive to errors in the parameter values: if the true values differ from those used during the optimization, the solution may, in fact, be far from optimal. There are many sources of uncertainty that need to be taken into account in the course of the treatment planning process. The segmentation of the tumor and the critical structures based on medical images is inherently uncertain and error prone. Furthermore, patient positioning uncertainties are relevant because the patient needs to be set up in the same position every day over the course of the treatment. Motion effects constitute another class of uncertainty.

There is no measurement (or procedure) in the radiation treatment process that can be performed perfectly. The main uncertainties we take into consideration in this research are as follows:

1) Setup uncertainty: this uncertainty is due to such factors as errors in the positioning of the patient and mechanical inaccuracies in the delivery.

2) Range uncertainty: it may arise from inaccuracies in the computed tomography (CT) imaging.

3) Anatomical change uncertainty: this error is caused by the motion of tumor and organs in the human body during a treatment session, tumor size and shape change and gain or loss weight.

Depending on the nature of the uncertainties, different approaches for taking them into account are preferable. Commonly, uncertainties are handled by using margins: The clinical target volume (CTV) is expanded into a planning target volume (PTV) and planning is performed to irradiate the latter. Margins are employed to combat everything from setup uncertainty to the motion to imaging artifacts. Their ubiquity in treatment planning is a testament to their effectiveness, relative ease of implementation, but also lack of dominant substitutes.

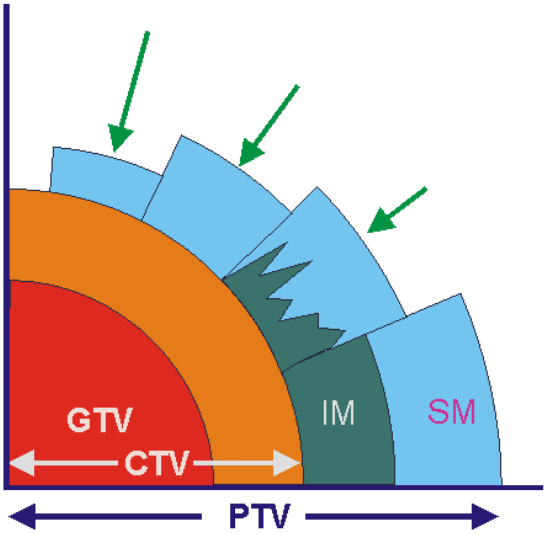

Figure 1.3: Clinical targets.

As alternatives to geometric margins, robust optimization methods that take uncertainties into account explicitly have been proposed. In these methods, dose distributions for multiple error scenarios are computed and the treatment plans are optimized with respect to all of these scenarios simultaneously. The methods differ in how they take the dose distributions into account: expected value optimization minimized the expectation of the objective value over the scenario doses [8]–[10], composite worst optimization minimizes the objective value of the worst case scenario [11], and voxelwise worst-case optimization minimizes the objective function applied to a worst-case dose distribution defined as the worst scenario dose to each voxel considered independently [12]. While these methods can produce robust plans also for sites of heterogeneous density, they result in qualitatively different plans than margin-based planning, even in situations where the static dose cloud approximation holds.

1.4 Biological Optimization

The current practice of proton therapy uses a constant relative biological effectiveness (RBE) value of 1.1 to account for biological effect in the treatment, as recommended by the International Commission on Radiation Units and Measurement (ICRU) [13]. This assumes that protons are 10% more effective than photons. Furthermore, it has been evidenced that RBE varies along the treatment field, i.e. with linear energy transfer (LET), the values of tissue-specific parameters defined by $(\alpha/\beta)x$ as well as the dose per fraction [14], [15]. But the use of variable RBE is hindered because of considerable model uncertainties for clinical tissues, mostly owing to the existing experimental biological data are insufficient to define a clear correlation between RBE and dose per fraction or $(\alpha/\beta)x$ for in vivo endpoints, included in RBE models [15]–[18]. If treatment planning objectives for target coverage are evaluated only in terms of variable RBE weighted dose, such methods typically lead to lower physical doses in parts of the target, based on the assumption that the RBE is larger than 1.1 in areas of high LET [19]. On the other hand, this could lead to overdosage to the critical structures if the RBE is underestimated [20].

Although the RBE-LET relationship depends on tissue type, endpoint, and dose, one can assume that the biological effectiveness increases with increasing LET [14], [21]–[24]. Unlike other biological parameters, LET can be calculated with high accuracy through analytical methods or Monte Carlo simulations [25]–[27]. Previous studies have demonstrated that active scanning offers the possibility of influencing the distribution of dose-averaged LET (i.e., the biological effect) without significantly

altering the distribution of physical dose. This can be explained as IMPT has a much higher degree of freedom for modulation than passively scattered proton therapy (PSPT) and single field optimized intensity modulated proton therapy (SFO-IMPT) [28]. Therefore, combining physical dose optimization with the goal of additionally influencing the LET distribution has been addressed to optimize biological dose in recent studies [16], [20], [21], [28]–[32]. Their primary focus was on increasing LET in radioresistant tumors or reducing it in critical normal tissues to achieve a better biological effect. However, they did not consider the robustness of physical dose and biological effect.

1.5 Objectives and Overview

The aim of this dissertation research is to develop biological effectiveness incorporated optimization approaches to improve the quality and robustness of biological effect meanwhile maintaining the coverage of physical dose.

In chapter 3, a LET-guided optimization method to study the feasibility of improving LET distribution in target volumes and reducing LET distribution in critical structures while keeping the physical dose distribution coverage. In this study, we considered LET as a physical surrogate of biological effect in treatment planning according to the approximated linear relationship between LET and RBE.

In chapter 4, a new mathematical model was come up with to increase the biological effect in radioresistant tumors and critical structures in such a way that a robust biological effect distribution can be achieved. In this method, the sum of the differences between the highest and the lowest biological effect in each voxel,

approximated by the product of dose and LET, was penalized to improve the robustness of biological effect distribution. Besides, an extra benefit of reduced biological effect distribution was achieved in the organs at risk.

In chapter 5, an influence index to quantify the contribution of the biological effect from each scanning spot on the basis of its topological relationship to different organs of interest. This method could be especially beneficial for patient cases where critical structures are adjacent to the target area. In addition, the DEAOpt approach is less complex computationally and therefore faster than the LETOpt approach.

As an important supplement, we proposed the LETBAO algorithm to investigate the impact of LETBAOpt on the biological effect of IMPT. BAO in IMPT has much high freedom than FMO because the evulation of each beam angle combination requires to fully solve an FMO model. Thus, it is feasible for LETBAO to generate a biological effect advanced treatment plan compared to biological effect-guided optimization in IMPT.

Chapter 2

Literature Review

2.1 Fluence Map Optimization problem

The fluence map optimization (FMO) is the core problem in radiation therapy treatment planning optimization. The objective of FMO problem is to optimize the optimal intensity map of beamlets to deliver a homogenous prescribed dose to the target while minimizing the radiation dose on critical structures, which is inherently contradictory because the targets and critical structures are near each other or overlapped. Usually, the objective function is used to penalize the difference between the prescribed dose distribution and the current dose distribution. However, there are many formulations have been proposed in FMO previous studies.

In FMO optimization, the most commonly used objective functions are dose based and dose-volume based objective functions [33]–[36]. The advantage of these objective functions is they are straightforward for the treatment plan evaluation. Wu and Mohan [37] proposed an objective function based on the equivalent uniform dose (EUD) for radiation therapy optimization. This objective function uses the biologically equivalent dose to evaluate the plan quality. Linear programming models also have been used to formulate the FMO problem [38].

To solve the FMO problem, a great number of algorithms have been proposed to find the optimal beamlets intensity profiles. These strategies can be grossly classified into two groups: global optimization (GO) and local optimization (LO). GO

approaches include linear programming [39], [40], mixed integer programming [41], [42], simulated annealing and genetic algorithms [43]–[45]. These approaches are designed to reach a global optimal solution. However, they all require an excessive amount of time for optimization, which is not practical in clinical treatment planning. In addition, the performance of these approaches depends heavily on the choice of parameters [39]. For example, simulated annealing and genetic algorithms, have the advantages of avoiding getting trapped in local minima in principle, they are slow and may also get trapped in local minima if the thermal cooling process is too fast in the case of simulated annealing, or if the population evolution is not realistic in the case of genetic algorithms. Linear programming methods can incorporate constraints and guarantee to have an optimal solution. However, they are limited to linear objective functions, which are poor indicators of the response of tumors and healthy tissue to radiation. On the other hand, LO approaches include gradient-based algorithms [12], [37], [46], [47], local neighborhood search [48] and iterative methods [49]. Due to the LO approaches are designed to obtain usable solutions within a clinically acceptable planning time window. So, LO approaches have been commonly used for clinical treatment planning optimization. However, it has been reported in the IMRT treatment planning literature that the gradient-based optimization methods, it can be easily trapped in local minima [50]–[53]. As noted by Llacer et al [54], the commonly used gradient-based methods often result in different solutions when different starting points are used. Due to the IMPT has even more degree of freedom (i.e., multiple energy layers) compare to IMRT. This can lead to a higher chance of being trapped in a local minimum, as was pointed out by Albertini et al [55].

Despite the fact that many solution approaches have been proposed to solve the FMO problem, solving the FMO problem is computationally difficult in practice due to the presence of uncertainties in radiation therapy.

2.2 Robust Optimization for Radiation Therapy

In the standard radiation treatment regime, the spatial and temporal dose distribution is optimized assuming the patient geometry is static over the course of treatment and a fixed dose of radiation is delivered in every treatment fraction. However, during the course of treatment, the patient geometry may deviate from the one observed in the image on which a treatment plan is based. These uncertainties add complexity to the inherent trade-off between minimizing the healthy tissue dose (or probability of side effects) and ensuring that the tumor receives a sufficient dosage of radiation.

To date, robust optimization is widely used to incorporate different uncertainties into the optimization process to improve the robustness of treatment plans. Many robust optimization models for radiation treatment planning were developed by researchers. Chu et al [56] proposed a robust optimization approach accounted for patient interfraction motion and setup uncertainties for IMRT. The results demonstrated that robust solution achieved better healthy tissue sparing than a clinical margin solution without compromising tumor coverage and robustness. Ólafsson and Wright [57] considered dose matrices calculation error and interfraction position uncertainties into an IMRT treatment planning problem formulation, and showed that a robust solution outperforms nominal solution (one which assumes a dose matrix in

known with certainty) in terms of tumor coverage and improved healthy tissue sparing when compared with margin solution. Li and Xing [58] use a three-dimensional Gaussian distribution function to simulate random organ motion for IMRT planning. Bortfeld et al [59] introduced a robust methodology for IMRT treatment planning under uncertainty and considered the specific case of intrafractional uncertainty induced by breathing motion. They incorporated the uncertainty in the probability mass function of breathing motion into the inverse planning optimization and ensured that all target voxels received sufficient expected dose for all probability distributions within a polyhedral set. Chan et al [60] generalized the robust optimization framework for IMRT planning without considering the probability distribution of uncertainties.

Worst case robust optimization is another main approach to consider uncertainties. Pflugfelder et al [12] proposed a “worst case” optimization method for IMPT by considering both setup uncertainty and range uncertainty. In this approach, the worst case dose in each voxel was calculated to evaluate the objective function. Fredriksson et al [11] use a minimax robust optimization method to handle setup and range uncertainties in IMPT planning. The worst scenario among the nominal and uncertainty cases was punished by optimization algorithm. Both of these approaches can work with a linear programming (LP) model [61] and a nonlinear programming (NLP) model [62]. The results of all these papers show that the robustness of IMPT plan can be significantly improved by robust optimization, while without loss nominal case target coverage and OAR sparing.

2.3 Linear Energy Transfer (LET) – Guided Optimization

The present study demonstrated that the LET-incorporated IMPT optimization can create preferred dose-averaged LET distributions while maintaining satisfactory dose distributions. The goal of LET-guided optimization is to maximization in target volumes and minimization in critical normal tissues is expected to boost the differential benefits of increasing the biological effect of protons in tumor and/or reducing it in healthy tissues compared to the current standard for brain tumor cases. Within dose-exposed volumes, evaluation of LET can be used as another measure of plan quality, in addition to dose. Moreover, one can also choose to use radiobiological models as additional indicators of plan quality, such as the linear quadratic (LQ) cell survival model, tumor control probability (TCP), normal tissue complication probability (NCTP), and RBE models.

LET painting approaches have been investigated for ion [29] and proton [30] therapies, in which planning methods such as splitting targets or adopting opposite beam arrangements are used to allocate the high LET protons within target instead of normal tissues. However, those techniques may require greater effort in planning, quality assurance, and delivery than does the current practice because they use more planning volumes and beam angles. In contrast, incorporating LET directly into the optimization process may have certain practical advantages over the LET painting techniques and it could be easily implemented in clinical settings.

One recent study discussed a multi-criteria optimization approach in which a set of IMPT plans were created using various dose based objectives and constraints, then

plans with superior dose and LET distributions were selected [16]. While the advantage of this method is that multiple competing plans can be generated, the disadvantage is that the performance on finding improved LET distributions may be compromised because LET criteria are not included in optimization.

In another recent study, a two-step prioritized optimization approach was proposed: first a plan was optimized using conventional dose criteria, and, in the second step, the plan was optimized solely based on the product of LET and dose as a surrogate of variable RBE weighted dose with constraints to limit the change to physical dose distribution from the first step [20]. Prioritized optimization may be an effective approach to managing the trade-off effect between dose and LET [28]. However, the optimality of LET optimization may be affected by the local minimum problem in nonconvex optimization, as the second round of prioritized optimization uses a warm start.

An et al [31] proposed a LET-guided robust planning model that simultaneously considered proton range and patient setup uncertainties and spares high RBE in the OARs. However, this study did not discuss if increasing LET in target could be achieved at the same time.

2.4 Monitor Unit Constraints

IMPT is currently performed using the active spot scanning technique. In this modality, a proton pencil beam can be scanned magnetically in two-dimensional directions perpendicular to the beam direction in order to form an irradiating field. Monoenergetic pencil beams with different energies can then be used to produce the

desired dose distributions to cover the three-dimensional tumor target [63]. By individually modulating the intensity of each scanning spot, an IMPT plan can thus be delivered [64]. The scanning schemecan be either continuous or discrete. The continuous scanning system sweeps a beam in a raster manner, whereas the discrete scanning system employs a stop-and-shoot process whereby the beam is turned off between spots [65]. The spot scanning system used at The University of Texas MD Anderson Cancer Center employs the discrete scanning scheme and is capable of generating protons with 94 non-equispaced energies from 72.5 to 221.8MeV using a scanning nozzle (Hitachi, Ltd, Tokyo, Japan and Hitachi America Ltd, Tarrytown, NY, USA) [64]. Proton beams range from 4 to 30.6 cm in steps of 1 mm for lower energies and up to 6mm for higher energies. This study focuses on the discrete scanning system at MD Anderson, although other discrete scanning systems would function on similar principles.

Smaller spot spacing has been shown to increase target dose homogeneity and lower the organ-at-risk (OAR) dose, but it also results in many low-intensity spots and reduces plan optimality [64]. There are minimum monitor unit (MU) constraints for delivering each pencil beam (spot) for the scanning spot system. A MU is defined by a fixed number of output pulses from the main dose monitor ion chamber in the scanning nozzle; hence, one M U value is used to represent spot intensity and its resolution at MD Anderson is 0.0001. To ensure delivery accuracy, the minimum MU (0.005 at MD Anderson) must be selected while taking into account two considerations: (1) the spot dose should be higher than the expected delayed dose, which is the dose delivered after the scanning termination signal is sent; and (2) the

accuracy of spot position measurement would be reduced if a lower minimum MU were used [66]. Note that at the Bragg peak, the dose delivered by a single spot with 0.005 MU is approximately 0.2 to 0.55 Gy, depending on different energies. However, deliverable minimum MU constraints are not considered in the current TPS. Instead, a post- processing procedure is performed to satisfy those constraints. MU values over 0.0025 are rounded up to 0.005 and MU values below 0.0025 are rounded down to 0. Rounding errors in this procedure can result in significant distortion from the optimized dose distributions to the delivered dose distributions [64]. Distortion is exacerbated when there are more spots with small MU values, which can be caused by small spot spacing. Therefore, when designing a treatment plan, a threshold value for spot spacing needs to be set in order to resolve the tradeoff between the dosimetric advantage and delivery constraints; hence, using spot spacings smaller than the threshold value is to be avoided when designing IMPT plans owing to the dose distribution deterioration caused by rounding errors.

Whereas the incorporation of MU constraints into inverse treatment planning for IMPT has not been much discussed thus far, the problem of limiting excessive MUs has been extensively studied in inverse treatment planning for intensity modulated radiation therapy with photons (IMXT). Most previous studies have focused on including beam segmentation constraints in the IMXT optimization process so that more continuous fluence maps can be generated in an optimized plan [67]–[69]. Coselmon et al [70] specifically discussed a strategy that assigns maximum intensity limits in IMXT optimization to improve delivery efficiency without significantly degrading plan quality. Overall, approaches proposed for IMXT optimization have to

address the question of deliverability with a multi-leaf collimator and are therefore not applicable to IMPT, in which intensities for all proton scanning spots can be modulated independently. A previously described method by Cao et al [32], regarding incorporating minimum deliverable MU constraint into the optimization, introduced a two stages optimization method. In the first stage, they performed an optimization using linear programming to find an intermediately optimized IMPT plan without the deliverable minimum MU constraints considered. In the second stage, they performed a boundary-constrained optimization, in which the optimizer would enforce lower bound constraints for every beamlet that has positive intensity after the first stage. All the beamlets with intensity less than the lower bound after the first stage would be turn off in the second stage. Therefore, the resultant plan might not be a local optimal solution to the original problem.

2.5 Beam Angle Optimization

The beam angle optimization (BAO) problem in radiotherapy treatment planning is a typical combinatorial optimization problem [61]. The optimization of beam irradiation directions can substantially improve treatment plan quality [71], [72]. However, the clinical use of equispaced beam angle ensembles is chanllenged by solving the BAO problem, a nonconvex problem with many local minima on a vast search space [73].

Usually, the BAO problem is guided by the optimal value of the fluence map optimization (FMO)—the problem of obtaining the most appropriate radiation intensities for each beam direction [74]. A combinatorial BAO formulation can be

obtained by considering a discrete subset of all possible angle directions in [0,360]. Many different algorithms have been used to address the combinatorial BAO problem, including gradient search [73], neighborhood search [48], [61], [75], response surface approaches [76], branch-and-prune [48], hybrid approaches [77], [78], genetic algorithms [78]–[80], artificial neural network [81], simulated annealing [82], or matheuristic approaches [83]. Alternative approaches consider all possible (continuous) angles resulting in a continuous BAO formulation [84], [85].

Most of the mentioned approaches applied sequential combination of two algorithms, where one algorithm solves for beam angles and the other algorithm approximates the beam intensities. These approaches involve many approximations in solving subproblems as well as the relaxation of integer constraints, which may lead to inefficient searching directions

Chapter 3

Linear Energy Transfer Incorporated Optimization for Intensity-Modulated Proton Therapy

3.1 Introduction

By using pencil beam scanning technique for treatment, intensity modulated proton therapy(IMPT) can modulate the intensity of beamlets independently. IMPT is more effective in delivering conformal dose distributions than conventional beam radiation therapy, such as IMRT, because it can set nonuniform intensities for different beamlets flexibly. However, there are problems arising in the stage of treatment planning and delivery of IMPT. Among them, how to measure the biological effect and improve it are two prominent issues.

The relative biological effectiveness (RBE), defined as the ratio of the photon (reference) dose and the proton dose necessary to cause the same level of effect, is used to calculate the biological effect of IMPT. The current practice of proton therapy applies a constant RBE value of 1.1 to account for the biological effect of the treatment, as recommended by the International Commission on Radiation Units and Measurements [13]. The constant RBE value reflects the basic assumption that protons are 10% more biologically effective than photons.

Although it is well known that RBE depends on the type of the particle, the dose-averaged linear energy transfer (LETd), the tissue type ($(\alpha/\beta)x$ ratio) and the dose level [19], it is hard to predict an accurate RBE value because of conspicuous model uncertainties for clinically relevant tissues, due to the lack of experimental data to

conclude precise (α/β)x values [16].There is research shows that (α/β)x values for many tissue types are often accompanied by more than 50% uncertainty [17]. If treatment planning objectives for target coverage are evaluated based on variable RBE, Therefore, use of these variable RBE models to evaluate proton treatment plans may lead to unwanted clinical consequences. For example, if the calculation of the target dose coverage is based on a variable RBE-weighted dose, the patient will be at risk of receiving a lower physical dose in parts of the tumor because variable RBE is assumed to be greater than 1.1 in areas of high LET. Critical structures are in danger of being exposed to a higher physical dose when the variable RBE is underestimated [20], [86].

RBE increases with increasing LET, whereas it decreases with increasing dose and (α/β)x. Experimental data show that proton RBE increases with increasing LET [14], [21]–[24]. Therefore, LET could be used as a good surrogate for indirect RBE optimization to avoid the controversy to calculate RBE from LET in proton therapy [20]. Previous studies have proven that IMPT has the ability to produce equivalent physical dose distributions but greatly different LET distributions [16], [87]. Therefore, recent studies begin to include both dose and LETd into objectives to study the method's feasibility and examine the tradeoff between doses and LETd values [16], [20], [21], [28]–[31], [88]. Unkelbach et al [20] proposed a prioritized optimization method to reoptimize IMPT plans in terms of their LET distributions while limiting the degradation of the best possible physical dose distribution. Cao et al [28] introduced a LET-incorporated IMPT optimization method, which was able to produce clinically satisfactory dose distributions while increasing dose-averaged LET in target volumes and reducing it in critical normal tissues for five selected brain tumor patient

cases. But, all these researches did not consider the uncertainties in IMPT. An et al [31] proposed a LET-guided robust planning model that simultaneously considered proton range and patient setup uncertainties and spares high RBE in the OARs.

This research aimed to investigate the impact of incorporating LET criteria directly into IMPT optimization. First, we would like to verify that both dose and LET distributions could be optimized simultaneously. The goal of this optimization was set to not only produce satisfactory dose distributions but also to achieve reduced LET distributions in critical structures and increased LET in target volumes.

3.2 Method and Materials

3.2.1 Linear energy transfer incorporated optimization

For each patient, two optimization approaches were evaluated in this study: conventional optimization, and LET-incorporated optimization. The goal of LET-incorporated optimization was to optimize dose and LET distributions simultaneously. The additive objectives of LET were, straightforwardly, maximization of LET in tumor targets and minimization of LET in critical tissues and normal tissues.

During IMPT, the patient receives irradiation in multiple proton beams with different incident angles. Each beam can be divided into thousands of beamlets and we used j as the index of beamlet. w_j^2 denotes the intensity of beamlet j to preserve the nonnegativity. With D_{ij} as the physical dose deposited to voxel i by beamlet j with unit intensity (so-called influence matrix), the physical dose of voxel D_i is calculated by:

$$D_i = \sum_j^{N_B} D_{ij} w_j^2, \tag{3.1}$$

where N_B denotes the total number of beamlets. The LET delivered to voxel i by beamlet j in unit intensity are indicated L_{ij}. By defining the dose-averaged LET L_i over all pencil beam contributions as follow:

$$L_i = \frac{\sum_j^{N_B} D_{ij} L_{ij} w_j^2}{\sum_j^{N_B} D_{ij} w_j^2}. \tag{3.2}$$

The conventional optimization model in IMPT we used in this research is as below:

$$F_P(w_j) = p_T \frac{1}{N_T} \sum_{i=1}^{N_T} \left(D_i - D_{0,T}\right)^2 + p_{OAR} \frac{1}{N_{OAR}} \sum_{i=1}^{N_{ORA}} H\left(D_i - D_{0,OAR}\right) \times \left(D_i - D_{0,OAR}\right)^2, \tag{3.3}$$

where N_T, and N_{OAR} are sets of voxels in target volumes and OARs, respectively. p terms denote the penalty weights of the corresponding organs to control the priorities between competing objectives. D_0 terms are the prescribed doses required by the treatment plans. The heavy-side step function $H\left(D_i - D_{0,OAR}\right)$ is a discontinuous function whose value is 0 for a nonpositive argument and 1 for a positive argument.

By adding two terms for maximizing dose-averaged LET in the target and minimizing it in OARs, the cost function for LET-incorporated optimization (LETOpt) was formulated as shown below:

$$F_L(w_j) = F_P(w_j) - p_{T,L} \frac{1}{N_T} \sum_{i=1}^{N_T} {L_i}^2 + p_{OAR,L} \frac{1}{N_{OAR}} \sum_{i=1}^{N_{ORA}} {L_i}^2. \tag{3.4}$$

The derivative function of Formulation 3.4 can be written as follow:

$$F'_L(w_j) = 4 * p_T \frac{1}{N_T} \sum_{i=1}^{N_T} \left(\sum_{j=1}^{m} D_{i,j} w_j^2 - D_{p,T}\right) D_{i,j} w_j + 4 *$$

$$p_{OAR} \frac{1}{N_{OAR}} \sum_{i=1}^{N_{OAR}} H\left(\sum_{j=1}^{m} D_{i,j} w_j^2 - D_{p,O}\right) \times \left(\sum_{j=1}^{m} D_{i,j} w_j^2 - D_{p,O}\right) D_{i,j} w_j - 4 *$$

$$p_{T,L} \frac{1}{N_T} \sum_{i=1}^{N_T} \left(\frac{\sum_{j=1}^{m} D_{i,j} L_{i,j} w_j^2}{\sum_{j=1}^{m} D_{i,j} w_j^2}\right) \left(\frac{D_{i,j} L_{i,j} w_j \sum_{j=1}^{m} D_{i,j} w_j^2 - D_{i,j} w_j \sum_{j=1}^{m} D_{i,j} L_{i,j} w_j^2}{\left(\sum_{j=1}^{m} D_{i,j} w_j^2\right)^2}\right) + 4 *$$

$$p_{O,L} \frac{1}{N_{OAR}} \sum_{i=1}^{N_{OAR}} \left(\frac{\sum_{j=1}^{m} D_{i,j} L_{i,j} w_j^2}{\sum_{j=1}^{m} D_{i,j} w_j^2}\right) \left(\frac{D_{i,j} L_{i,j} w_j \sum_{j=1}^{m} D_{i,j} w_j^2 - D_{i,j} w_j \sum_{j=1}^{m} D_{i,j} L_{i,j} w_j^2}{\left(\sum_{j=1}^{m} D_{i,j} w_j^2\right)^2}\right). \tag{4.4}$$

The calculation of D_{ij} and L_{ij} was carried out by a previously validated fast Monte Carlo system [89].

3.2.2 Patient cases and treatment planning

For the LETOpt study, we selected five brain tumor patients which had been treated with proton therapy at UT MD Anderson, including one glioblastoma, one anaplastic astrocytoma and three ependymoma cases. In all these cases, one or more critical structures, e.g. brainstem or optic chiasm, were adjacent to or overlapped with gross target volumes (GTVs) and clinical target volumes (CTVs). The prescriptions to target volumes and field arrangements were the same as those used in the clinical treatments. The doses prescribed to all OARs are set to zero in optimization. Table 3.1 lists patient information and specific treatment planning parameters.

Table 3.1: Patient information and treatment planning parameters.

Patient #	Prescription Dose (Gy)	Number of Fractions	Beam Angle (Couch, Gantry)	OARs included in Optimization
1	1.8 (CTV)	30	(10,260), (350,100), (0,180)	Brainstem, Brain
2	1.85 (CTV)	32	(90,265), (0,100), (0,260), (0,180)	Brainstem, Spinal Cord, Brain
3	1.85 (CTV)	32	(0,180), (350,95), (10,265)	Brainstem, Spinal Cord, Brain
4	1.8 (CTV)	30	(0,180), (0,250), (0,110)	Brainstem, Brain
5	1.8 (CTV)	30	(355,105), (5,255), (95,290)	Brainstem, Brain

3.3 Results

The statistics of the dose and LETd distribution of five cases were summarized in Table 3.2. Compare to DoseOPT, the LETOpt plans can significantly reduce the LET value in the brainstems. For example, in case 1, the mean value of LET in the brainstem was reduced from 6.18 keV/um to 4.13 keV/um. Meanwhile, the $\mathrm{LETd}_{5\%}$ and $\mathrm{LETd}_{2\%}$ of LET distribution also show the same result. The LETd in the target volumes was markedly improved by the LETOpt approach for most of the cases. However, for case 2, we noticed that the $\mathrm{LETd}_{98\%}$ of LETd distribution in CTV slightly decreased from 1.36 keV/um to 1.21 keV/um. But the $\mathrm{LETd}_{2\%}$ increased from 2.87 keV/um to 4.22 keV/um. Meanwhile, the difference of dose distributions by these two methods in five cases were kept in a very small range. Table 3.2 and Figure 3.1

shows that the tradeoff effect between dose and LETd metrics happened in all patient cases, while its magnitude and sensitivity to changing optimization priorities varied among cases

Table 3.2: Statistics of dose (Gy) and LETd (keV/um) of the IMPT plans optimized by DoseOpt and LETOpt for the five brain tumor patients.

Patient	Plan		CTV		Brainstem		
			98%	2%	5%	2%	Mean
1	DoseOpt	Dose	54.00	58.04	52.63	54.06	27.08
		LETd	3.16	5.14	9.21	9.68	6.18
	LETOpt	Dose	54.00	58.47	52.85	54.32	29.97
		LETd	3.85	5.07	5.85	6.14	4.13
2	DoseOpt	Dose	59.20	63.97	60.47	61.74	28.64
		LETd	1.36	2.87	4.57	5.21	2.44
	LETOpt	Dose	59.20	64.96	60.80	62.08	32.00
		LETd	1.21	4.22	2.20	2.47	1.02
3	DoseOpt	Dose	59.20	64.24	57.85	59.87	22.54
		LETd	1.64	4.44	6.61	7.08	4.35
	LETOpt	Dose	59.20	64.95	57.84	59.87	23.34
		LETd	1.70	3.79	3.96	4.43	2.45
4	DoseOpt	Dose	54.00	58.48	53.72	55.68	29.10
		LETd	2.63	4.18	4.43	4.77	3.02
	LETOpt	Dose	54.00	59.06	53.72	55.97	30.09
		LETd	2.95	4.36	4.04	4.33	2.66
5	DoseOpt	Dose	54.00	57.62	55.39	56.23	33.69
		LETd	2.55	4.48	6.09	6.58	4.06
	LETOpt	Dose	54.00	58.20	55.39	56.24	35.53
		LETd	3.02	5.84	4.98	5.27	3.10

Figure 3.1 shows the DVH, LETd and cLETxD volume histogram for the CTV and the brainstem for the two differently optimized IMPT plans in the five brain tumor case. Solid lines were for DoseOpt and dash lines were for LETOpt. The DVH for the CTV and brainstem were at the same level for the DoseOpt and LETOpt plans, indicating that LETOpt plan can generate almost equal physical dose distribution compared to DoseOpt plan. In contrast, the LETd and c LETxD distribution in the

CTV was markedly improved and in the brainstem was significantly reduced by the LETOpt approach.

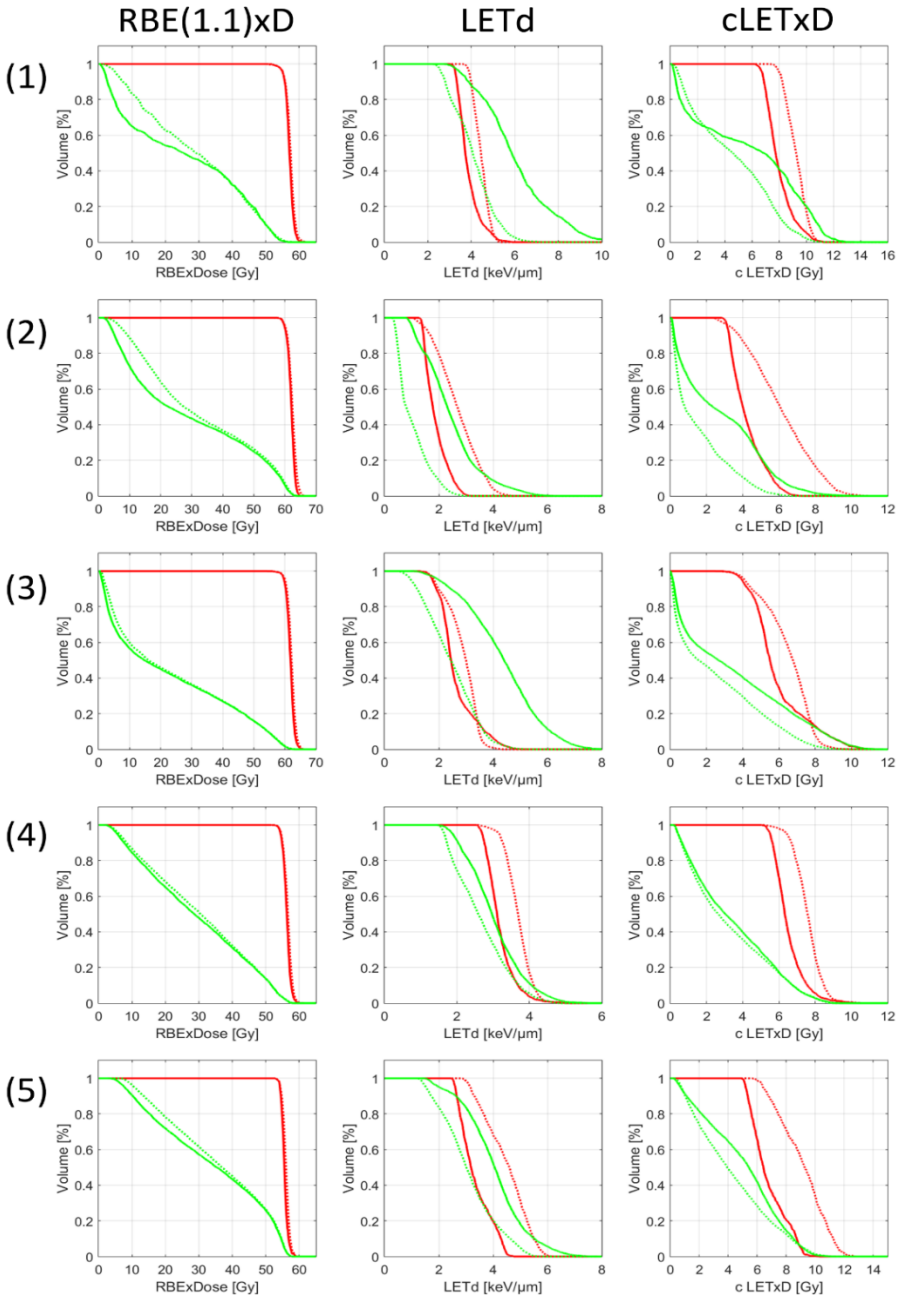

Figure 3.1: Comparison of DoseOpt and LETOpt plans for five patients. Dose, LET and cLETxD-volume histograms for the target (red contour), and brainstem (black contour) were shown in each column. Solid lines were for DoseOpt and dash lines were for LETOpt.

Figure 3.2 further illustrates the difference of LET distributions of the DoseOpt and the LETOpt for case 1 (one typical head and neck cancer patient). Figures 3.2(a) and (b) show the dose distribution of DoseOpt and LETOpt assuming a fixed RBE of 1.1; Figures 4.2 (d) and (e) show the distribution of LET, respectively; Figures 3.2 (c) and (f) show the difference of two plans in dose and LET. There is almost no difference between these two plans in dose distribution. But compared with DoseOpt, LETOpt plan forced the high LET distribution part from the target area to the brainstem area.

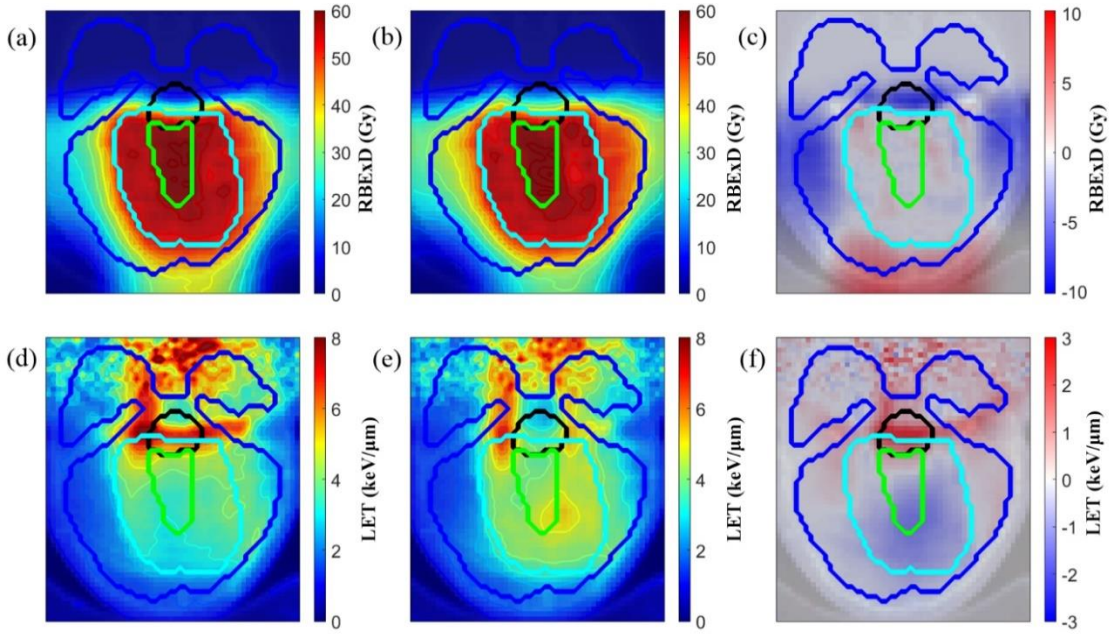

Figure 3.2: Comparison between DoseOpt and LETOpt plans for patient case 1. GTV, CTV, brain, and brainstem are contoured in green, cyan, blue, and black.

3.4 Discussion

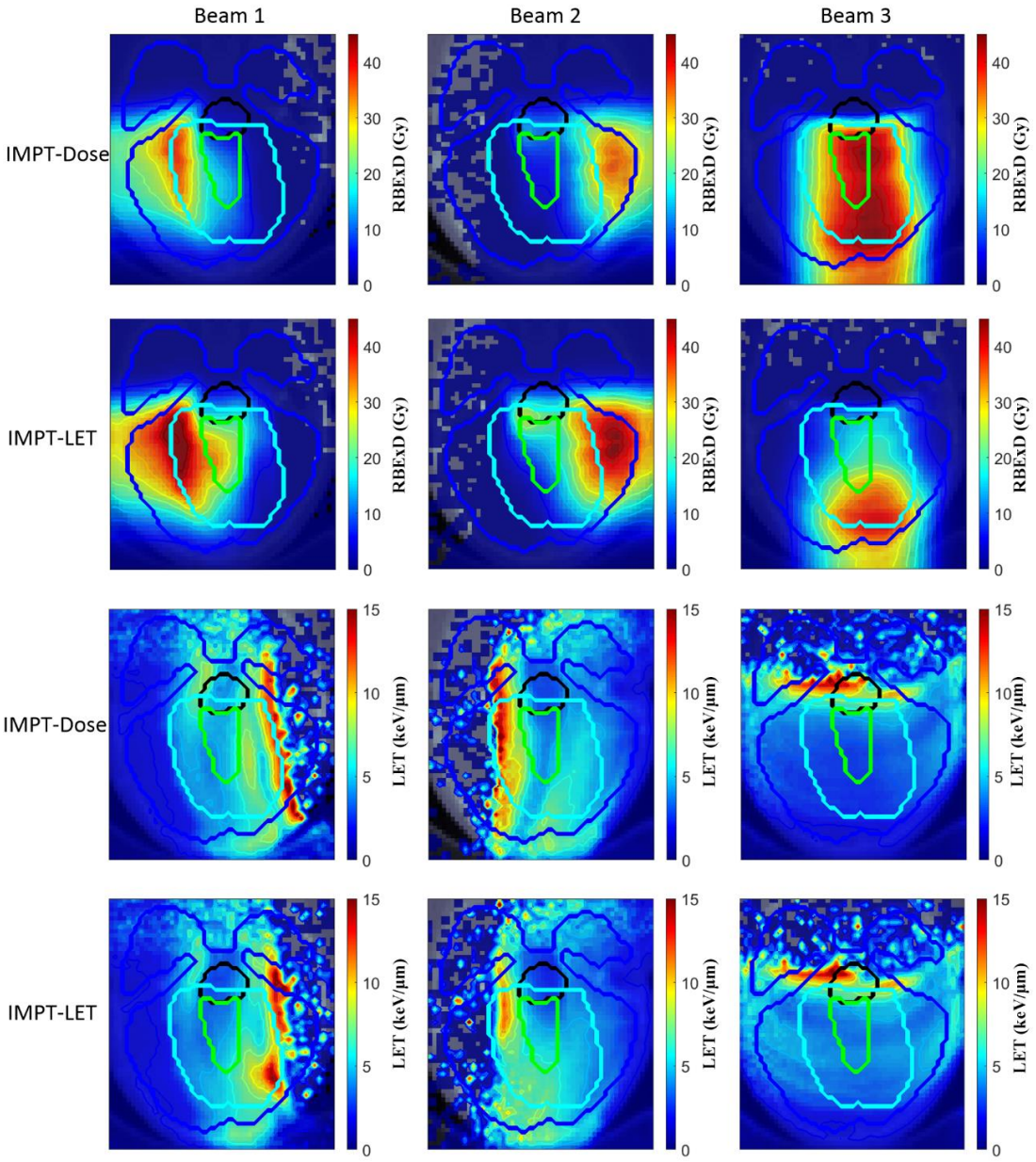

Figure 3.3: Comparison of each beam between DoseOpt and LETOpt plans for patient case 1. GTV, CTV, brain, and brainstem are contoured in green, cyan, blue, and black.

By analysing of the dose and LET distributions in each beam of the DoseOpt and LETOpt plans, we found out the dose contribution from beam 3 in the LETOpt plan

was reduced compared to the DoseOpt plan. Since the LET is calculated by the method of dose-average LET, the total LET inside the brainstem was reduced because the weighting factor (dose) for the LET in beam 3 decreased. Even though the LET distribution in each beam was similar for the DoseOpt and LETOpt plans, the change of dose distribution could impact the total dose-average LET distribution significantly (Figure 3.3).

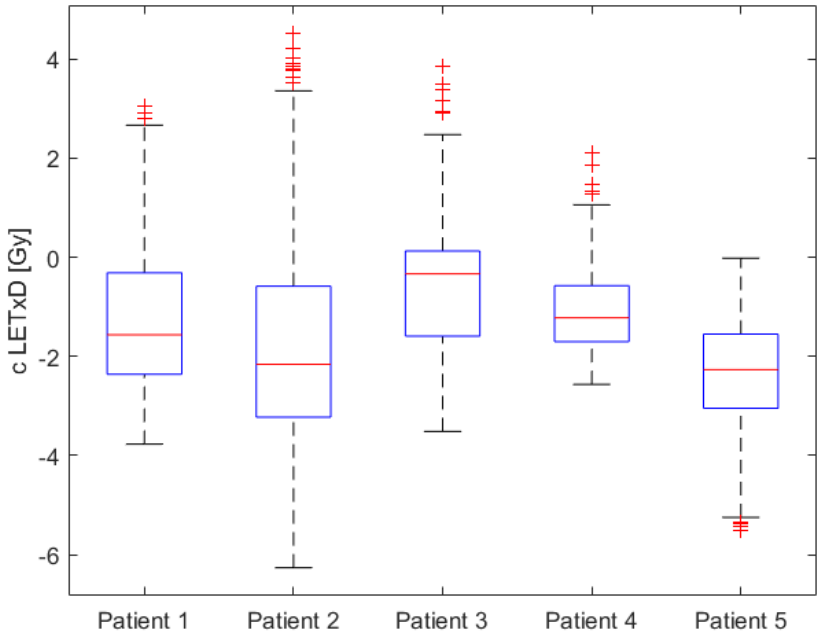

Figure 3.4: Scaled LET-weighted (cLETxD) dose comparison in the target volume for the DoseOpt and LETOpt plans. The bar chart shows the mean (red line) and range of the difference of c LETxD in each voxel of target volume between the DoseOpt and LETOpt plans.

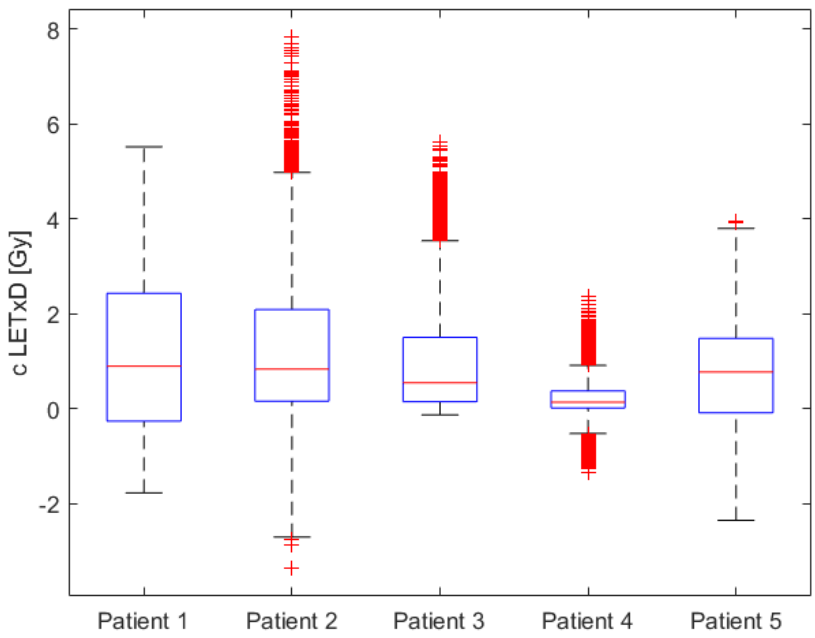

Figure 3.5: Scaled LET-weighted dose (cLETxD) comparison in the brainstem volume for the DoseOpt and LETOpt plans. The bar chart shows the mean (red line) and range of the difference of c LETxD in each voxel of brainstem volume between the DoseOpt and LETOpt plans.

As shown in Figure 3.4 and 3.5, the difference of cLETxD between the DoseOpt and LETOpt methods is negative for all the five patients in the target volume, which means the biological effect in the target volume for the DoseOpt plans is higher than for the LETOpt plans. And the positive difference between the DoseOpt and LETOpt approachs indicates the biological effect in the brainstem for the DoseOpt plans is lower than for the LETOpt plans.

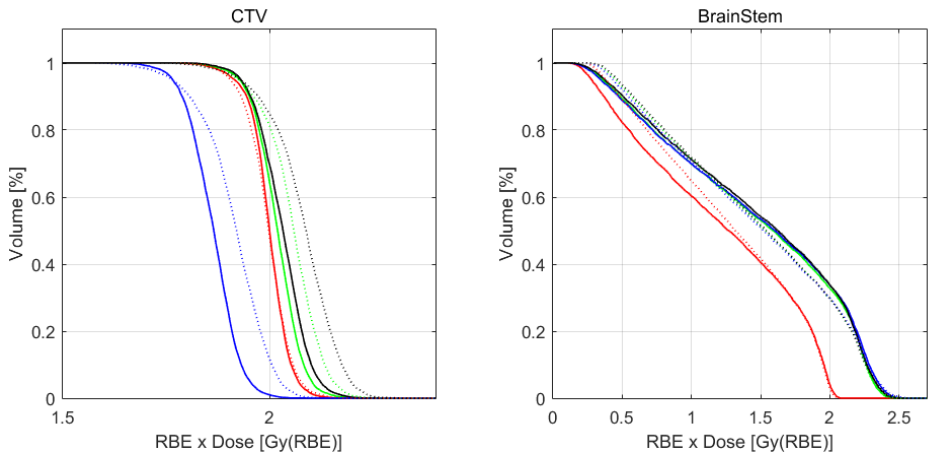

Figure 3.6: Dose volume histograms (per fraction) based on different RBE models of the DoseOpt (solid lines) and LETOpt (dashed lines) optimized plans for patient 5. The RBEs of constant 1.1, Carabe, Wedenberg, and McNamara are indicated in red, blue, black and green, respectively.

Current RBE models are imprecise because of the considerable uncertainties in predicating the (α/β)x. However, the RBE value has an almost linear relationship with the LET. As shown by Figure 3.6, the variable RBE weighted dose volume histograms calculated by Carabe, Wendenberg, and McNamara models in the target for the LETOpt plan were all higher than for the DoseOpt plan. We do not know which variable RBE model is more accurate, but they all show the same phenomena that increase LET in the target can improve the biological effect.

Here, the effect of adding two terms for maximizing dose-averaged LET in the target and minimizing it in OARs to voxel-based worst-case RO model (Formulation 4.5) was also investigated. The new model is shown as LETRO. The results for a prostate tumor case and a brain tumor case are shown in Figure 3,7 and 3.8. The differences in dose and LETxD distributions among the three IMPT plans were similar for the prostate and brain tumor cases. Thus, we proved that optimizing dose-averaged LET directely works for robust optimization.

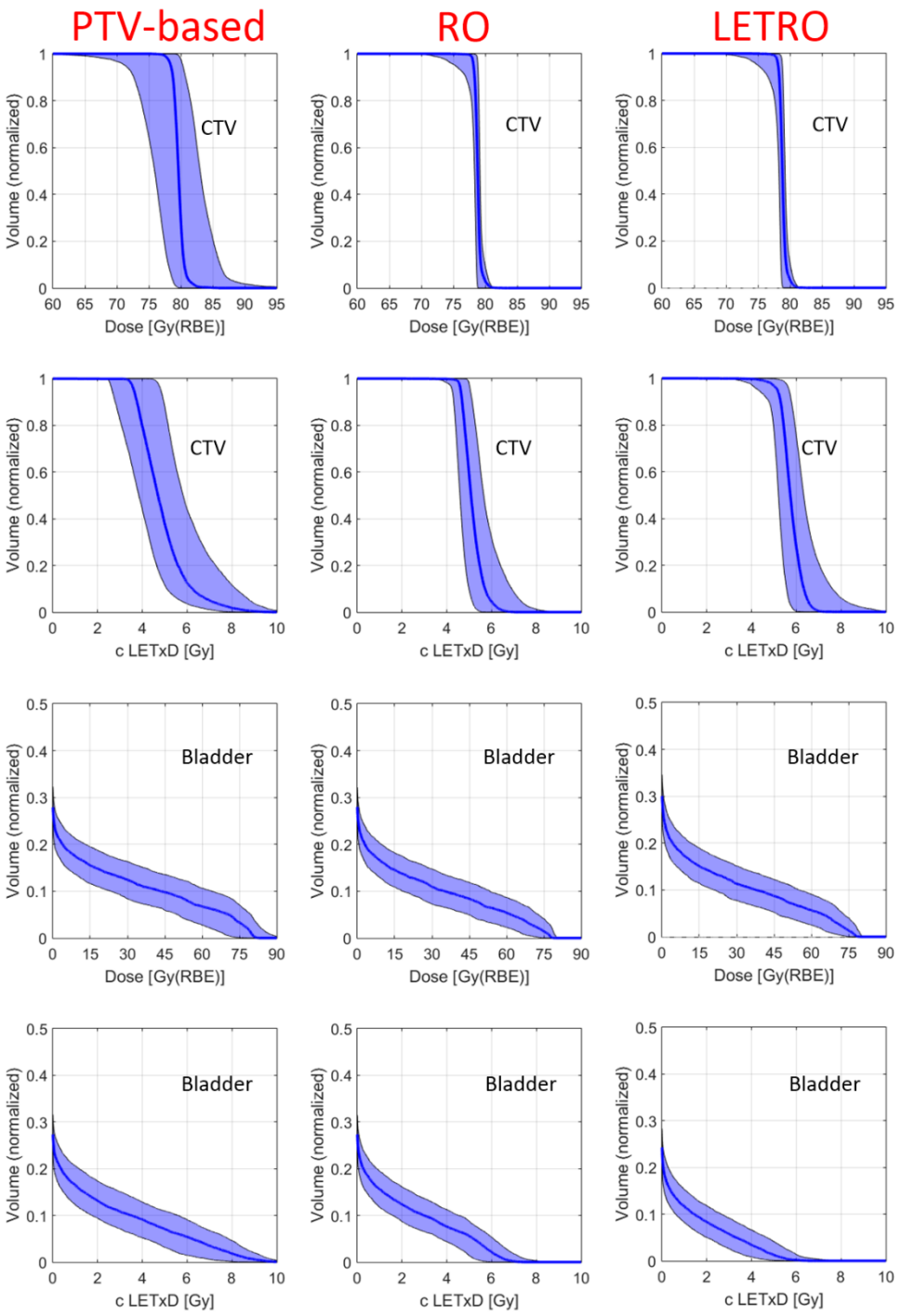

Figure 3.7: Dose-volume histograms (DVHs) for the clinical target volume (CTV) and the bladder for three IMPT plans in a prostate tumor patient case. The DVH bands were constructed on the basis of nine uncertainty scenarios with various range shifts and setup errors. The bold lines indicate the nominal distributions.

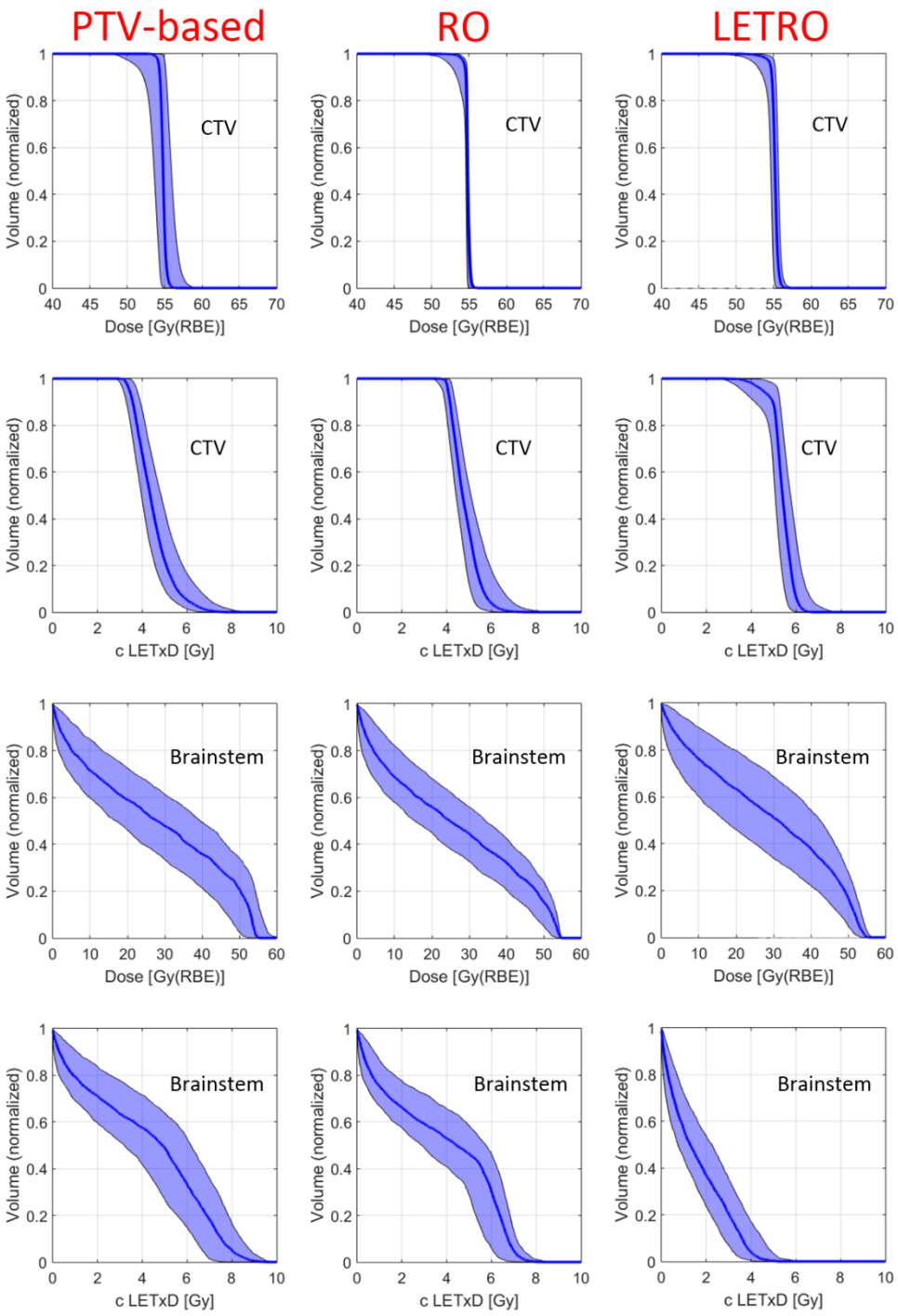

Figure 3.8: Dose-volume histograms (DVHs) for the clinical target volume (CTV) and the brainstem for three IMPT plans in a brain tumor patient case. The DVH bands were constructed on the basis of nine uncertainty scenarios with various range shifts and setup errors. The bold lines indicate the nominal distributions.

3.4 Conclusion

In this work, the LET-incorporated method was introduced to conventional dose-based optimization. This method was able to simultaneously optimize dose and LET. No matter if we take uncertainties into consideration, this method was able to hedge against high LET in OARs and improve the low LET in the targets while maintaining adequate dose coverage and robustness.

Chapter 4

Robust Optimization to Reduce the Impact of Biological Effect Variation from Physical Uncertainties

4.1 Introduction

Proton beams have the ability to deposit dose over a confined distance at the end of the beam range, namely the Bragg peak, and almost no dose is released beyond the peak. This characteristic of proton beams provides an accurate localization of dose in three dimensions. As a result, intensity-modulated proton therapy (IMPT) delivered by pencil-beam scanning can generate highly conformal and homogeneous doses to target volumes with complex shapes while minimizing the undesired dose to adjacent organs at risk (OARs) [5]. However, proton beams are more sensitive to uncertainties that arise during treatment than are photon beams [90]. Indeed, in the most advanced form of IMPT, multifield optimized IMPT, the final dose distribution is obtained by superimposing all individual inhomogeneous proton fields, which may make IMPT even more sensitive to uncertainties than conventional proton modalities such as passive scattering proton therapy (PSPT) or single field uniform dose (SFUD) IMPT [91]. To address this issue of uncertainty, robust optimization (RO) is commonly used in IMPT treatment planning [8], [10]–[12], [92]–[94].

The current practice of proton therapy uses a constant relative biological effectiveness (RBE) value of 1.1 to account for the biological effect of the treatment, as recommended by the International Commission on Radiation Units and Measurements [13]. This value reflects the basic assumption that protons are 10%

more biologically effective than photons. However, RBE varies along the treatment field, for instance with linear energy transfer (LET), tissue-specific parameters (defined by α and β), dose per fraction, and other factors [14], [15]. The use of variable RBE in treatment planning is challenging because of considerable model uncertainties for clinical tissues; existing experimental biological data are insufficient to clearly correlate RBE and dose per fraction or (α/β)x for in vivo endpoints [15]–[18]. Moreover, treatment plans that use a variable RBE-weighted dose often deliver low physical doses in parts of the target because they assume that RBE is greater than 1.1 in areas of high LET [19]. On the other hand, if RBE is underestimated, critical structures may receive overdosage [20].

Although factors such as tissue type, endpoint, and dose affect the relationship of RBE to LET, generally, biological effectiveness increases as LET increases [14], [21]–[24]. Unlike other biological parameters, LET can be calculated with high accuracy using analytical methods or Monte Carlo simulations [25]–[27]. Previous studies have demonstrated that active scanning can shape the distribution of dose-averaged LET (i.e., the biological effect) without significantly altering the distribution of physical dose [16], [21] because IMPT has a much higher degree of freedom for modulation than do other proton therapy modalities [28]. Therefore, recent studies have attempted to optimize biological dose by simultaneously optimizing physical dose and LET distribution [16], [20], [21], [28]–[31], [88]. The primary focus of these studies was on increasing LET in radioresistant tumors or reducing it in critical normal tissues. However, the impact of IMPT delivery uncertainties on biological effect has not been carefully evaluated or included in optimization.

The aim of this work is: (1) introduce an RO model for IMPT treatment plans that can achieve a robust biological effect distribution while maintaining satisfactory robust dose coverage in target volumes and sparing of critical structures; (2) use nominal optimization and RO to compare the robustness of variable RBE weighted dose, and try to prove physical dose based robust optimization will also make the biological dose robust and homogeneous.

4.2 Method and Materials

In IMPT, each beam consists of multiple beamlets that irradiate the tumor volume. The physical dose and LET delivered to voxel i by beamlet j in unit intensity are indicated as D_{ij} and L_{ij}. w_j^2 was used to denote the intensity of beamlet j to preserve the nonnegativity. Thus, for beamlet set N_B, the total dose D_i, dose-averaged LET L_i, and LET-weighted dose (LETxD) LD_i in voxel i can be calculated as follows:

$$D_i = \sum_j^{N_B} D_{ij} w_j^2, \tag{4.1}$$

$$L_i = \frac{\sum_j^{N_B} D_{ij} L_{ij} w_j^2}{\sum_j^{N_B} D_{ij} w_j^2}, \tag{4.2}$$

and

$$LD_i = \sum_j^{N_B} D_{ij} L_{ij} w_j^2. \tag{4.3}$$

A research treatment planning platform, matRad [95], was used to calculate D_{ij} and L_{ij} using a singular value decomposed pencil beam algorithm [96].

Commonly, IMPT uncertainties are handled by using margins. The clinical target volume (CTV) is expanded into the planning target volume (PTV), and planning is performed to irradiate the latter [11], [94], [97]. For PTV-based optimization, a standard quadratic objective function is minimized as follows [98]:

$$F_P(w_j) = p_T \frac{1}{N_T} \sum_{i=1}^{N_T} \left(D_i - D_{0,T}\right)^2 + p_{OAR} \frac{1}{N_{OAR}} \sum_{i=1}^{N_{ORA}} H\left(D_i - D_{0,OAR}\right) \times \left(D_i - D_{0,OAR}\right)^2, \tag{4.4}$$

where N_T, and N_{OAR} are sets of voxels in target volumes and OARs, respectively. p terms denote the penalty weights of the corresponding organs to control the priorities between competing objectives. D_0 terms are the prescribed doses required by the treatment plans. The heavy-side step function $H\left(D_i - D_{0,OAR}\right)$ is a discontinuous function whose value is 0 for a nonpositive argument and 1 for a positive argument.

As alternatives to geometric margins, optimization methods that explicitly take setup and range uncertainties into account have been proposed [8], [11], [62], [99], [100]. In these methods, dose distributions for multiple uncertainty scenarios are computed, and treatment plans are optimized with respect to all of the scenarios simultaneously. In this study, a voxel-based worst-case RO [62] method was used to penalize excessively high and low doses to target volumes and excessively high doses to OARs:

$$F_R(w_j) = p_{T,max} \frac{1}{N_T} \sum_{i=1}^{N_T} \left(D_{i,max} - D_{0,T}\right)^2 + p_{T,min} \frac{1}{N_T} \sum_{i=1}^{N_T} \left(D_{i,min} - D_{0,T}\right)^2$$

$$+ p_{OAR} \frac{1}{N_{OAR}} \sum_{i=1}^{N_{ORA}} H\left(D_{i,max} - D_{0,OAR}\right) \times \left(D_{i,max} - D_{0,OAR}\right)^2. \quad (4.5)$$

Note that $D_{i,max} = \max\left(D_{i,m}\right)$ and $D_{i,min} = \min\left(D_{i,m}\right)$ indicate the maximum and minimum dose, respectively, among m possible scenarios of voxel i.

According to Unkelbach et al [20], the RBE-weighted dose b_i can be given using equation (4.6):

$$b_i = \sum_j^{N_B} \left(1 + cL_{ij}\right) D_{ij} w_j^2 = D_i + cLD_i, \quad (4.6)$$

where c is a scaling parameter set to 0.04 μm/keV. It consists of two components, a physical component (D_i) and a biological component (cLD_i). We consider the latter as an approximation of the biological effect from all incident proton fields for a given voxel. $LD_{i,max} = \max(LD_i^m)$ and $LD_{i,min} = \min(LD_i^m)$ denote the maximum and minimum LET-weighted dose, respectively, over all m scenarios of voxel i.

To reduce the variation in biological effect in each voxel i, we propose to add minimization of the uncertainty gap, i.e., $LD_{i,max} - LD_{i,min}$, into the conventional RO model. This approach follows the principles of info-gap decision theory [101], [102], which seeks to maximize the robustness of a decision given minimum performance requirements. In other words, only the robustness of biological effect is optimized; biological effect itself is not maximized or minimized in either target or normal tissues.

Therefore, we added the L2-norm of the uncertainty gap of biological effect to (4.5) to construct the quadratic objective function for the biological effect-based RO (BioRO):

$$F_B(w_j) = F_R(w_j) + p_{T,gap}\frac{1}{N_T}\sum_{i=1}^{N_T}\left(LD_{i,max} - LD_{i,min}\right)^2 + p_{OAR,gap}\frac{1}{N_{OAR}}\sum_{i=1}^{N_{OAR}}\left(LD_{i,max} - LD_{i,min}\right)^2. \quad (4.7)$$

In this study, PTV-based optimization, conventional RO, and BioRO models were solved by a quasi-Newton method, the limited-memory Broyden-Fletcher-Goldfarb-Shanno algorithm [103]. We implemented each of the models in our in-house IMPT treatment planning system [32]. Calculations of dose and LET using unit beamlet intensity were performed using matRad, as mentioned earlier.

4.3 Biological effect-based robust optimization (BioRO)

4.3.1 Patient cases and treatment planning

Three IMPT plans were generated to illustrate the PTV-based, RO, and BioRO methods for three clinical cases: a brain tumor case, a prostate tumor case and a head & neck tumor case (Table 4.1). For the brain tumor case, three sets of angle combinations (gantry and couch) were used: (260°, 10°), (100°, 350°), and (180°, 0°). Setup uncertainties of ± 3 mm in three dimensions and range uncertainties of ± 3.5% of the nominal range were assumed. Two beams, (90°, 0°) and (270°, 0°), were used for the prostate tumor case, with setup uncertainties of ± 5 mm and range uncertainties of ± 3.5% of the nominal range. Similarly, setup uncertainties of ±3 mm and range uncertainties of ± 3.5% of the beams' nominal range were assumed in the head and neck tumor case under three beams: (180°, 0°), (65°, 345°) and (300°, 20°). Therefore, both RO and BioRO considered nine scenarios, i.e., one nominal scenario (without the

consideration of uncertainties), and eight uncertainty scenarios, including six setup uncertainty scenarios by shifting the patient's CT image [104] and two range uncertainty scenarios by scaling the nominal beamlet ranges [105]. The prescribed dose to target volumes and field arrangements were the same as those used in the clinical treatments. More planning details are listed in Table 4.1. The doses prescribed to all OARs were set to 0 in the optimizations.

Table 4.1: Patients information and treatment planning parameters.

Cancer type	Prescription dose (Gy/fx)	Number of fractions	Beam angles (gantry, couch)	Number of beamlets	Volumes included in optimization
Prostate	1.8 (CTV)	30	(90°, 0°)	5532	CTV, PTV, bladder, femoral heads, rectum
			(270°, 0°)	5525	
Brain	2 (CTV)	39	(260°, 10°)	3808	CTV, PTV, brainstem, optic chiasm, spinal cord, brain
			(100°, 350°)	3902	
			(180°, 0°)	3927	
H&N	2 (CTV)	33	(180°, 0°)	23758	CTV, PTV, left parotid, right parotid, larynx, spinal cord, mandible, left cochlea, right cochlea, brainstem, esophagus
			(65°, 345°)	25656	
			(300°, 20°)	25352	

Abbreviations: CTV, clinical target volume; PTV, planning target volume.

Upon the completion of the optimization step for each of the three approaches, fixed RBE (1.1)-weighted dose (RWD) and LETxD were calculated for each of the nine scenarios. Note that each of the three plans was normalized to have 98% of the CTV covered by the prescribed dose. Dose-volume histograms (DVHs) and LETxD-volume histograms for the nominal scenario were used to quantify the plans' quality. To evaluate and compare the plan robustness, the envelope of all DVHs or LETxD-volume histograms in band graphs [106] and maps of the uncertainty gap for all nine

scenarios were displayed. The difference between the worst and best value of a DVH point, such as Dv%, is considered as the bandwidth at Dv% for a given organ.

4.3.2 Results

Figure 4.1 shows the DVH and LETxD volume histogram bands for the CTV and the brainstem for the three differently optimized IMPT plans in the brain tumor case. The DVH bands for the CTV were narrower for the RO and BioRO plans than for the PTV-based plan, indicating that the RO and BioRO plans were less sensitive to setup and range uncertainties than was the PTV-based plan. As we expected, the BioRO approach was able to generate robust physical dose distributions in the target volume that were comparable to those generated by the RO approach. Moreover, the DVH bands for the brainstem were similar for all three optimization techniques. We should note that the mean dose to the brainstem increased from 25.9 Gy with the RO plan to 27.8 Gy with the PTV-based plan and 28.3 Gy with the BioRO plan. However, the maximum dose to the brainstem was similar in all three plans; the maximum values (worst-case) of D2% were 57.9 Gy, 54.5 Gy, and 54.8 Gy for the PTV-based, RO, and BioRO plans, respectively (Table 4.2).

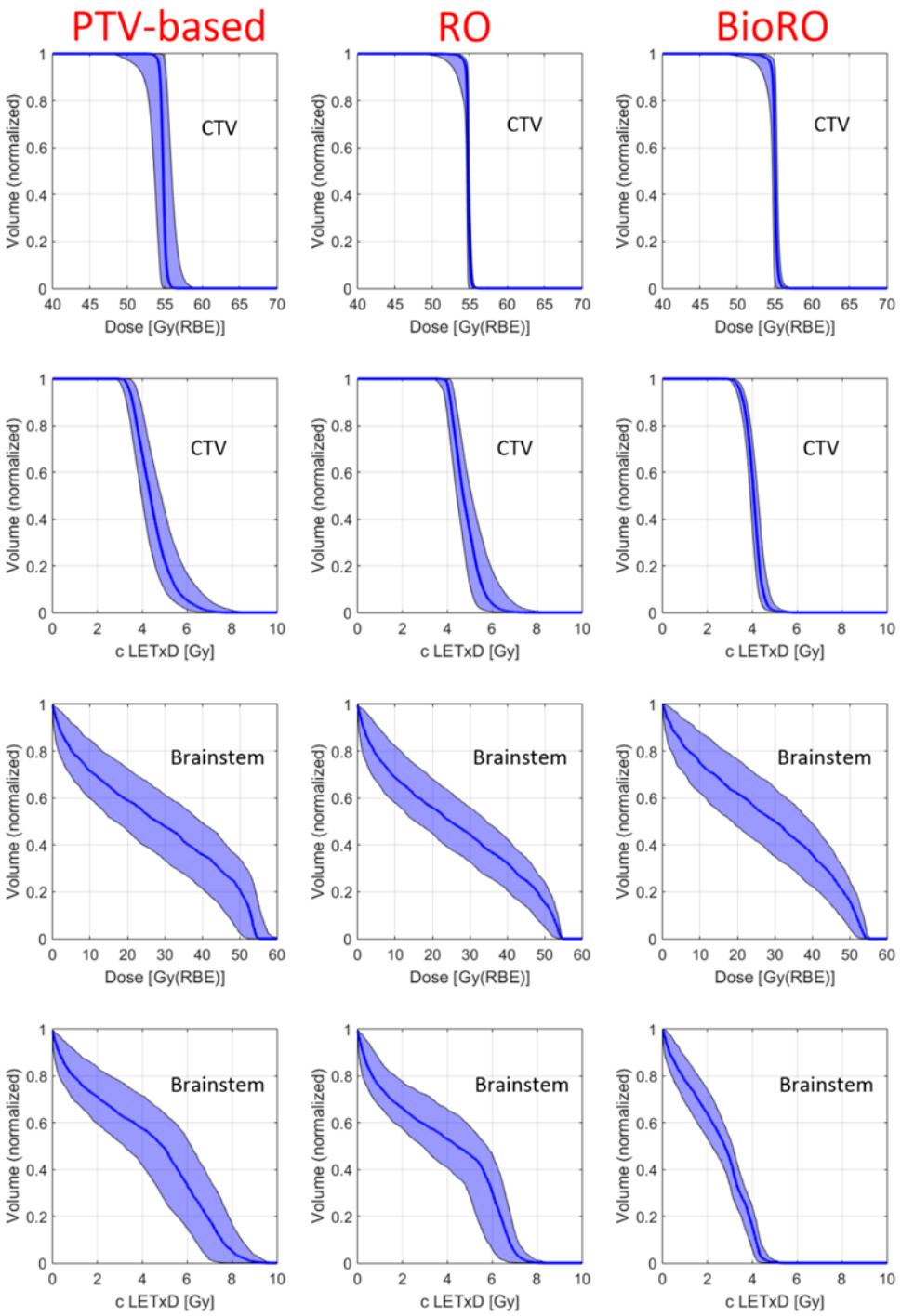

Figure 4.1: Dose-volume histograms (DVHs) and c LETxD-volume histograms of the clinical target volume (CTV) and the brainstem for three IMPT plans in a brain tumor patient case. The bold lines indicate the nominal distributions.

Table 4.2: Dose and LET-weighted dose (LETxD; scaled by c = 0.04 μm/keV) values in the clinical target volume (CTV) and the brainstem.

Tissue	**Dosimetric Parameter**	**PTV-based**			**RO**			**BioRO**		
		Nom	Max	Min	Nom	Max	Min	Nom	Max	Min
CTV	$D_{98\%}$ (Gy[RBE])	54.0	55.0	49.6	54.0	54.4	51.4	54.0	54.8	51.3
	$D_{2\%}$ (Gy[RBE])	55.6	58.0	54.6	55.3	55.5	54.8	55.8	56.2	55.1
	c LETx$D_{98\%}$ (Gy)	3.6	4.0	3.3	4.4	4.5	4.0	3.6	3.8	3.4
	c LETx$D_{2\%}$ (Gy)	7.2	8.4	6.4	6.9	8.1	6.0	5.3	5.7	5.0
Brainstem	$D_{2\%}$ (Gy[RBE])	54.3	57.9	50.4	54.0	54.5	51.6	53.8	54. 8	51.2
	D_{mean} (Gy[RBE])	27.8	35.2	20.4	25.9	31.9	19.9	28.3	35.0	21.4
	c LETx$D_{2\%}$ (Gy)	9.4	10.2	7.6	8.0	8.6	7.0	4.9	5.3	4.6
	c LETxD_{mean} (Gy)	4.7	6.0	3.4	4.2	5.2	3.2	2.7	3.2	2.3

Abbreviations: RBE, relative biological effectiveness; Nom, nominal

In contrast, LETxD volume histogram bands of the three plans exhibited pronounced differences (Figure 4.1). The robustness of the LETxD distributions in both the CTV and the brainstem was markedly improved by the BioRO approach. For instance, the bandwidth at D98% of c LETxD in the CTV was 0.4 Gy for the BioRO plan, 0.7 Gy for the PTV-based plan, and 0.5 Gy for the RO plan. The bandwidth at D2% of c LETxD in the CTV was 0.7 Gy for the BioRO plan, but 2.0 Gy and 2.1 Gy for the PTV-based plan and the RO plan, respectively. Similarly, the bandwidth at D2% of c LETxD in the brainstem was 0.7 Gy for the BioRO plan, smaller than the 2.6 Gy and 1.6 Gy bandwidths for the PTV-based and RO plans. The bandwidth at the mean value of c LETxD in the brainstem was also lower for the BioRO plan, 0.9 Gy compared to 2.6 Gy and 2.0 Gy for the PTV-based plan and the RO plan, respectively (Table 4.2).

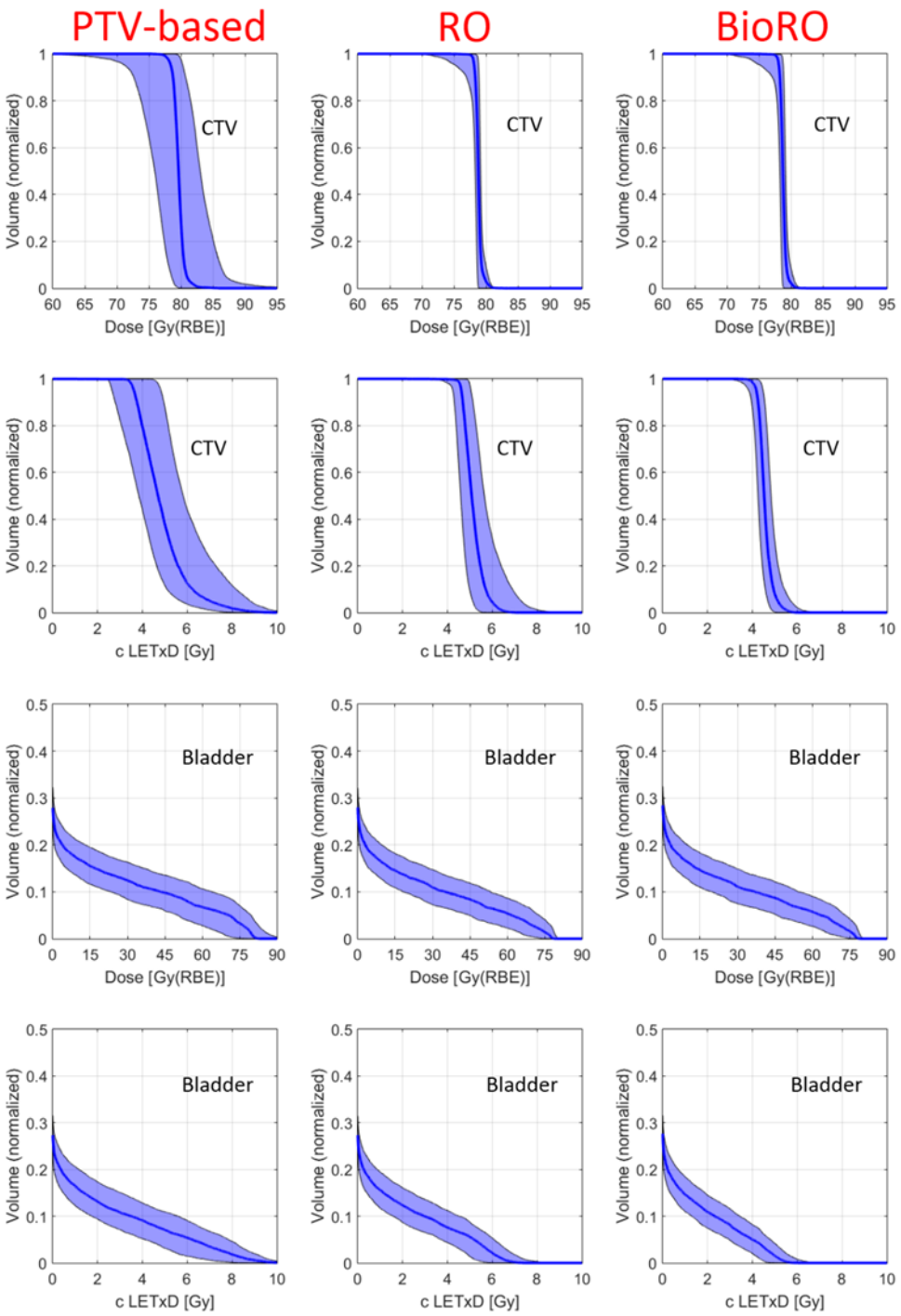

Figure 4.2: Dose-volume histograms (DVHs) and c LETxD-volume histograms of the clinical target volume (CTV) and the bladder for three IMPT plans in a prostate tumor patient case. The bold lines indicate the nominal distributions.

Table 4.3: Dose and LET-weighted dose (LETxD; scaled by c = 0.04 μm/keV) values in the clinical target volume (CTV), rectum, and bladder.

Tissue	**Dosimetric Parameters**	**PTV-based**			**RO**			**BioRO**		
		Nom	Max	Min	Nom	Max	Min	Nom	Max	Min
CTV	$D_{98\%}$ (Gy[RBE])	78.0	80.0	68.2	78.0	78.8	73.5	78.0	78.7	73.5
	$D_{2\%}$ (Gy[RBE])	81.8	89.6	79.0	80.3	80.8	78.8	80.1	80.8	78.7
	c LETx$D_{98\%}$ (Gy)	3.6	5.2	2.8	5.0	5.5	4.5	4.5	4.9	4.0
	c LETx$D_{2\%}$ (Gy)	8.7	10.4	7.2	6.9	8.6	5.8	5.9	6.6	5.3
Rectum	$D_{2\%}$ (Gy[RBE])	72.0	81.2	49.7	71.9	78.4	51.1	71.7	78.2	52.1
	$D_{2\%}$ (Gy[RBE])	72.0	81.2	49.7	71.9	78.4	51.1	71.7	78.2	52.1
	c LETx$D_{2\%}$ (Gy)	5.8	8.2	3.9	3.9	5.0	2.6	3.5	4.4	2.3
	c LETxD_{mean} (Gy)	0.7	1.2	0.3	0.4	0.7	0.2	0.4	0.6	0.2
Bladder	$D_{2\%}$ (Gy[RBE])	78.4	84.1	63.7	73.3	78.4	61.6	73.6	78.3	62.3
	D_{mean} (Gy[RBE])	8.7	12.0	5.7	7.6	10.4	5.1	7.8	10.6	5.3
	c LETx$D_{2\%}$ (Gy)	8.7	9.9	6.1	6.6	7.6	5.4	5.4	6.1	4.4
	c LETxD_{mean} (Gy)	0.9	1.2	0.5	0.7	1.0	0.5	0.6	0.8	0.4

Abbreviations: RBE, relative biological effectiveness; Nom, nominal

The results for the prostate tumor case are shown in Figure 4.2 and Table 4.3. The differences in dose and LETxD distributions among the three IMPT plans were similar for the prostate and brain tumor cases. Note that the improvement in the robustness of LETxD with the BioRO plan in the bladder and rectum was modestly lower than in the brainstem as shown by the brain tumor case because of the anatomy and the beam arrangement. The bandwidth at D2% of c LETxD in the bladder was 1.7 Gy for the BioRO plan, smaller than the 3.8 Gy and 2.2 Gy bandwidths for the PTV-based plan and the RO plan, respectively (Table 4.3). The bandwidth at the mean value of c LETxD in the bladder was 0.4 Gy for the BioRO plan, 0.5 Gy for the PTV-based plan, and 0.7 Gy for the RO plan. In the rectum, the bandwidth at D2% of c

LETxD was 2.1 Gy for the BioRO plan, compared to 4.3 Gy and 2.4 Gy for the PTV-based plan and the RO plan, respectively. The bandwidth at the mean value of c LETxD in the rectum was 0.4 Gy for the BioRO plan, compared to 0.5 Gy and 0.9 Gy for the PTV-based plan and the RO plan.

The DVHs, c LETxD volume histograms and their statistics for the head and neck tumor case are shown in Figure 4.3, 4.4 and Table 4.4. The BioRO approach produced plan with more robust LETxD distribution than did the RO and PTV-based methods, and similar dose distribution compared to RO plan which is better than the PTV-based plan. The bandwidth at D2% of c LETxD in the larynx was 0.8 Gy for the BioRO plan, 2.1 Gy for the PTV-based plan, and 1.2 Gy for the RO plan. The bandwidth at the mean value of c LETxD in the larynx was 0.4 Gy for the BioRO plan, 0.8 Gy for the PTV-based plan, and 1.0 Gy for the RO plan. In the parotid (right), the bandwidth at D2% of c LETxD was 0.8 Gy for the BioRO plan, smaller than the 1.5 Gy and 1.2 Gy bandwidths for the PTV-based and RO plans; and the bandwidth at mean value of c LETxD was 0.4 Gy for the BioRO plan, smaller than the 0.7 Gy and 0.6 Gy bandwidths for the PTV-based and RO plans. Similarly, the bandwidth at D2% of c LETxD in the parotid (left) was 1.1 Gy for the BioRO plan compared to 1.3 Gy for the PTV plan and 2.2 Gy for the RO plan; the bandwidth at mean value of c LETxD in the parotid (left) was 0.2 Gy for the BioRO plan compared to 0.2 Gy for the PTV plan and 0.3 Gy for the RO plan.

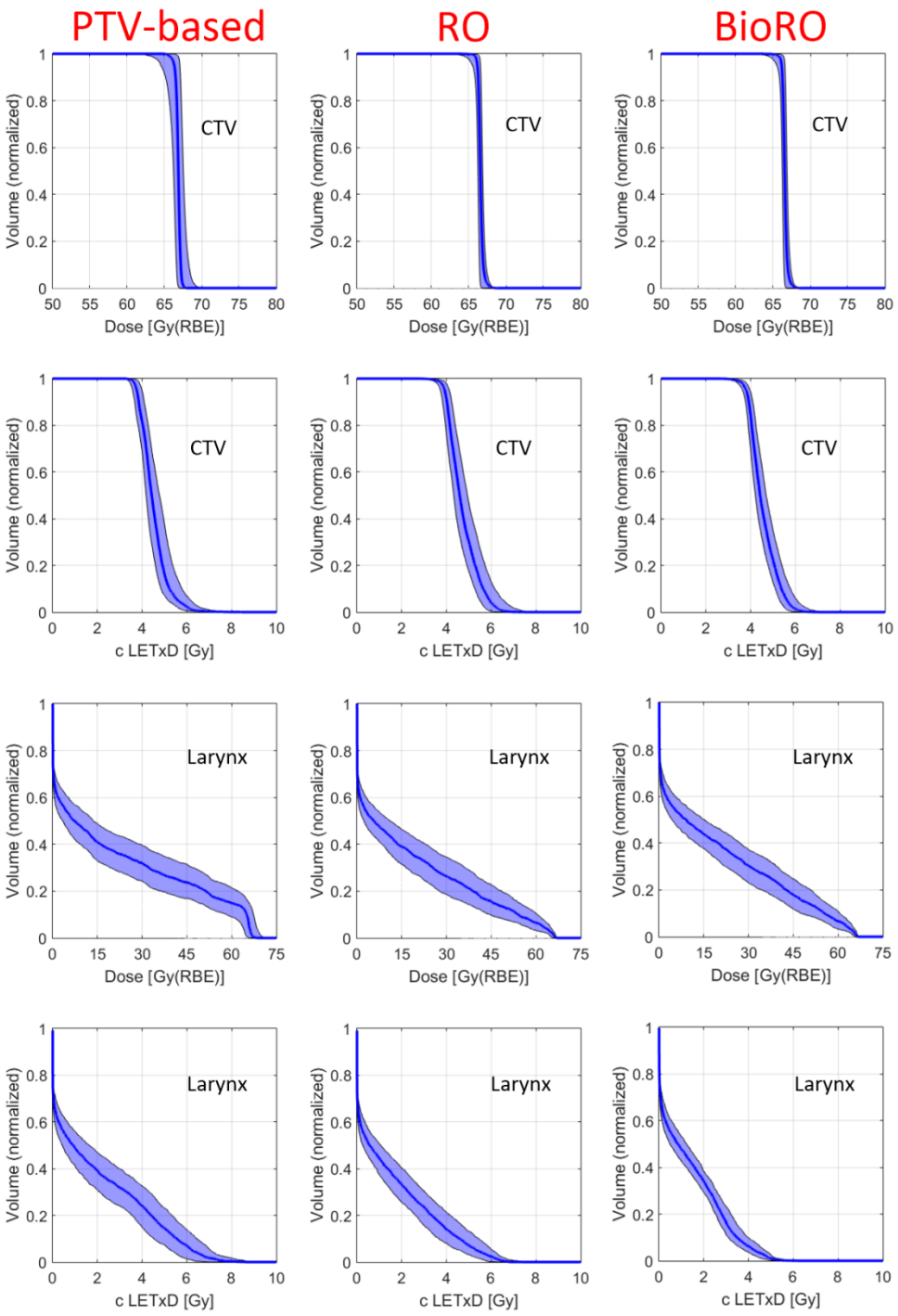

Figure 4.3: Dose-volume histograms (DVHs) and c LETxD-volume histograms of the clinical target volume (CTV) and the larynx for three IMPT plans in a head & neck tumor patient case. The bold lines indicate the nominal distributions.

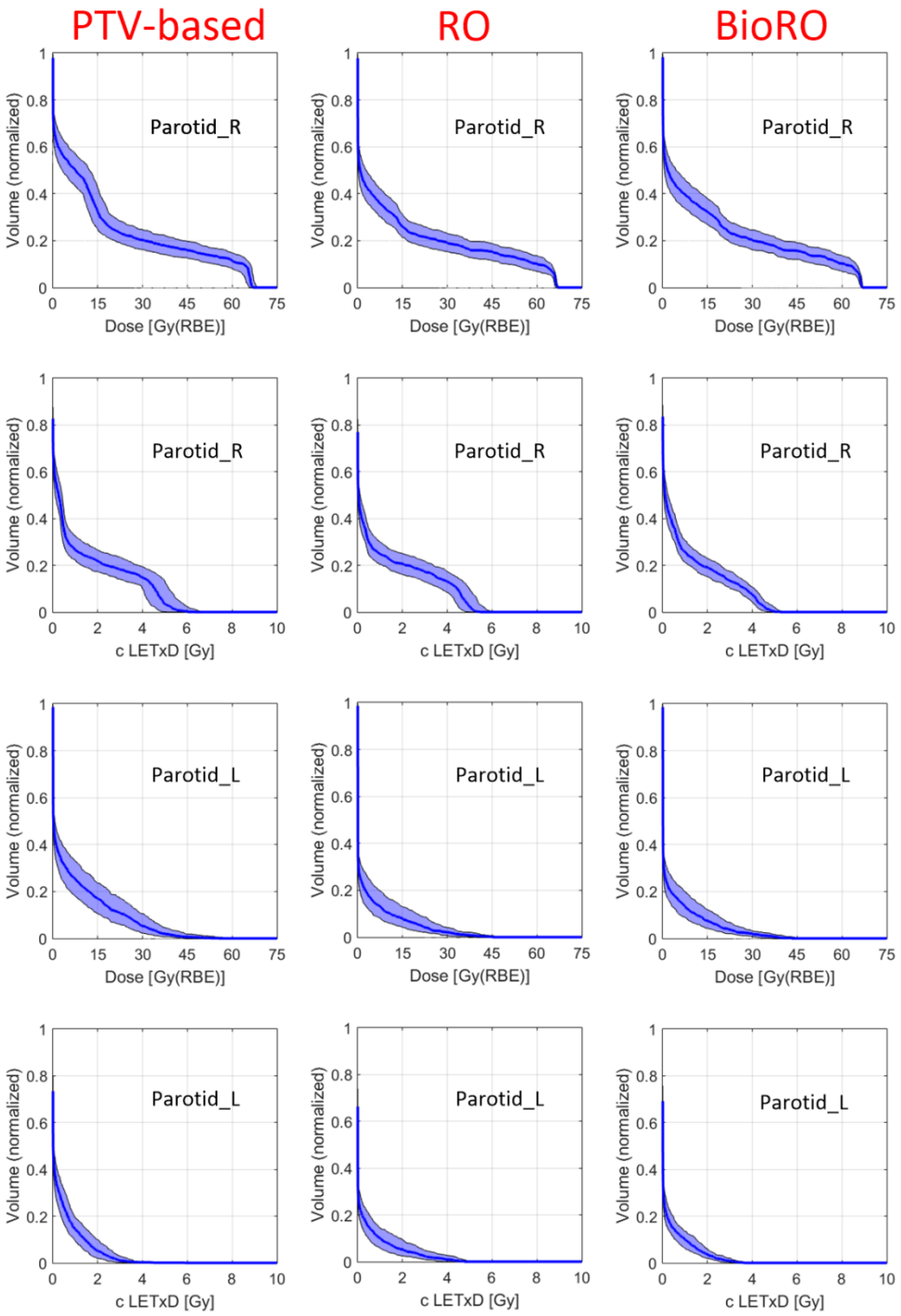

Figure 4. 4: Dose-volume histograms (DVHs) and c LETxD-volume histograms of the parotid (right & left) for three IMPT plans in a head & neck tumor patient case. The bold lines indicate the nominal distributions.

Table 4.4: Dose and LET-weighted dose (LETxD; scaled by c = 0.04 μm/keV) values in the clinical target volume (CTV), larynx and parotid (right & left) for a H&N tumor case.

Tissue	Dosimetric Parameters	PTV-based			RO			BioRO		
		Nom	Max	Min	Nom	Max	Min	Nom	Max	Min
CTV	$D_{98\%}$ (Gy[RBE])	66.0	67.0	63.8	66.0	66.5	64.5	66.0	66.5	64.9
	$D_{2\%}$ (Gy[RBE])	67.4	69.0	66.8	67.5	67.8	66.6	67.4	67.8	66.6
	c LETx$D_{98\%}$ (Gy)	3.7	3.9	3.5	3.8	4.0	3.6	3.6	3.8	3.4
	c LETx$D_{2\%}$ (Gy)	6.1	6.6	5.6	6.2	7.0	5.7	5.9	6.4	5.5
Larynx	$D_{2\%}$ (Gy[RBE])	66.5	69.3	64.5	65.6	66.4	63.8	65.4	66.2	63.6
	D_{mean} (Gy[RBE])	20.8	25.9	16.1	17.3	21.6	13.3	19.4	23.3	15.5
	c LETx$D_{2\%}$ (Gy)	6.9	7.9	5.8	6.1	6.5	5.3	4.8	5.1	4.3
	c LETxD_{mean} (Gy)	2.0	2.5	1.5	1.5	2.0	1.2	1.4	1.6	1.2
Parotid_R	$D_{2\%}$ (Gy[RBE])	66.3	67.7	64.8	66.4	66.8	65.8	66.4	66.8	65.8
	D_{mean} (Gy[RBE])	16.5	19.9	13.3	13.8	16.7	11.1	15.1	18.1	12.2
	c LETx$D_{2\%}$ (Gy)	5.3	6.1	4.6	5.0	5.7	4.5	4.6	5.0	4.2
	c LETxD_{mean} (Gy)	1.1	1.5	0.8	1.0	1.3	0.7	0.9	1.1	0.7
Parotid_L	D_{mean} (Gy[RBE])	37.6	44.4	31.4	30.8	38.5	23.0	30.0	36.4	23.1
	c LETx$D_{2\%}$ (Gy)	6.1	8.7	4.0	3.0	4.8	1.8	3.0	4.5	1.9
	c LETxD_{mean} (Gy)	2.7	3.3	2.0	3.2	4.4	2.4	2.4	3.0	1.9
	c LETxD_{mean} (Gy)	0.4	0.5	0.3	0.3	0.5	0.2	0.3	0.4	0.2

Abbreviations: RBE, relative biological effectiveness; Nom, nominal.

Figure 4.4 shows uncertainty maps for the three plans for the brain tumor case. The top row shows the difference distributions for dose (based on a constant RBE of 1.1). The bottom row shows difference distributions for LET weighted dose (LETxD) (scaled by c =0.04 μm/keV). The RO method was the most robust in terms of physical dose distribution in the target and brainstem. Moreover, the RO plan was more robust than the PTV-based plan in terms of LETxD. The BioRO method, which minimized the variation in biological effect, led to a remarkable reduction of LETxD hot spots,

especially in the brainstem. Meanwhile, the robustness of the physical dose distribution for the BioRO plan was improved compared to the PTV-based plan.

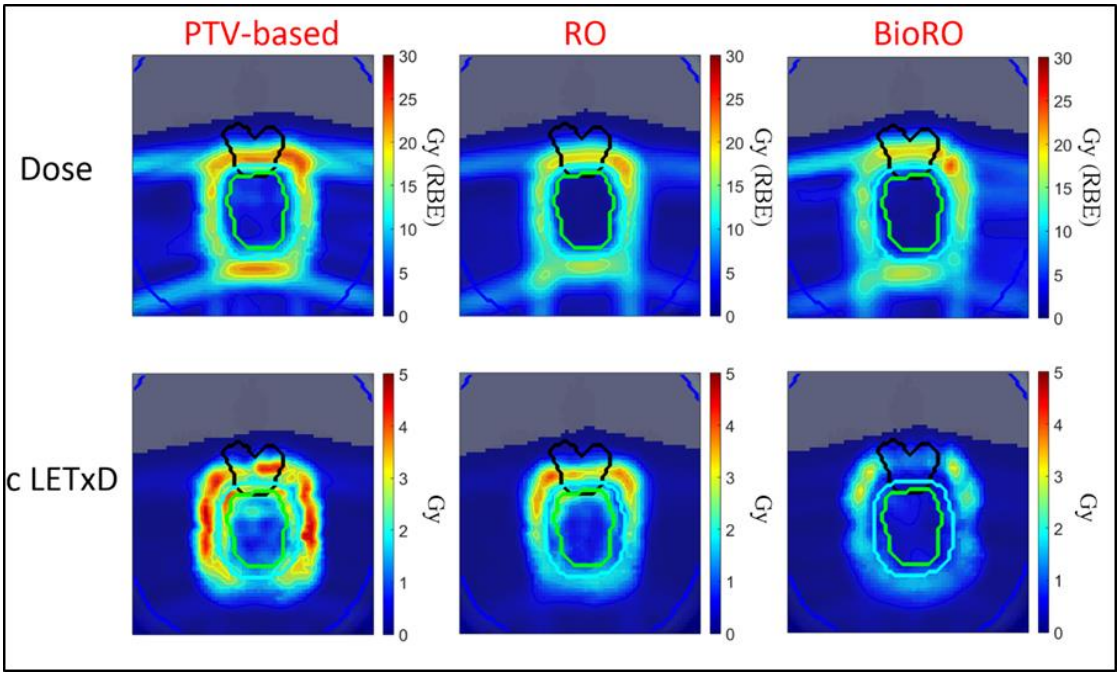

Figure 4.5: Distribution of differences between the maximum and minimum values in each voxel. The green and black contours indicate the clinical target volume (CTV) and brainstem, respectively.

As shown in Figure 4.6, the biological effect in the nominal scenario was the lowest for the BioRO plan, especially in critical organs. Panels (a), (b), and (c) show dose distributions (based on a constant RBE of 1.1) for the nominal scenario for PTV-based, RO, and BioRO plans , respectively. Panels (A), (B), and (C) show LET-weighted dose (LETxD) distributions (scaled by c = 0.04μm/keV) for the nominal scenario for PTV-based, RO, and BioRO plans, respectively. Panel (a – b) illustrates the absolute difference of (a) and (b), calculated by subtracting the value in (b) from the value in (a) for each voxel. The same method was applied for (a-c), (b-c), (A-B), (A-C), and (B-C). However, there was almost no difference among the three plans in

the physical dose distributions for the nominal scenario (see subfigure (a-b), (a-c) and (b-c)).

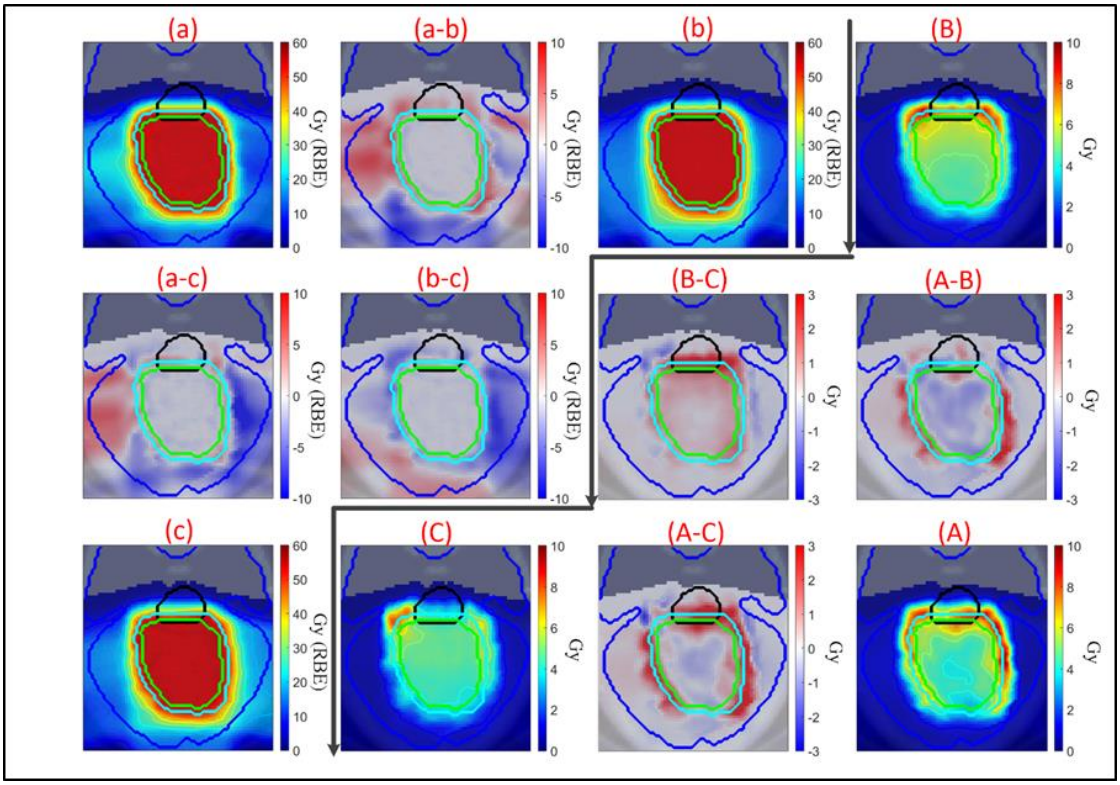

Figure 4.6: Comparison of PTV-based, robust optimization (RO), and biological effect-based RO (BioRO) plans for the brain tumor patient case. The green and black contours indicate the clinical target volume (CTV) and brainstem, respectively.

4.3.3 Discussion

Three has been a growing interest in LET-based IMPT planning, including novel forward planning techniques and optimization methods [16], [20], [21], [28]–[31], [88]. The primary goal of LET-based planning is to place areas of higher LET to achieve a greater biological effect in radioresistant tumors while minimizing LET in critical structures to avoid unnecessary tissue damage. At the same time, LET-based planning keeps physical dose distributions as similar as possible to those currently

used in proton therapy with fixed RBE planning. These methods have demonstrated the potential of increasing LET in target regions and/or reducing LET in normal tissues without excessively compromising current dose requirements. However, the challenge of IMPT delivery uncertainties has been largely ignored. The BioRO approach to IMPT planning proposed in the present study focuses on minimizing the variation in biological effect attributable to physical uncertainties for both target and normal tissues. The uncertainty gap minimization method was effective in reducing the spread of LETxD-volume histogram bands in this study. In other words, this approach could produce treatment plans with a high certainty of biological effect with satisfactory physical dose plan quality.

RO has been shown to deliver IMPT more safely than conventional PTV-based optimization [8], [11], [12], [62], [99]. RO provides dose distributions that are robust against delivery uncertainties, especially because it limits the impact of shifted Bragg peaks at the beam's distal edge, close to the target boundary. Therefore, researchers have proposed that unlike PTV-based plans, RO plans may alleviate increased LET or LETxD in OARs adjacent to the target [107]. Our study confirmed that this is the case. For example, compared to the PTV-based plan, LETxD for 2% of the volume and mean LETxD for the brainstem were reduced by 15% and 11%, respectively, with RO. Similarly, LETxD for 2% of the volume and mean LETxD for the rectum were reduced by 33% and 43%, respectively.

Interestingly, the BioRO plan further reduced LETxD in OARs than the RO plan for both patient cases. For example, for the brain tumor case, compared to the PTV-based plan, LETxD for 2% of the volume and mean LETxD for the brainstem were

reduced by 48% and 43%, respectively. Similarly, for the prostate tumor case, LETxD for 2% of the volume and mean LETxD for the rectum were reduced by 40% and 43%, respectively. This finding may be nonintuitive, as the minimization of LETxD was not specified in the BioRO cost function. Instead, the uncertainty gap of LETxD was minimized. We conjecture that the reduction of LETxD in BioRO plans is attributable to the positive correlation between the uncertainty gap of LETxD and the nominal LETxD. For instance, a higher LETxD leads to a larger uncertainty gap, as either nominal LETxD or LETxD in various uncertainty scenarios is modulated by the same set of beamlet intensities, i.e., $LD_i = \sum_j^{N_B} D_{ij} L_{ij} w_j^2$. In all patient cases, we found that the sum of all beamlet intensities for the BioRO plan was the lowest among the three plans. However, these reduced total intensities did not necessarily lead to a cold plan in terms of dose, as seen in this study, because of the solution degeneracy of IMPT optimization.

We also note that our method is similar to ones proposed by Giantsoudi et al [107] and An et al [31] in which biological effect was included in the robust optimization framework. But our method is different in terms of its objectives that minimize the impact of physical uncertainties on biological effect, i.e., those uncertainty gap terms, instead of minimizing worst-case biological effect. The difference among methods is worth investigating in future studies. Moreover, the information gap concept could also be applied in the robust optimization of dose, compared to the worse case optimization strategies extensively used in the literature. However, this may require a comprehensive comparison study and is beyond the scope of this paper concerning biological effect robustness.

Moreover, the BioRO plan also reduced LETxD in the target for all patient cases. However, the reduction in the target dose was much smaller than it was in OARs. The main reason for this difference may be that the BioRO plan enforced the requirement of prescribed dose to the target, but not to OARs, for which there was no lower dose limit. One straightforward method to avoid the reduction of LETxD in the target could be to use an additional objective to maximize the nominal or minimum LETxD for target voxels. Such a method for managing the trade-off between optimality and robustness with regard to biological effect needs to be explored in future research.

The gain in LET or LETxD while maintaining dose requirements is mainly achievable because IMPT provides a higher degree of freedom for optimization, i.e., intensity modulation. Our study demonstrated that plan robustness to biological effect can be improved by redistributing LETxD. Similarly, previous studies showed that LET and LETxD were improved by redistributing them [20], [28], [88]. Because large uncertainties in proton RBE models remain a challenge to implementing RBE-based optimization in clinical practice, LET- or LETxD-based optimization is a promising method for improving the current proton treatment by moving toward biological effect-based IMPT planning.

4.3.4 Conclusion

We presented a proof-of-concept study of biological effect-based IMPT robust optimization in order to reduce the impact of variation in protons' biological effect while limiting the degradation of the physical dose distribution from a voxel-based worst-case RO plan. By minimizing the uncertainty gap of the biological effect

(approximated by the product of LET and physical dose) in each voxel, the BioRO approach provided robust distributions of biological effect to both target and critical structures. This approach does not depend on tissue parameters or variable RBE models, which are associated with large uncertainties. In addition, our three patient case studies demonstrated that BioRO can avoid elevating biological effect in critical structures.

4.4 Impact of robust optimization on relative biological effectiveness

4.4.1 Patient cases and treatment planning

Two IMPT plans were generated to illustrate the CTV-based optimization and RO methods for two cases from MD Anderson Cancer Center (MDACC), e.g. a prostate cancer and a head-and-neck (HN) cancer. The uncertainties paramters used for the prostate case and head and neck (H&N) case are as same as we 4.3.2 section. The prescribed dose to target volumes and field arrangements were the same as those used in the clinical treatments. The doses prescribed to all OARs were set to 0 in the optimizations. More planning details are listed in Table 4.5.

Table 4.5: Patients information and treatment planning parameters.

Cancer type	Beam angle	Number of beamlets	Organs	Number of voxels
Prostate	(90°, 0°)	5532	CTV	6716
	(270°, 0°)	5525	Bladder	10087
			Femoral heads	21686
			Rectum	5614
H&N	(105°, 0°)	3808	CTV	12906
	(180°. 0°)	3902	Brain	347816
	(255°, 0°)	3927	Brainstem	2996
			Optic chiasm	64

Abbreviations: CTV, clinical target volume; PTV, planning target volume.

4.4.2 Results

4.4.2.1 Homogeneous of plans

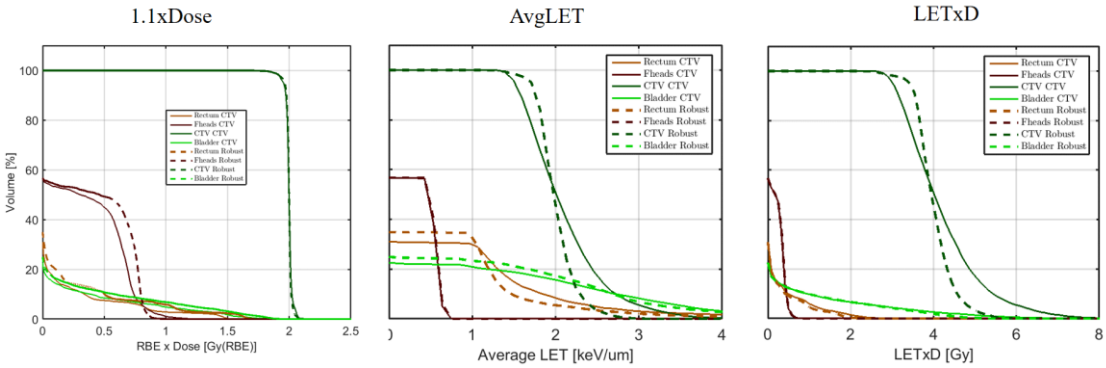

Figure 4.7: Physcial dose, LET and scaled LETxD histograms of prostate case.

For the prostate case, as shown by the Figure 4.7, both Robust optimization and CTV-based optimization give the same dose volume histogram in the nominal scenario. But robust optimization gives a higher LET volume histogram in target,

which makes the LET weight dose distribution of robust optimization plan is more homogeneous.

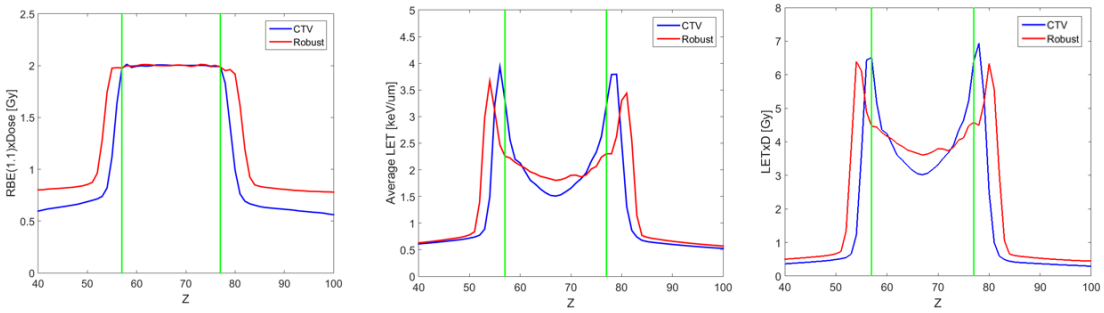

Figure 4.8: Physcial dose, LET and biological dose profiles of prostate case. The green lines show the region of the CTV.

Compared to the CTV-based optimization plan, the profile of LET weighted dose in the RO plan will be more uniform due to the LET distribution is more homogeneous (see Figure 4.8). Thus, the variable RBE (McNamora model) [14] weighted dose for the CTV-based optimization plan has more hot points and cold points inside the CTV region, especially in the distal edge of the target (Figure 4.9).

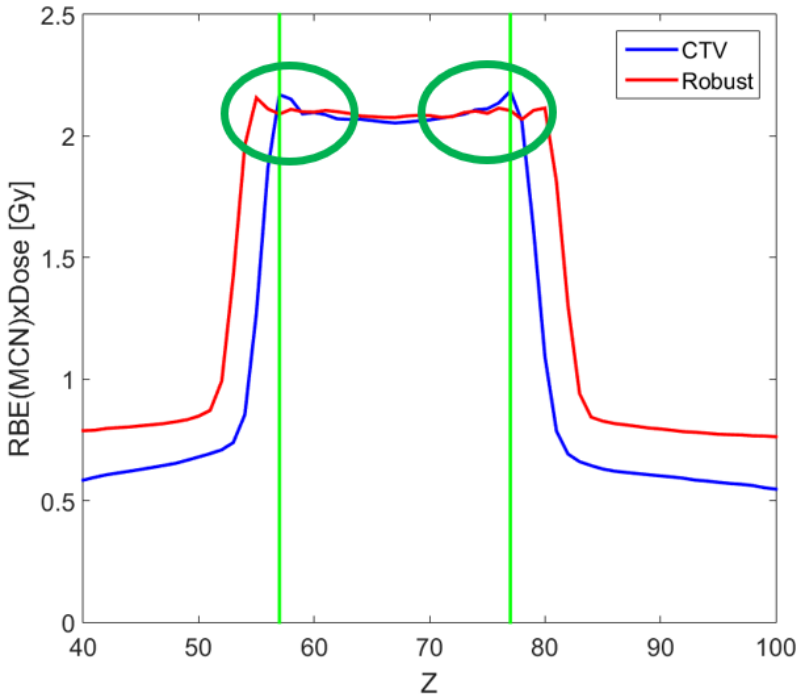

Figure 4.9: Variable RBE (McNamara model) weighted dose profles of prostate case. The green lines show the region of the CTV.

This can also be proved by the N&H case (4.10).

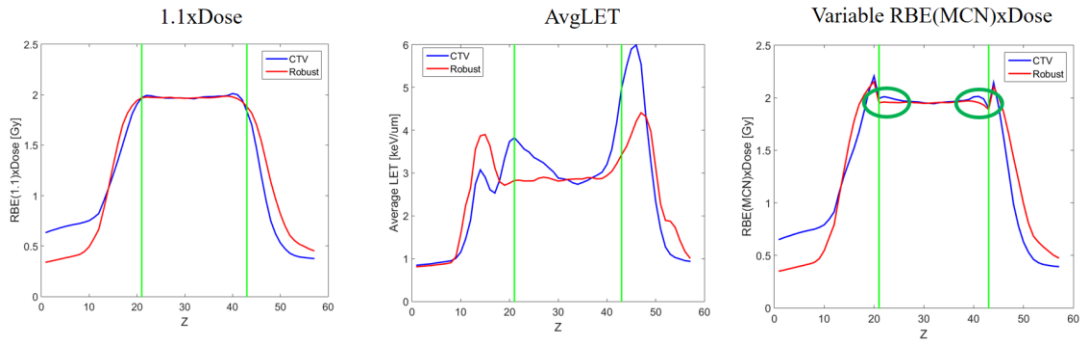

Figure 4.10: Physcial dose, LET and biological dose profiles of prostate case. The green lines show the region of the CTV.

4.4.2.2 Robustness of the plans

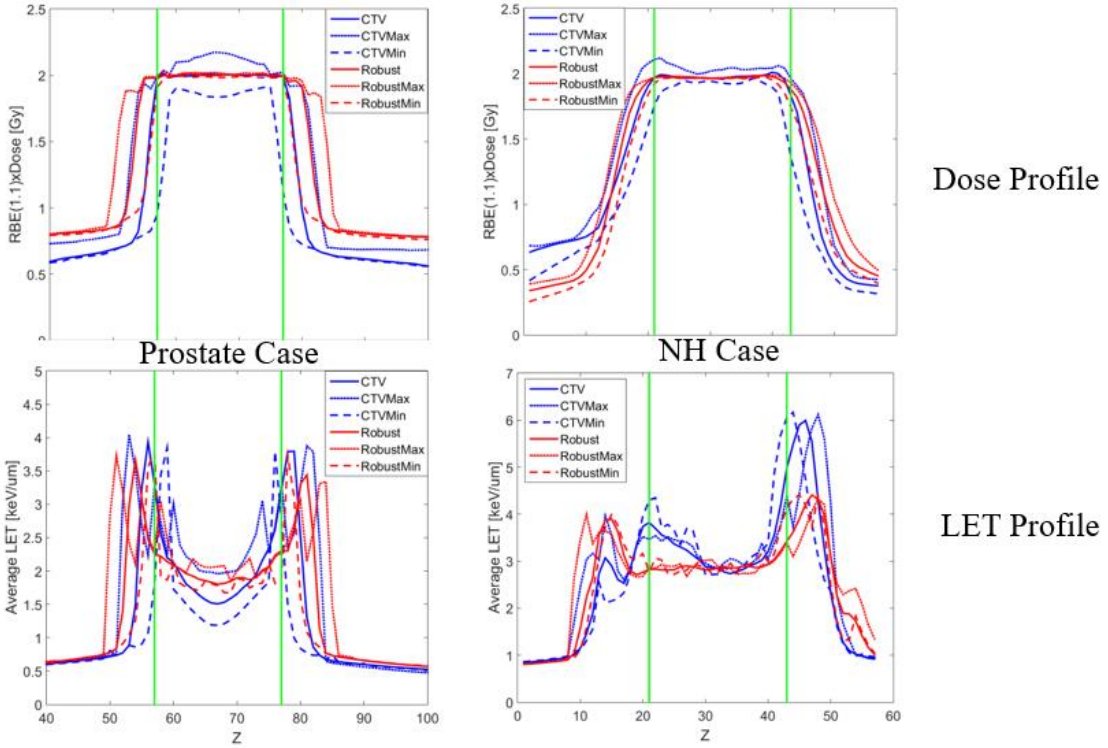

Figure 4.11: Physical dose and LET profiles of three cases over maximal value (dotted line), minimal value (dash line) and nominal scenarios (solid line).

By comparing the profile of worst case, best case, and nominal case, we can easily find out the robust optimization will keep the physical dose (inside target region) in a narrow band (Figure 4.11, 4.12). At the same time, the LET band will also stay robust because he LET distribution will be impacted by dose distribution by the dose averaged ratio, even we do not optimize the LET factor.

The robust optimization is approved to be more robust in the biological effect while achieving the physical dose robustness compared to the CTV-based optimization. The constant RBE weighted dose band and variable RBE (McNamara model) weighted dose band of two plans also show the same conclusion (Figure 4.12). The brain tumor case was optimized by CTV-based optimization and robust

optimization methods, both based on a constant RBE = 1.1. Then the results were compared based on the constant RBE band (blue) and variable RBE (McNamora model) band (red). As we saw, the variable RBE bands for the robust optimization plan keep the robustness compared to the variable RBE bands for the CTV-based optimization plan. More than that, we find out the variable RBE band was lower than the constant RBE band in the target and higher than the constant RBE band in the brainstem. This is because the $(\alpha/\beta)x$ ratios used for the target and OAR are different. For the brain tumor case, the variable RBE in the target and brainstem is usually evaluated by $(\alpha/\beta)x$ ratios 10 and 2. This indicated the lower $(\alpha/\beta)x$ ratio could result in a variable RBE value higher than 1.1.

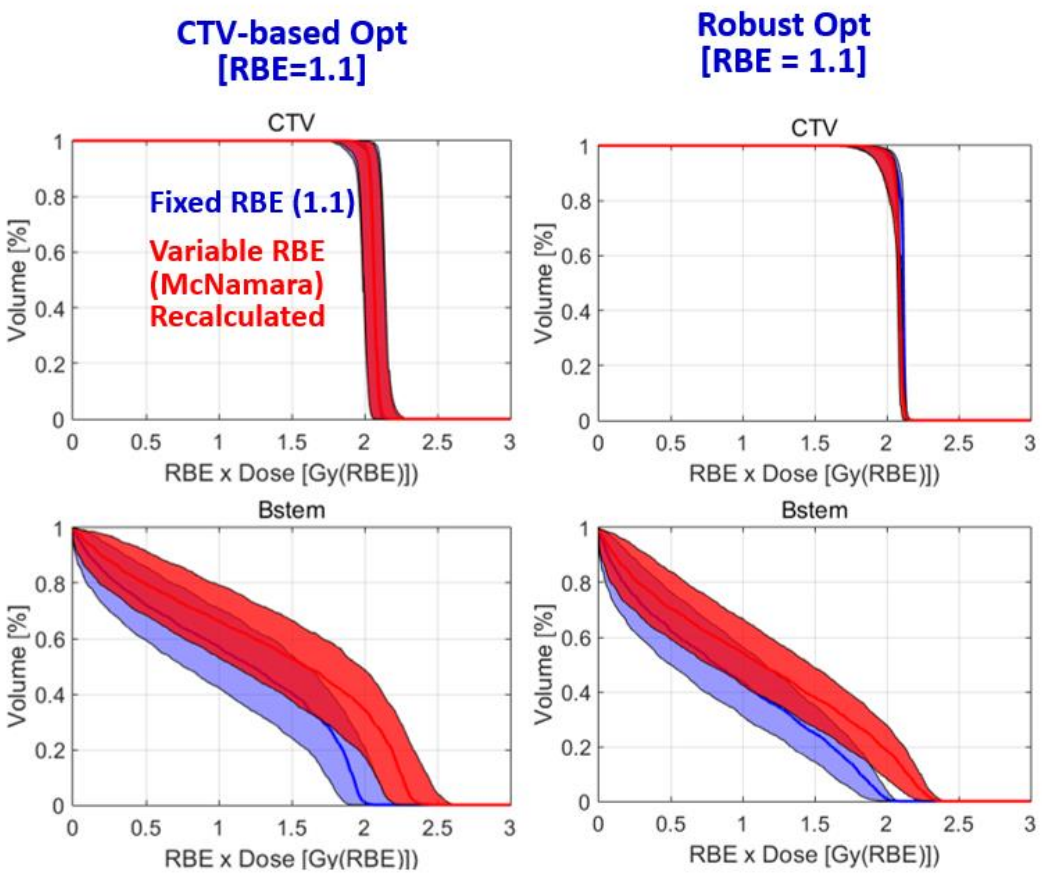

Figure 4.12: Physical dose and variable RBE weighted dose band of N&H case.

4.4.3 Conclusion

The voxel-based worst-case RO method could enhance the variable RBE weight dose robustness compare to the CTV-based optimization approach. This is because RO plans show an advantage in the robustness of physical dose which plays the most important role in the variable RBE models. Furthermore, RO method also makes the LET distribution more comformal, which also promotes the the stability of variable RBE among all scenarios. The results of comparison between the RO method and PTV-based optimization method are listed in the Appendices A.

Chapter 5

A Biological Effect-Guided Optimization Approach using Beam Distal-Edge Avoidance for Intensity-Modulated Proton Yherapy

5.1 Introduction

Proton beams deposit dose slowly along their incoming path before reaching a sharp peak known as the Bragg peak. Beyond the Bragg peak, the deposited dose rapidly falls to almost zero. This physical property of proton beams enables intensity-modulated proton therapy (IMPT): delivery of a highly conformal dose enclosing the tumor while sparing adjacent normal tissue [5]. In addition, the biological effect of proton beams is greater than that of photons. The biological effect is usually measured by the relative biological effectiveness (RBE), i.e., the ratio of the doses of two types of ionizing radiation needed to reach the same biological effect [15], [108]. A constant RBE value of 1.1 (i.e., 10% more effective than a photon beam) is currently used in recommendations for clinical proton treatment planning from the International Commission on Radiation Units and Measurements [13].

RBE varies depending on linear energy transfer (LET), tissue-specific parameters (defined by α and β), dose per fraction, and other factors [14], [15], [23], [109], [110]. However, existing experimental biological data are insufficient to clearly correlate RBE and dose per fraction or $(\alpha/\beta)_x$ for *in vivo* endpoints [15], [17], [107]. Therefore, the use of these variable RBE models to evaluate proton treatment plans may lead to unwanted clinical consequences. For example, if the calculation of the target dose

coverage is based on a variable RBE-weighted dose, the patient will be at risk of receiving a lower physical dose in parts of the tumor because variable RBE is assumed to be greater than 1.1 in areas of high LET. Critical structures are in danger of being exposed to a higher physical dose when the variable RBE is underestimated [20], [86].

To resolve this problem, recent studies have attempted to optimize a biological dose approximated by both physcial dose and LET. This is because the biological effectiveness of a proton beam increases with the increase in LET toward the end of the proton range [20], [30] and LET can be predicted precisely using analytical methods or Monte Carlo simulations [25]. Several studies have developed methods to take advantage of LET to maximize biological effectiveness in proton therapy. In order to increase LET to achieve a higher biological effect in radioresistant tumors, Bassler et al [29] introduced a "LET-painting" method that can generate mixed-modality treatment plans using protons and carbon ions to shape a high-LET region throughout the planning target volume. Fager et al [30] used multiple radiation fields to cover different segments of the target so that the dose prescriptions could be reduced by the increased LET in the target. Tseung et al [111] took advantage of graphics processing unit acceleration to optimize the biological dose for head and neck cancer cases. To reduce the risk of normal tissue complications, Unkelbach et al [20] applied a two-step optimization method to avoid high scaled LET-weighted dose values in critical structures. To reduce LET and RBE in organs at risk (OARs), Traneus and Ödén [112] noticed the location of the proton track-end and added it into an objective function.

Various LET optimization techniques have also been developed to take care of the biological effect in both target volumes and critical structures, Giantsoudi et al [16] presented a multicriteria optimization method to find plans with higher dose-averaged LET in tumor targets and lower dose-averaged LET in normal tissue structures. Inaniwa et al [88] minimized the physical dose and dose-averaged LET based on prescribed values in a quadratic cost function, while Cao et al. added two terms for maximizing LET-weighted dose in the target and minimizing it in OARs without considering any prescription. To deal with plan robustness under proton range and patient setup uncertainties, An et al [113] minimized the highest LET in OARs while maintaining the same dose coverage and robustness in tumor targets as the conventional robust IMPT treatment plan model, while Bai et al [114] penalized the sum of the differences between the highest and lowest biological effect in each voxel, approximated by the product of dose and LET, to achieve the robust biological effect and physical dose distributions in both target and critical structures. However, these approaches typically use optimization priorities to control the trade-off dynamic between dose and LET objectives. The intrinsic relationship between dose and LET of protons was not incorporated in the cost function.

Notably, LET keeps increasing beyond the location of the Bragg peak in the patient volume. This property could be explicitly considered in the optimization. Therefore, we investigated the impact of directly including the scanning spot position in IMPT optimization. We introduced an influence index for each scanning spot based on its topological relationship to different organs of interest and added this index to a

conventional dose-based objective function. Both physical dose and LET distributions can be optimized simultaneously in the proposed approach.

5.2 Methods and Materials

This work evaluated the effectiveness of distal-edge avoidance-guided optimization (DEAOpt) by comparing its results with those of conventional dose-based optimization (DoseOpt) and LET-incorporating optimization (LETOpt) using four clinical cases.

5.2.1 Distal-edge avoidance-guided optimization (DEAOpt)

IMPT treatment planning using the 3D spot scanning technique [115] can deposit physical dose D_{ij} and LET L_{ij} to voxel i by the jth beamlet with unit intensity. The total dose D_i, dose-averaged LET (LETd) L_i, and LET-weighted dose (LETxD) LD_i in the voxel i are calculated by:

$$D_i = \sum_j^{N_B} D_{ij} w_j^2, \tag{5.1}$$

$$L_i = \frac{\sum_j^{N_B} D_{ij} L_{ij} w_j^2}{\sum_j^{N_B} D_{ij} w_j^2}, \tag{5.2}$$

and

$$LD_i = \sum_j^{N_B} D_{ij} L_{ij} w_j^2, \tag{5.3}$$

respectively, where w_j^2 is the intensity of beamlet j among beamlet set N_B to preserve the nonnegativity. The dose and LET calculations in this study were performed with

an open-source treatment planning platform, matRad [95], using a singular-value decomposed pencil-beam algorithm [96].

For DoseOpt, a standard quadratic objective function was used to minimize the mean square deviation between the calculated dose distribution and the ideal prescription over the entire volume [116]. Different weighting factors, λ_T and λ_{OAR}, and prescription values, $D_{0,T}$and $D_{0,OAR}$, for the structures were applied to control the balance between target coverage and critical structure sparing. The objective function is given by [117]:

$$F_N(w_j) = \lambda_T \frac{1}{N_T} \sum_{i=1}^{N_T} \left(D_i - D_{0,T}\right)^2 + \lambda_{OAR} \frac{1}{N_{OAR}} \sum_{i=1}^{N_{OAR}} H\left(D_i - D_{0,OAR}\right) \times \left(D_i - D_{0,OAR}\right)^2. \quad (5.4)$$

Here, N_T and N_{OAR} are the sets of voxels in target volumes and OARs, respectively. The Heaviside function, denoted by $H\left(D_i - D_{0,OAR}\right)$, is a discontinuous function whose value is zero if $D_i \leq D_{0,OAR}$ and one if $D_i > D_{0,OAR}$.

Because the scaled LETxD (c LETxD) can be regarded as the additional biological dose contributed by the LET effect [20], two LETxD terms were added to Function (4) to maximize the biological dose in the target and minimize it in the OARs for the LETOpt [20], [28], [88]. The optimization weighting factors for the two objective terms were θ_T and θ_{OAR}. The cost function of LETOpt was formulated as shown in (5.5):

$$F_L(w_j) = F_N(w_j) - \theta_T \frac{1}{N_T} \sum_{i=1}^{N_T} LD_i^2 + \theta_{OAR} \frac{1}{N_{OAR}} \sum_{i=1}^{N_{OAR}} LD_i^2. \quad (5.5)$$

According to Unkelbach et al [20], a threshold value LD^{ref}, such that 95% of the target volume receives LD_i values higher than LD^{ref}, can be used for normal tissues. In our case, we did not involve the prescriptions for the LETxD terms because there was a large difference in the LET distributions for different cases, and even for the same case with different beam angles. Our goal was to increase the biological dose in the target and reduce it in OARs as much as possible. Because increasing the biological dose in the target often comes at the cost of increasing the biological dose in the OARs, one can adjust the weighting factors (θ_T and θ_{OAR}) in Formulation (5.5) to find a balance between the target and the OARs. However, the threshold LD^{ref} can easily be added to Formulation (5.5) for both the target and critical structures.

For each lateral position, the proton beam energy was chosen so that the Bragg peak of the depth dose curve coincided with the distal target edge [117]. Since LET keeps rising beyond the Bragg peak, the highest value of the LETxD appeared at position p_j, which is a distance d_j away from the scanning spot location s_j along the beam direction $\overrightarrow{b_j}$. This distance depends on the beam energy and tissue type:

$$p_j = s_j + \overrightarrow{b_j} \cdot d_j. \tag{5.6}$$

In order to limit the high biological dose in the target area and protect critical structures, we examined the topological relationship between the peak LETxD position, the target location, and the critical structure locations in four situations, shown in Figure 1. For Situation A, the position of the peak LETxD value p_j falls into the OAR areas and outside the target region; a penalty θ_A was assigned to this beamlet. For Situation B, where p_j is in the overlap area of the target and OAR, θ_B was the

assigned penalty. For Situation C, where a subregion formed by the center p_j and semidiameter R_j overlaps with an OAR but not the target area [118], the penalty was θ_C. Finally, in Situation D, where the subregion is outside the OAR and overlaps with the target volume, the penalty was θ_D.

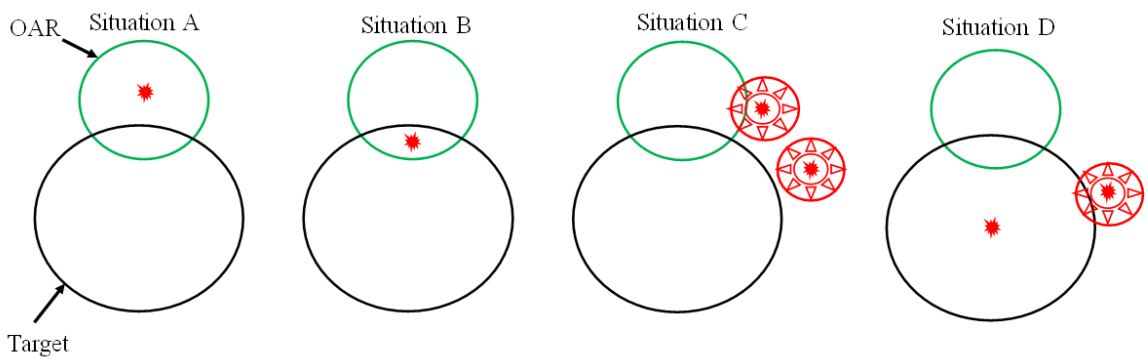

Figure 5.1: Topological relationship between peak scaled linear energy transfer-weighted dose location and different organs of interest. OAR, organ at risk.

The semidiameter R_j is the proximal 80% to distal width of the most distal peak of beamlet j [94], [118]. The values of penalty θ were set based on Formulation (5.7) and case preferences. For example, if the treating physician preferred to maintain a high biological dose in the area where the target and OARs overlap, a low value of θ_B was assigned according to the fomulation (5.7):

$$\theta_A \geq \theta_C \geq \theta_B \geq \theta_D. \tag{5.7}$$

Thus, we added an L_1-norm sparsity term, in which the penalty for beamlet intensity was based on the topological relationship shown above, to Formulation (5.4) to construct the objective function for the DEAOpt:

$$F_S(w_j) = F_N(w_j) + \frac{1}{N_B}\sum_{j=1}^{N_B} \theta_j w_j^2. \tag{5.8}$$

In this paper, the DoseOpt, LETOpt, and DEAOpt models were solved by the interior-point optimizer package IPOPT [119]. which is a free software package for large-scale nonlinear optimization problems.

5.2.2 Patient data and treatment planning

Table 5.1: Patient information and treatment planning parameters.

Tumor location	**Prescription dose (Gy/fx)**	**Number of fractions**	**Beam angles (gantry, couch)**	**Number of beamlets**	**Volumes included in optimization**
1. Brain	1.8 (CTV)	30	(260, 0)	1813	CTV, PTV, brainstem,
			(100, 0)	1829	optic chiasm, spinal cord, brain
			(180, 0)	1826	
2. Brain	1.8 (CTV)	30	(265, 90)	1417	CTV, PTV, brainstem,
			(260, 0)	1388	optic chiasm, spinal cord, brain
			(100, 0)	1410	
			(180, 0)	1335	
3. H&N	2.0 (CTV)	33	(180, 0)	2505	CTV, parotid, larynx, spinal cord, mandible, cochlea, brainstem, esophagus
			(65, 345)	2800	
			(300, 20)	2580	
4. H&N	2.0 (CTV)	33	(300, 15)	4123	CTV, parotid, larynx, spinal cord, mandible, cochlea, brainstem, esophagus
			(60, 345)	4217	
			(180, 0)	4114	

Abbreviations: CTV, clinical target volume; PTV, planning target volume; H&N, head and neck.

We implemented the proposed DEAOpt method, the conventional DoseOpt method, and the LETOpt method in four clinical cases retrospectively selected from our patient database: two patients with brain cancer and two with head-and-neck (H&N) cancer. For brain tumor patients, a prescribed dose of 1.8 Gy (RBE = 1.1) per fraction to the target volumes was planned in 30 fractions. The prescription dose of 2.0 Gy (RBE = 1.1) per fraction to the target volumes was applied for H&N cancer

patients in 33 fractions. To simplify the problem, the doses prescribed to OARs were set to 0 in the optimizations. For all patients, beam angles were the same as those used in the clinical treatment. Although the target volume and location varied among the patient cases, at least one critical structure was close to or overlapped with the clinical target volumes (CTVs) or the planning target volumes (PTVs) in each case. More planning details are listed in Table 1.

5.2.3 Plan evaluation

To evaluate the quality of the treatment plans generated by the three optimization methods, fixed RBE (1.1)-weighted dose-volume histograms (DVHs) and c LETxD-volume histograms were calculated and displayed. The $D_{98\%}$ and $D_{2\%}$ of the DVHs in the targets were used to reflect the dose coverage and homogeneity, meanwhile, the $D_{2\%}$ and D_{mean} of the DVHs in the OARs were used to assess the risk of exposure. To measure the improvement in the tumor volume coverage and protection of the OARs due to the biological effect, c $LETxD_{98\%}$, c $LETxD_{2\%}$, and c $LETxD_{mean}$ of the LVHs were compared. All the plans were normalized to have 98% of the CTV covered by the prescribed dose. In this study, $D_{v\%} = d$ means the dose level *d*, for a given *v%* volume of a structure, receives a dose of *d* Gy or higher.

5.3 Results

Figure 5.2 shows the dose-, LETd-, and c LETxD-volume histograms of the CTV and brainstem for the IMPT plans optimized by DoseOpt, LETOpt, and DEAOpt in the brain tumor cases. The doses in the CTV and brainstem generated by the three

approaches were comparable. For case 1, the $D_{2\%}$ in the CTV was 56.67 Gy for the DoseOpt plan, 56.71 Gy for the LETOpt plan, and 56.72 Gy for the DEAOpt plan. The $D_{2\%}$ in the brainstem was 56.95 Gy for the DoseOpt plan, 56.73 Gy for the LETOpt plan, and 56.75 Gy for the DEAOpt plan. The mean dose in the brainstem was 23.80 Gy, 23.44 Gy, and 23.77 Gy for the DoseOpt, LETOpt, and DEAOpt plans, respectively (Table 5.2).

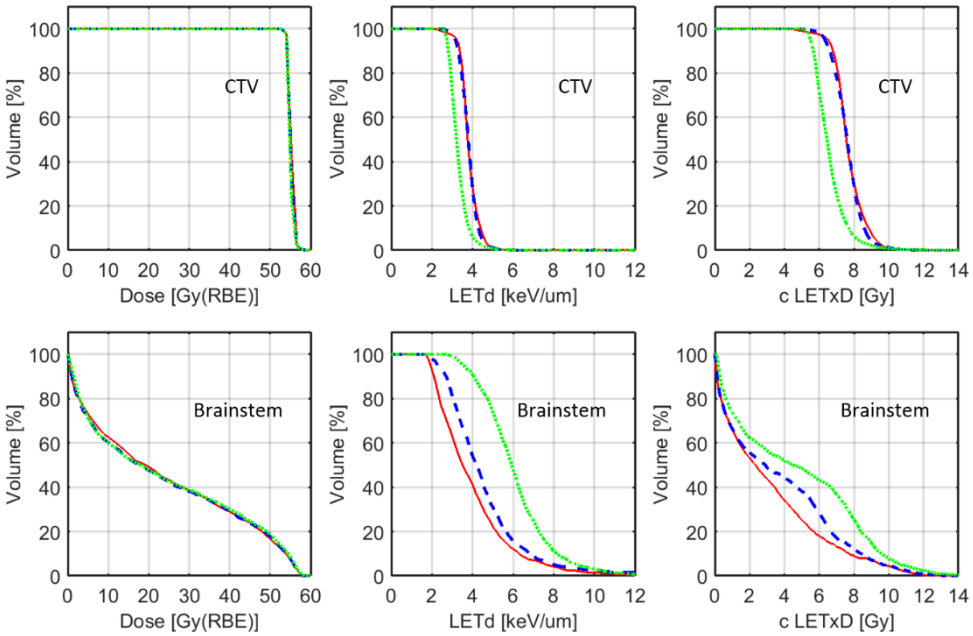

Figure 5.2: Dose-volume histograms (first column), dose-averaged LET (LETd)-volume histograms (second column), and scaled LET-weighted dose (c LETxD)-volume histograms (third column) of the clinical target volume (CTV; top row) and the brainstem (bottom row) for three intensity-modulated proton therapy plans in brain tumor patient case 1. DoseOpt plan (green line), LETOpt plan (blue dashed line), and DEAOpt plan (red line).

Table 5.2: Dose and linear energy transfer (LET)-weighted dose (LETxD; scaled by c = 0.04 μm keV−1) values in the clinical target volume (CTV) and the brainstem for two brain tumor cases optimized by DoseOpt, LETOpt, and DEAOpt approaches.

Tissue	**Dosimetric parameters**	**Brain tumor case 1**			**Brain tumor case 2**		
		DoseOpt	LETOpt	DEAOpt	DoseOpt	LETOpt	DEAOpt
CTV	$D_{98\%}$ (Gy[RBE])	54.00	54.00	54.00	54.00	54.00	54.00
	$D_{2\%}$ (Gy[RBE])	56.67	56.71	56.72	55.24	55.65	55.76
	c $LETxD_{98\%}$ (Gy)	5.36	6.08	5.63	4.97	5.94	5.33
	c $LETxD_{2\%}$ (Gy)	9.06	9.59	9.63	7.30	7.75	8.79
Brainstem	$D_{2\%}$ (Gy[RBE])	56.95	56.73	56.75	56.54	56.73	57.97
	D_{mean} (Gy[RBE])	23.80	23.44	23.77	36.42	36.83	35.57
	c $LETxD_{2\%}$ (Gy)	12.31	11.22	10.99	9.66	7.53	8.51
	c $LETxD_{mean}$ (Gy)	4.76	3.70	3.19	5.21	3.27	3.45
Calculation Time (s)		176.86	300.48	202.34	394.96	774.40	563.92

Abbreviations: RBE, relative biological effectiveness.

In terms of biological effect, both LETOpt and DEAOpt improved the LETd in the CTV and spared it in the brainstem. Since the dose distributions in the target and critical structures were similar for all three methods, the biological effect distributions had the same character as the LETd distributions. The c $LETxD_{98\%}$ in the CTV was 5.36 Gy for the DoseOpt plan, smaller than the 6.08 Gy for the LETOpt plan and 5.63 Gy for the DEAOpt plan. The c $LETxD_{2\%}$ in the CTV was 9.06 Gy for the DoseOpt plan, compared to 9.59 Gy and 9.63 Gy for the LETOpt plan and the DEAOpt plan, respectively. For the brainstem, the c $LETxD_{2\%}$ was 12.31 Gy for the DoseOpt plan, 11.22 Gy for the LETOpt plan, and 10.99 Gy for the DEAOpt plan. The mean value of

c LETxD was 4.76 Gy for the DoseOpt plan, higher than the 3.70 Gy for the LETOpt plan and 3.19 Gy for the DEAOpt plan (Table 5.2).

Table 5.3: Dose and linear energy transfer(LET)-weighted dose (LETxD; scaled by c = 0.04 μm keV−1) values in the clinical target volume (CTV) and the organs at risk (OARs) for two head and neck (H&N) tumor cases optimized by DoseOpt, LETOpt, and DEAOpt approaches.

Tissue	**Dosimetric parameters**	**H&N tumor case 1**			**H&N tumor case 2**		
		DoseOpt	LETOpt	DEAOpt	DoseOpt	LETOpt	DEAOpt
CTV	$D_{98\%}$ (Gy[RBE])	66.00	66.00	66.00	66.00	66.00	66.00
	$D_{2\%}$ (Gy[RBE])	68.39	68.55	68.64	68.36	68.71	69.09
	c LETx$D_{98\%}$ (Gy)	7.12	7.11	7.17	5.72	6.07	6.28
	c LETx$D_{2\%}$ (Gy)	11.66	12.11	12.52	8.78	9.40	9.91
Larynx	$D_{2\%}$ (Gy[RBE])	53.13	52.90	53.43	66.45	66.69	66.72
	D_{mean} (Gy[RBE])	5.37	5.12	5.11	10.84	10.92	11.12
	c LETx$D_{2\%}$ (Gy)	7.13	6.54	6.49	9.90	8.39	8.36
	c LETxD_{mean} (Gy)	0.96	0.81	0.78	1.76	1.38	1.25
Right parotid	$D_{2\%}$ (Gy[RBE])	67.21	67.16	67.22	71.09	71.85	72.27
	D_{mean} (Gy[RBE])	6.74	6.67	7.06	17.90	17.99	18.34
	c LETx$D_{2\%}$ (Gy)	8.38	8.26	8.56	10.94	10.93	10.63
	c LETxD_{mean} (Gy)	0.81	0.81	0.80	2.43	2.39	2.12
Left parotid	$D_{2\%}$ (Gy[RBE])	10.01	9.57	9.29	0.14	0.13	0.07
	D_{mean} (Gy[RBE])	0.77	0.70	0.67	0.02	0.02	0.02
	c LETx$D_{2\%}$ (Gy)	0.93	0.76	0.63	0.01	0.01	0.01
	c LETxD_{mean} (Gy)	0.07	0.06	0.05	0.01	0.01	0.00
Calculation Time (s)		357.34	600.75	402.73	581.58	1044.14	746.23

Abbreviation: RBE, relative biological effectiveness.

The results for brain tumor patient case 2 are shown in Figure 5.3 and Table 5.2. The differences in dose and c LETxD distributions among the three IMPT plans were similar for the two brain tumor cases.

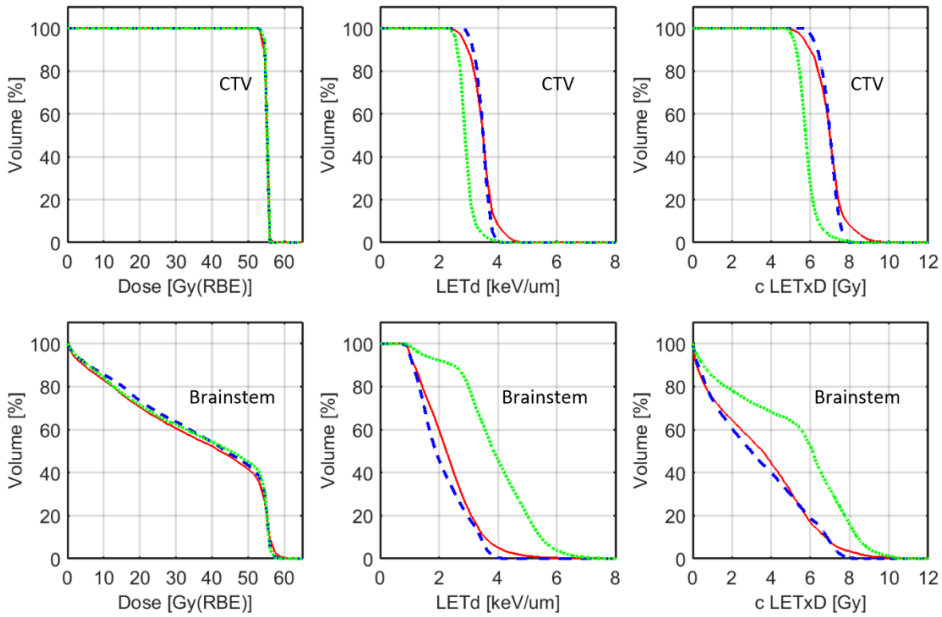

Figure 5.3: Dose-volume histograms (first column), dose-averaged LET (LETd)-volume histograms (second column), and scaled LET-weighted dose (c LETxD)-volume histograms (third column) of the clinical target volume (CTV; top row) and the brainstem (bottom row) for three intensity-modulated proton therapy.

The improvement in the target coverage and reduction of c LETxD to the critical structures with the LETOpt and DEAOpt plans for the H&N cancer cases was modestly lower than for the brain tumor cases, as illustrated in Figure 5.4, 5.5, and Table 5.3. Compared with DoseOpt plans, the DEAOpt plans reduced the mean value of c LETxD by an average of 23.87% in the larynx for the H&N cancer cases and by an average of 33.38% in the brainstem for the brain tumor cases. Meanwhile, the DEAOpt plans increased the c $LETxD_{98\%}$ by 5.25% and the c $LETxD_{2\%}$ by 10.13% on average in the CTV for the H&N cancer cases, lower than the average increment rate

of 7.24% for the c LETx$D_{98\%}$ and 13.35% for the c LETx$D_{2\%}$ in the brain tumor cases. Thus, the DEAOpt plans improved the biological effect to the same degree as the LETOpt plans in both types of cases. However, the plans were not exactly the same. For example, the LETOpt plan increased the c LETx$D_{2\%}$ in the CTV to 7.75 Gy, while the DEAOpt plan increased it to 8.79 Gy in brain tumor case 2. In this case, the LETOpt plan achieved a c LETx$D_{98\%}$ value of 5.94 Gy in the CTV, higher than the 5.33 Gy for the DEAOpt plan.

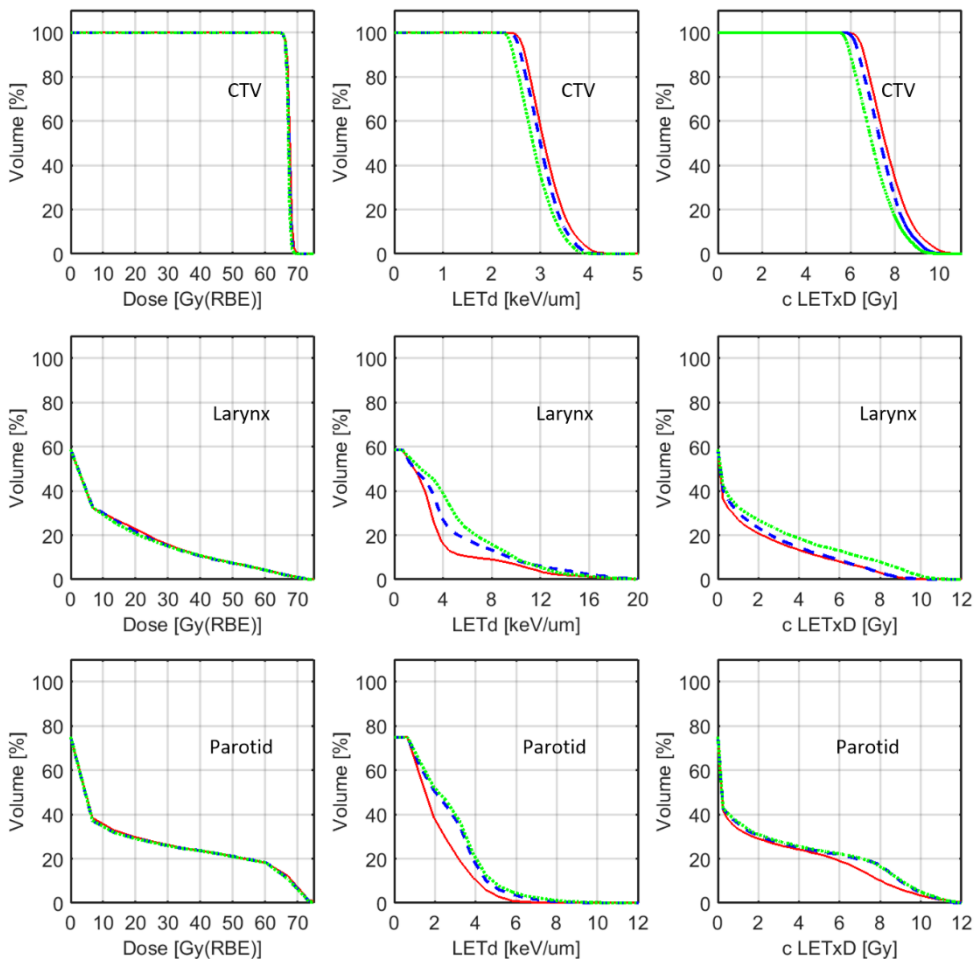

Figure 5.4: Dose-volume histograms (first column), dose-averaged LET (LETd)-volume histograms (second column), and scaled LET-weighted dose (c LETxD)-volume histograms (third column) of the clinical target volume

(CTV; top row) and parotid glands (bottom row) for three intensity-modulated proton therapy plans in head and neck cancer patient case 2:.DoseOpt plan (green line), LETOpt plan (blue dashed line), and DEAOpt plan (red line).

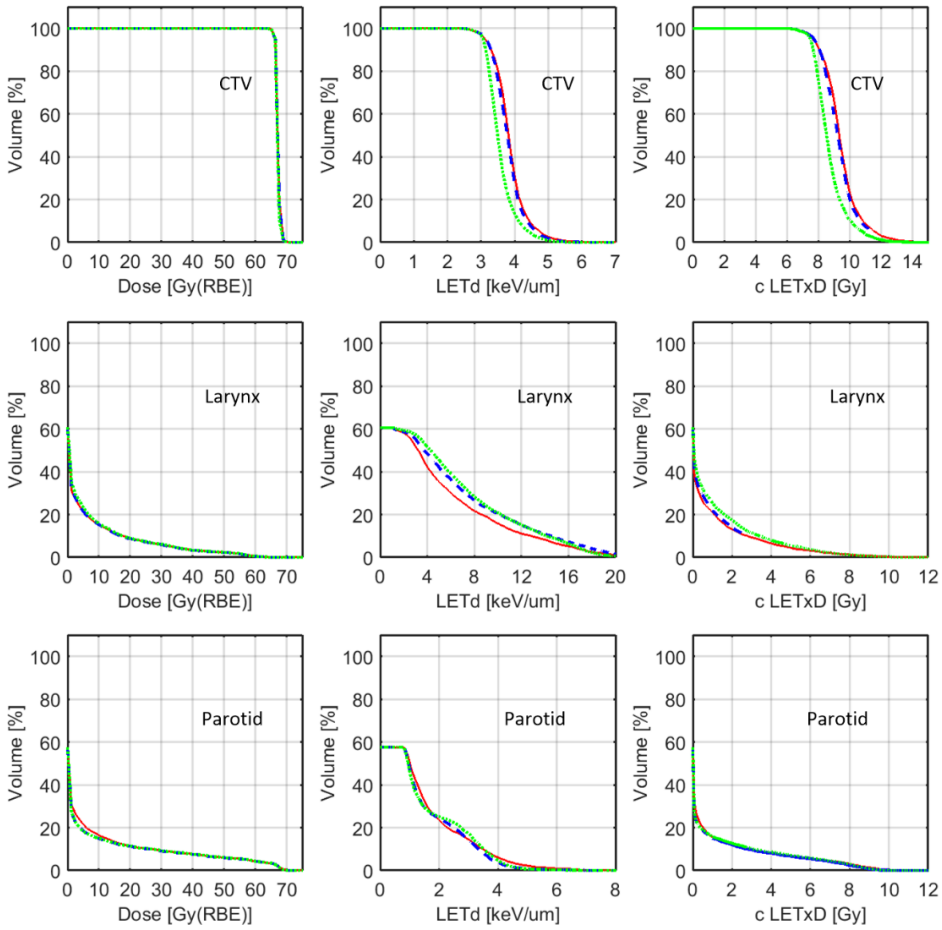

Figure 5.5: Dose-volume histograms (first column), dose-averaged LET (LETd)-volume histograms (second column), and scaled LET-weighted dose (c LETxD)-volume histograms (third column) of the clinical target volume (CTV; top row) and the organs at risk (larynx, middle row; parotid gland, bottom row) for three intensity-modulated proton therapy plans in head and neck tumor patient case 1. DoseOpt plan (green line), LETOpt plan (blue dashed line), and DEAOpt plan (red line).

Figure 5.6 shows the dose and biological effect distributions for brain tumor case 1. For physical dose, there was no difference among the three plans. Both the DEAOpt plan and LETOpt plan avoided the hot spots of c LETxD in the overlap area of the

brainstem and the target. Comparison with the DoseOpt plan also shows that c LETxD in the target improved for both DEAOpt and LETOpt plans. However, it is noteworthy that the DEAOpt plan restricted the high biological effect inside the target border more effectively than did the LETOpt plan, which caused the normal tissue adjacent to the target to receive a lower biological effect.

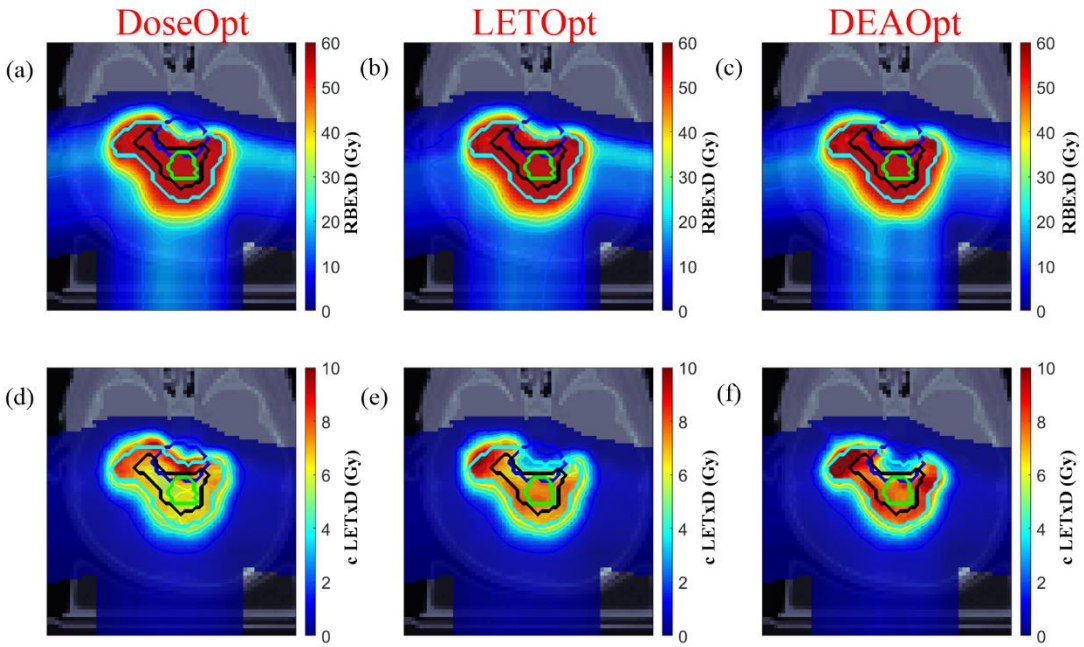

Figure 5. 6: Plan comparison for the brain tumor patient case 1. The top row shows the dose distributions (based on a constant RBE of 1.1). The bottom row shows the distributions of LET-weighted dose scaled by c = 0.04 μm keV−1 (c LETxD). The gross target volume, clinical target volume, planning target volume, and brainstem are contoured by green, black, cyan, and blue, respectively.

5.4 Discussion

Current LET-based optimization methods [20], [28], [30], [31], [88], [112] use LET as a surrogate for RBE optimization [20], [31] because of the considerable uncertainties in the validity of RBE models and the almost linear relationship between

LET and RBE [16]. In addition, the high degree of freedom of the IMPT plan makes it feasible to produce satisfactory dose distributions while achieving desirable LET distributions [28]. However, a drawback to the existing methods is that they use the inverse planning approach to optimize the LET distribution, which adds extra complexity [117]. To overcome this challenge, our method includes a regularization term for each scanning spot to reduce the complexity of the first and second derivatives. The runtime of the DEAOpt was, on average, 30.37% faster than that of LETOpt and 24.52% slower than that of DoseOpt (Table 5.2 and Table 5.3). The boost of computing time did not sacrifice plan quality; the DEAOpt plan's biological effect and physical dose distributions were comparable with those of the LETOpt plan.

In proton beams, LET continues to increase beyond the Bragg peak. We classified the scanning spots into four categories according to the topological relationship between their peak LETxD positions and different organs of interest (Figure 5.1). In Situation A, the peak LETxD position falls into the OAR area and outside the target region, meaning that the dose intensity in this scanning spot may aggravate toxicities in critical structures. Of course, this scanning spot also contributes to the dose in the border of the target, but it can be replaced by other scanning spots from different beams. In Situation B, where the peak LETxD position is in the overlap area of the target and OARs, the priority of treatment planning decides the penalty set. For example, if the first priority is to kill the tumor cells, we allow for a high biological effect in this area, which makes the penalty in this scanning spot close to 0; if protecting critical structures is the priority, a high penalty should be assigned to this scanning spot to restrain the biological effect in this area. For other situations, the peak

LETxD position's radius may cover the edge of OARs or the target. When the irradiated region overlaps with the target, the corresponding scanning spot will guarantee the homogeneity and coverage of the physical dose in the tumor. Sometimes, when the overlap is with OARs, we should limit the intensity in this scanning spot. If the peak LETxD position is far away from all OARs, a high penalty should be set for this scanning spot to protect healthy tissues and promote the biological effect in the target.

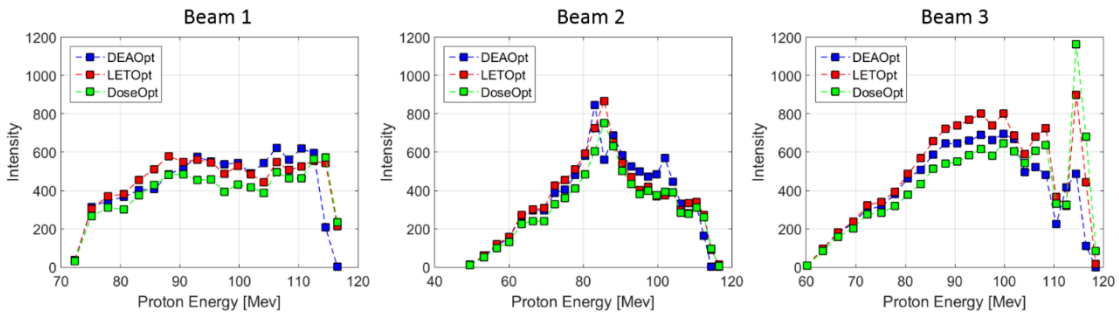

Figure 5. 7: Comparisons of the intensity in each proton energy layer for three beams with the DEAOpt plan, LETOpt plan, and DoseOpt plan in head and neck tumor case 2.

Regardless of the optimization approach used to optimize the physical dose and LET, the objective is achieved mostly by shifting LET hot spots to other regions nearby or inside the target [20]. Conventional treatment planning usually places the Bragg peaks at the distal edge of the target to maintain the dose coverage, which inevitably causes the region of high LET to be located in the periphery of the target. To keep protons stopping within the target region, the location of the scanning spot at the distal edge of the target should be avoided. This would protect the normal tissue adjacent to the target from the risk of side effects associated with high LET. As shown in Figure 5.7, the DEAOpt plan deposits lower intensity at the last two proton energies

in each beam than do the LETOpt and DoseOpt plans. These two energy layers have the potential to release LET outside of the target. Nonetheless, there was no substantial difference in total intensity among the three plans, and their dose distributions were similar because the high degree of freedom of IMPT enables it to replenish each voxel with physical dose from multiple scanning spot combinations.

Our research confirmed that biological effect optimization can be achieved by optimizing the location of scanning spots directly instead of using the inverse optimization method. The effectiveness of DEAOpt is highly dependent on the geometry of structures and the spot arrangement. As shown in Figure 5.7, our method tends to avoid spots in the beam distal edge because of the trade-off effect between dose and LET. In our H&N cancer cases, DEAOpt methods made a smaller difference than in our brain tumor cases because more OARs need to be protected during the irradiation of H&N tumors. This phenomenon was also observed with the LETOpt plans.

5.5 Conclusion

In this study, we proposed and developed a distal-edge avoidance-guided optimization method to optimize IMPT plans in terms of their c LETxD distributions without degrading the physical dose distributions, which are comparable to those of LET optimization plans. We used an influence index to quantify the contribution of the biological effect from each scanning spot on the basis of its topological relationship to different organs of interest. This method could be especially beneficial for patient cases where critical structures are adjacent to the target area. In addition,

the DEAOpt approach is less complex computationally and therefore faster than the LETOpt approach.

Chapter 6

Biological Effect Incorporated Beam Angle Optimization for Intensity-Modulated Proton Therapy

6.1 Introduction

Design a treatment plan of intensity modulated proton therapy (IMPT) requires to optimize four parameters/variable: first, beam angles selection; second, proton energy level selection; third, optimization of scanning spot intensity, which is mentioned as fluence map optimization (FMO) in chapter 2; finally, spot size, spot space and scanning path. However, for most commercial treatment planning system, the proton energy level and scanning path are decided by the machine used for treatment. Spot size and spot space are consistant with the grid size, and there are not many options. In clinical practice, the FMO is based on the beam angles selected by the doctor or physicist according to their experience and patient cancer sites in clinical practice. Although initial studies have illustrated BAOpt for particle therapy treatment planning can significantly improve the plan quality [61], BAO methods incorporated biological effect has not yet been explored.

The goal of this study is to investigate the impact of BAOpt on the biological effect of IMPT. BAO in IMPT has much high freedom than FMO because the evaluation of each beam angle combination requires to fully solve an FMO model. Thus, it is feasible for BAO to generate a biological effect advanced treatment plan compared to biological effect-guided optimization in IMPT.

6.2 Method and Materials

The total dose D_i, dose-averaged LET (LETd) L_i, and LET-weighted dose (LETxD) LD_i deliverd to the voxel i in beam angle optimization problem are formulated by:

$$D_i = \sum_a^{\mathrm{A}} \sum_j^{N_a} D_{iaj} w_{aj}^2, \tag{6.1}$$

$$L_i = \frac{\sum_a^{\mathrm{A}} \sum_j^{N_a} D_{iaj} L_{iaj} w_{aj}^2}{\sum_a^{\mathrm{N}} \sum_j^{N_a} D_{iaj} w_{aj}^2}, \tag{6.2}$$

and

$$LD_i = \sum_a^{\mathrm{A}} \sum_j^{N_a} D_{iaj} L_{iaj} w_{aj}^2, \tag{6.3}$$

respectively, where D_{iaj} and L_{iaj} denote the dose and LET contributions to voxel i from the beamlet j in beam angle a at the unit weight. w_{aj}^2 is defined as the intensity of the beamlet j in the beam angle a and N_a is defined as the beamlet set for the beam angle a while the beam angle set is A. Here we use the square of w_{aj} instead of w_{aj} itself to represent the intensity because the quadratic formation decision variable can preserve the nonnegativity.

The dose and LET calculations in this study were performed with an open-source treatment planning platform, matRad [95], using a singular-value decomposed pencil-beam algorithm [96].

6.2.1 Beam angle optimization model (BAO)

For conventional dose-based optimization model (DoseOpt), a quadratic objective function is used to measure the treatment plan qualty under a given beam

angle set $A^b (A^b \subseteq A)$. The penalty factors, λ_T and λ_{OAR}, and prescription dose, $D_{0,T}$ and $D_{0,OAR}$, are applied to the target and critical structures, respectively. The priority of penalty factors can be used to control the balance between target coverage and critical structure sparing. The objective function is fomulated as below:

$$F_D(\mathrm{A}^b, w_{aj}) = \lambda_T \frac{1}{N_T} \sum_{i=1}^{N_T} (D_i - D_{0,T})^2 + \lambda_{OAR} \frac{1}{N_{OAR}} \sum_{i=1}^{N_{OAR}} H(D_i - D_{0,OAR}) \times (D_i - D_{0,OAR})^2, \tag{6.4}$$

where N_T and N_{OAR} are the sets of voxels in target volumes and OARs. The Heaviside function, denoted by $H(D_i - D_{0,OAR})$, is a discontinuous function whose value is zero if $D_i \leq D_{0,OAR}$ and one if $D_i > D_{0,OAR}$.

If all possible continuous beam angle combinations are considered for the treatment plan, the above DoseOpt model (Formulation 6.4) becomes a BAO model. Let n be defined apriori by the treatment planner as the required number of beam irradiation directions for a treatment plan, and N be defined as the total number of candidate beam angles. The BAO model can be given by:

$$\min_{A^b, w_{aj}} \{F_D(A^1, w_{aj}), F_D(A^2, w_{aj}), F_D(A^3, w_{aj}), \dots, F_D\left(A^{\binom{N}{n}}, w_{aj}\right)\},$$
$$s.t.\ (A^1, A^2, A^3, \dots, A^{\binom{N}{n}}) \in R^n. \tag{6.5}$$

6.2.2 LET- incorporated beam angle optimization model (LETBAO)

As introduced by chapter 3, the LET-incorporated optimization (LETOpt) model can be formulated by adding two terms for maximizing dose-averaged LET (LETd) in the target and minimizing it in OARs to DoseOpt model:

$$F_L(A^b, w_{aj}) = F_D(A^b, w_{aj}) - p_{T,l}\frac{1}{N_T}\sum_{i=1}^{N_T} {L_i}^2 + p_{OAR,l}\frac{1}{N_{OAR}}\sum_{i=1}^{N_{ORA}} {L_i}^2. \quad (6.6)$$

Because the LET component in the above cost function is a ratio of two linear questions, we use LET-weighted dose (LETxD) to replce the dose-average LET (LETd) to simply the question [20], [28]. The new LETBAO model can be formed as:

$$F_L(A^b, w_{aj}) = F_D(A^b, w_{aj}) - p_{T,l}\frac{1}{N_T}\sum_{i=1}^{N_T} {LD_i}^2 + p_{OAR,l}\frac{1}{N_{OAR}}\sum_{i=1}^{N_{ORA}} {LD_i}^2. \quad (6.7)$$

Use LETOpt model to evaluate the quality of the treatment plan, we can build the LETBAO model as below:

$$\min_{A^b, w_{aj}} \{F_L(A^1, w_{aj}), F_L(A^2, w_{aj}), F_L(A^3, w_{aj}), \dots, F_L\left(A^{\binom{N}{n}}, w_{aj}\right)\},$$

$$s.t.\ (A^1, A^2, A^3, \dots, A^{\binom{N}{n}}) \in R^n. \quad (6.8)$$

6.2.3 Local neighborhood search algorithm

Solving the BAO and LETBAO models can be computationally challenging when there are a large number of candidate beam angles. In this study, we introduced a local neighborhood search (LNS) algorithm to find a local optimal solution subject to the neighborhood for a given initial feasible solution.

The neighborhood of a beam angle set can be obtained by altering one or more angles of the set with a neighbor of the corresponding angles. However, allowing more angles to be exchanged at one time can introduce additional complexity to the problem due to the increased neighborhood size [48]. Thus, a one-angle-exchange algorithm [120], which only swaps one angle of the current set with another angle that is not in the set, was applied to this research to construct the neighborhood of the beam angle

set. Given an initial beam angle set $\bar{A}$, where $\bar{A} \subseteq A$, $|\bar{A}| = n$, the neighborhood of $\bar{A}$ can be defined as below:

$$N(\bar{A}) = \{\bar{A}' : \bar{A}' = (\bar{A} \cup \{a_v\}) \backslash \{a_\mu\}, \text{ for } a_v \in \Theta(a_\mu), a_\mu \in \bar{A}\}, \tag{6.9}$$

where the neighborhood of a fixed beam angle a_μ is defined as follow:

$$\Theta(a_\mu) = \{a'_\mu : a'_\mu = [a_\mu - \theta, a_\mu + \theta], \text{for } a_\mu \in A \; and \; a_\mu \notin \bar{A}\} \; mod \; 360^o. \tag{6.10}$$

We take modular arithmetic with 360 to keep the beam angle non-negative. θ is the user-defined parameter that decides the size of the neighborhood region. For example, if the solution pool $A = \{0, 10, 20, \ldots 350\}$ and $\theta = 30$, the neighbors of beam angle 10 are located within its proximal region $[10 - 30, 10 + 30] mod \; 360$, and $\Theta(10) = \{340, 350, 0, 20, 30, 40\}$. The size of the neighborhood set $N(\bar{A})$ is determined by θ. The size of the neighborhood set $N(\bar{A})$ is determined by θ. The process of LNS algorithm is explained as follows:

Local Neighborhood Search Algorithm

```
0. Start;
1. Set k = 0, A^0 ∈ [0,360]^n, obj = f(A^0), lib = 0;
2. do{
      (a). Generate neighborhood N(A^k)_i, i = 1, 2,3 ..... |N(A^k)|;
      (b). for i =1:1: |N(A^k)|
                  if (N(A^k)_i ∉ lib)
                        if(f(N(A^k)_i) < obj)
                              obj = f(N(A^k)_i);
                              A^{k+1} = N(A^k)_i;
                     end
                        lib = [lib, N(A^k)_i];
               end
            end
      (c). obj = f(A^{k+1});
      (d). k = k + 1;
    } while (f(A^{k-1}) > f(A^k))
3. Stop. The final local optimizal solution is A* = A^{k-1}.
```

The starting solution A^0 to the LNS algorithm can be any set of angles. Usually, a set of equally spaced beam angles is the simplest choice. Beyond that, a beam angles set selected by the doctor or heuristic model will be more effective [48].

6.2.4 Patient data and treatment planning

Four IMPT plans were generated to illustrate the DoseOpt, BAO, LETOpt and LETBAO methods for one phantom case (AAPM,TG119, C-shape) [121], and two brain tumor cases selected from our patient database. For all the cases, 36 equispaced coplanar beam angles were considered as candidate beam angles for selecting a constant number of optimal treatment angles. For the phantom case, a prescribed dose of 2 Gy (RBE = 1.1) per fraction to the target volumes was planned in 25 fractions. The prescription dose of 1.8 Gy (RBE = 1.1) per fraction to the target volumes was

applied for brain cancer patients in 30 fractions. The doses prescribed to all OARs were set to 0 in the optimizations. More planning details are listed in Table 6.1.

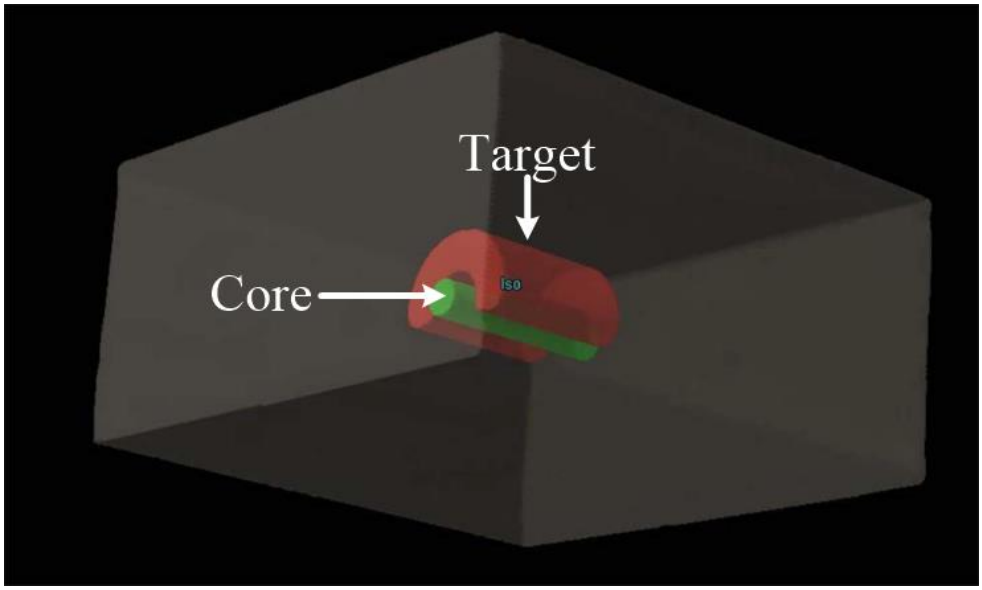

Figure 6.1: Geometry of the phantom case (AAPM,TG119, C-shape)

Table 6.1: Patients information and treatment planning parameters.

Cancer Type	Prescription dose (Gy/fx)	Number of fractions	Tissue Type	Number of voxels
Phantom (TG 119)	2 (Target)	25	Target	7429
			Core	1280
			Body	599440
Brain case 1	1.8 (CTV)	30	CTV	4332
			PTV	7440
			Brainstem	2304
			Optic Chiasm	56
Brain case 2	1.8 (CTV)	30	CTV	4308
			PTV	8729
			Brainstem	1047
			Optic Chiasm	49

Abbreviations: CTV, clinical target volume; PTV, planning target volume.

6.3 Results

For the brain tumor patients, three-beam plans were optimized based on the angles used in the clinical treatment. And the two-beam plan was applied to BAO and LETBAO optimization in the phantom case. Here we only consider the gantry angles and set all the couch angles to 0. Beam angles sets (92, 270), (95, 180, 265) ,and(100, 180, 260) were used for the DoseOpt and LETOpt treatment planning, and initial solution of BAO and LETBAO, respectively. Note that all treatment plans were normalized to have 98% of the tartget or CTV covered by the prescribed dose.

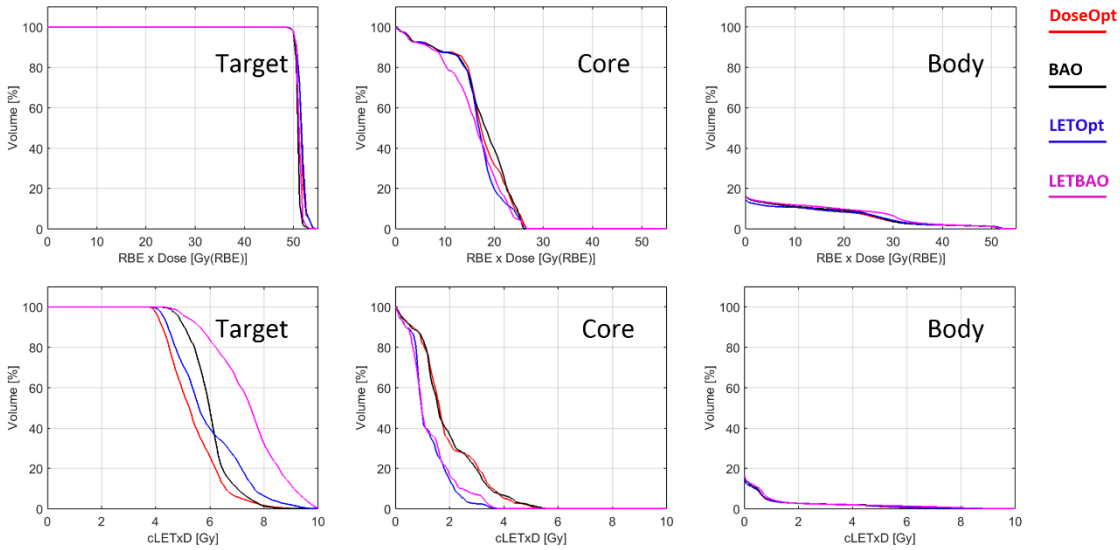

Figure 6.2: Dose-volume histograms (first row) and scaled LET-weighted dose (c LETxD)-volume histograms (second row) of the target volume and the core (critical structure) for the phantom case TG 119.

Figure 6.2 compares dose and scaled LETxD volume histograms for the target and core for the plans with DoseOpt, BAO, LETOpt, and LETBAO in the phantom case. The doses in the target and core generated by the four methods were comparable, and the BAO method shows a slight adavantage in target homogeneity. The $D_{2\%}$ in the

target was 51.87 Gy for the BAO plan, which is lower than 53.59 Gy for the DoseOpt plan, 53.66 Gy for the LETOpt plan, and 53.32 Gy for the LETBAO plan. The mean dose in the core was 17.17 Gy, 17.39 Gy, 16.33 Gy, and 15.69 Gy for the DoseOpt, BAO, LETOpt and LETBAO plans, respectively (Table 6.2).

Table 6.2: Dose and linear energy transfer (LET)-weighted dose (LETxD; scaled by c = 0.04 μm keV−1) values in the target volume and the core for phantom case TG119 optimized by DoseOpt, BAO, LETOpt, and LETBAO approaches.

Tissue Type	**Dosimetric parameters**	**Phantom (TG 119)**			
		DoseOpt	**BAO**	**LETOpt**	**LETBAO**
Target	$D_{98\%}$ (Gy[RBE])	50.00	50.00	50.00	50.00
	$D_{2\%}$ (Gy[RBE])	53.59	51.87	53.66	53.32
	c $LETxD_{98\%}$ (Gy)	3.96	4.61	4.15	4.84
	c $LETxD_{2\%}$ (Gy)	7.86	7.88	8.96	9.77
Core	$D_{2\%}$ (Gy[RBE])	26.04	25.52	25.93	25.96
	D_{mean} (Gy[RBE])	17.17	17.39	16.34	15.69
	c $LETxD_{2\%}$ (Gy)	4.85	4.92	3.27	3.46
	c $LETxD_{mean}$ (Gy)	1.91	1.90	1.18	1.21
Beam Angles		(90, 270)	(100, 260)	(90, 270)	(80,260)

For the biological effect, both LETOpt and LETBAO approaches can improve the c LETxD in the target and spared it in the core compared to DoseOpt and BAO approaches. And LETBAO method achieves the best results. The c $LETxD_{98\%}$ in the target was 4.84 Gy for the LETBAO plan, 22% higher than the 3.96 Gy for the DoseOpt plan, 5% higher than the 5.63 Gy for the BAO plan, and 17% higher than the 4.15 Gy for the LETOpt plan. The c $LETxD_{2\%}$ in the target was 9.77 Gy for the LETBAO plan, which is 24%, 24%, 7% higher than the DoseOpt, BAO, and LETOpt plans, respectively. The mean value of c LETxD in the core was 1.21 Gy for the BAO

plan, 1.91 Gy for the DoseOpt plan, 1.90 Gy for the BAO plan and 1.18 Gy for the LETOpt plan (Table 6.2). The dose and biological effect distributions for the four plans are illustrated in Figure 6.3. The biological effect (c LETxD) distribution in the target area for the LETBAO plan is significantly higher than the other three plans.

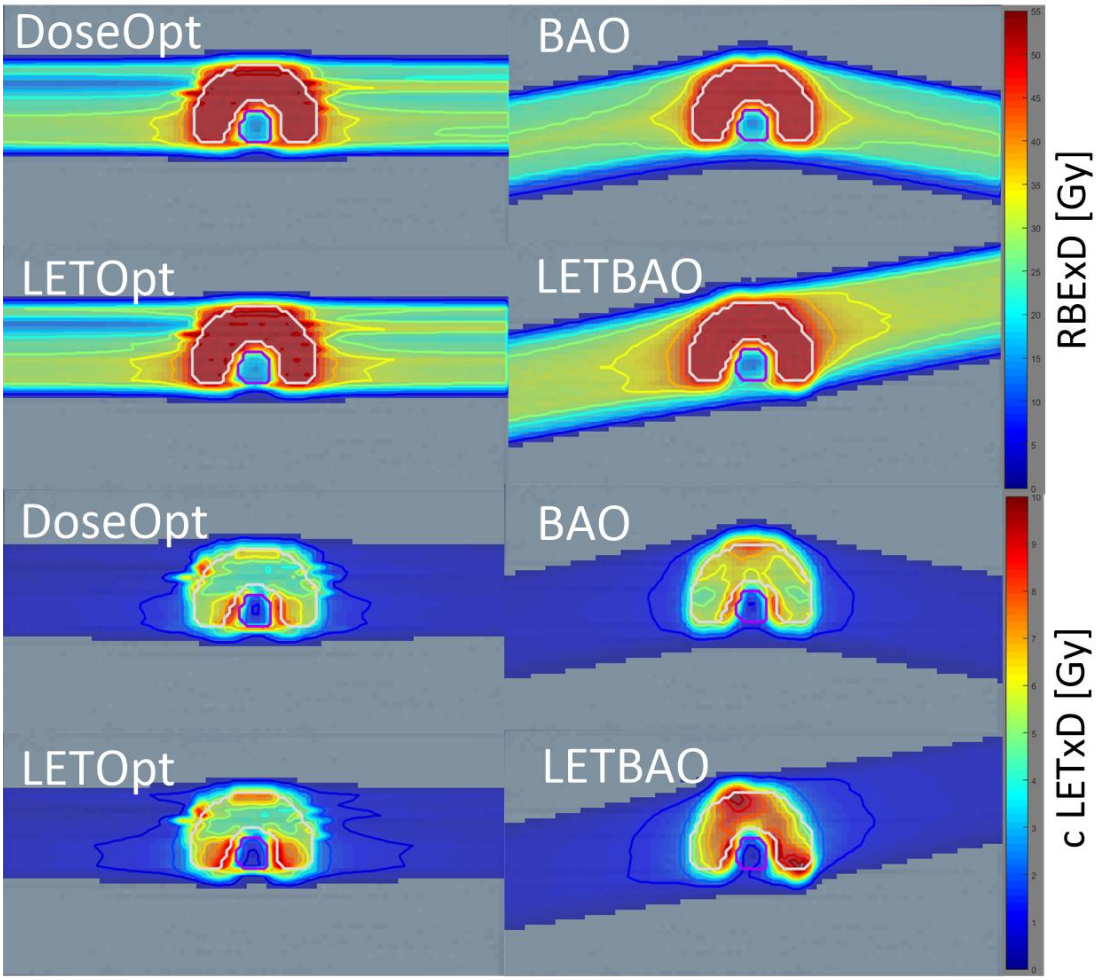

Figure 6.3: Plan comparison for the phantom case. The top two rows show the dose distributions (based on a constant RBE of 1.1). The bottom two rows show the distributions of LET-weighted dose scaled by c = 0.04 μm keV−1 (c LETxD). The target volume and core are contoured by the color white and purple.

Table 6.3: Dose and linear energy transfer (LET)-weighted dose (LETxD; scaled by c = 0.04 μm keV−1) values in the CTV and the brainstem for brain tumor case 1 optimized by DoseOpt, BAO, LETOpt, and LETBAO approaches.

Tissue Type	**Dosimetric parameters**	**Brain Case 1**			
		DoseOpt	**BAO**	**LETOpt**	**LETBAO**
CTV	$D_{98\%}$ (Gy[RBE])	54.00	54.00	54.00	54.00
	$D_{2\%}$ (Gy[RBE])	56.70	56.41	56.94	56.98
	c $LETxD_{98\%}$ (Gy)	5.26	4.95	7.14	7.15
	c $LETxD_{2\%}$ (Gy)	9.42	9.37	13.86	15.04
Brainstem	$D_{2\%}$ (Gy[RBE])	56.23	56.15	56.41	56.61
	D_{mean} (Gy[RBE])	18.81	18.38	18.93	19.01
	c $LETxD_{2\%}$ (Gy)	10.89	12.46	10.59	10.65
	c $LETxD_{mean}$ (Gy)	3.50	4.01	3.18	3.04
Beam Angles		(95,180,265)	(105,190,225)	(95,180,265)	(95,160,265)

Table 6.4: Dose and linear energy transfer (LET)-weighted dose (LETxD; scaled by c = 0.04 μm keV−1) values in the CTV and the brainstem for brain tumor case 2 optimized by DoseOpt, BAO, LETOpt, and LETBAO approaches.

Tissue Type	**Dosimetric parameters**	**Brain Case 2**			
		DoseOpt	**BAO**	**LETOpt**	**LETBAO**
CTV	$D_{98\%}$ (Gy[RBE])	54.00	54.00	54.00	54.00
	$D_{2\%}$ (Gy[RBE])	56.97	56.96	57.64	57.65
	c $LETxD_{98\%}$ (Gy)	3.64	3.91	5.16	7.43
	c $LETxD_{2\%}$ (Gy)	8.92	8.89	9.86	11.72
Brainstem	$D_{2\%}$ (Gy[RBE])	57.22	57.21	57.65	57.69
	D_{mean} (Gy[RBE])	24.05	24.05	24.33	24.26
	c $LETxD_{2\%}$ (Gy)	11.87	10.94	9.64	8.65
	c $LETxD_{mean}$ (Gy)	4.78	4.68	2.74	2.96
Beam Angles		(100,180,260)	(90,180,270)	(100,180,270)	(70,180,290)

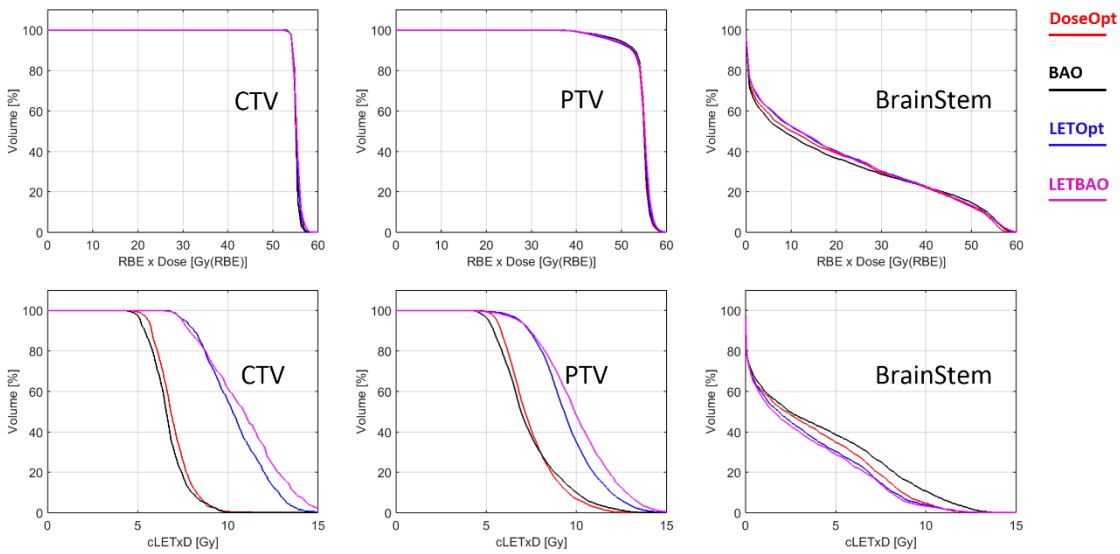

Figure 6.4: Dose-volume histograms (first row) and scaled LET-weighted dose (c LETxD)-volume histograms (second row) of the CTV and the brainstem for the brain tumor case 1.

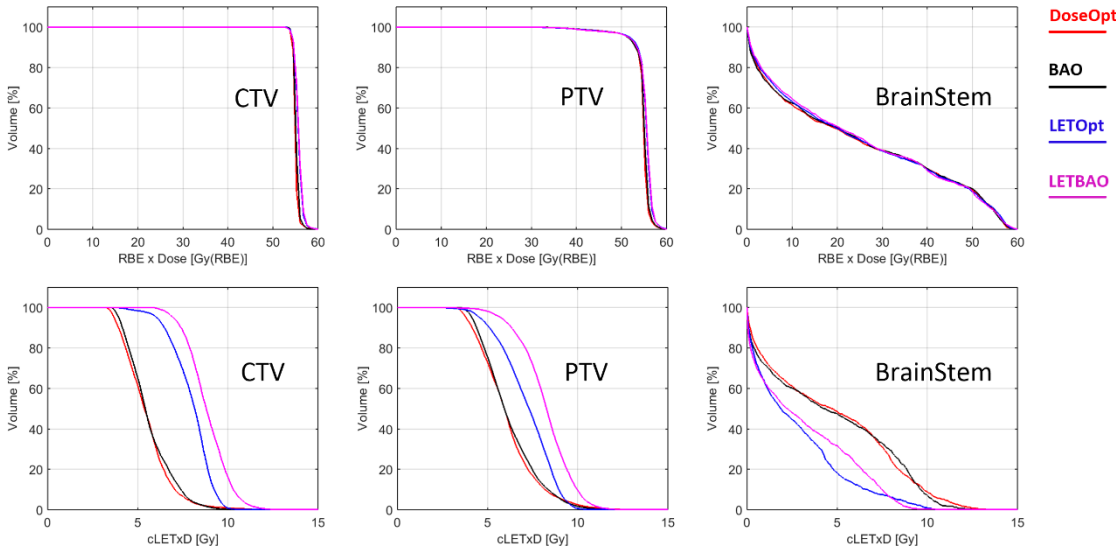

Figure 6.5: Dose-volume histograms (first row) and scaled LET-weighted dose (c LETxD)-volume histograms (second row) of the CTV and the brainstem for the brain tumor case 2.

The DVHs, c LETxD volume histograms and their statistics for the head and neck tumor case are shown in Figure 6.4, 6.5 and Table 6.3, 6.4. The differences in

dose and c LETxD distributions among the four IMPT plans were similar for the two brain tumor cases compare to the phantom case. The LETBAO approach produced plans with higher quality LETxD distribution and machable dose coverage compared to the DoseOpt, LETOpt and BAO methods. For the brain tumor cases, the c $LETxD_{98\%}$ in the CTV was improved by the LETBAO plans on an average of 70%, 67%, 22% compared with the DoseOpt, BAO and LETOpt plans, respectively. The average increase rate of c $LETxD_{2\%}$ by the LETBAO method in CTV was 46% for the DoseOpt method, 46% for the BAO method, and 14% for the LETOpt method. More than that, on average, the LETBAO approach can reduce the c $LETxD_{mean}$ in the brainstem by 51% and 31% for the DoseOpt and BAO approachs. However, LETOpt can reach the same effect in reducing the biological effect in the OARs for the brain tumor cases.

Figure 6.6, 6.7 show the dose and biological effect distributions for brain tumor cases. For physical dose, there was nearly no difference between the four plans. Both the LETOpt plan and the LETBAO plan avoided the hot spots of c LETxD in the overlap area of the brainstem and the target. Comparison with the DoseOpt plan also shows that c LETxD in the target improved for both the LETOpt and the LETBAO plans. However, it is noteworthy that the improvement of the biological effec in the LETBAO plans is much higher than in the LETOpt plans.

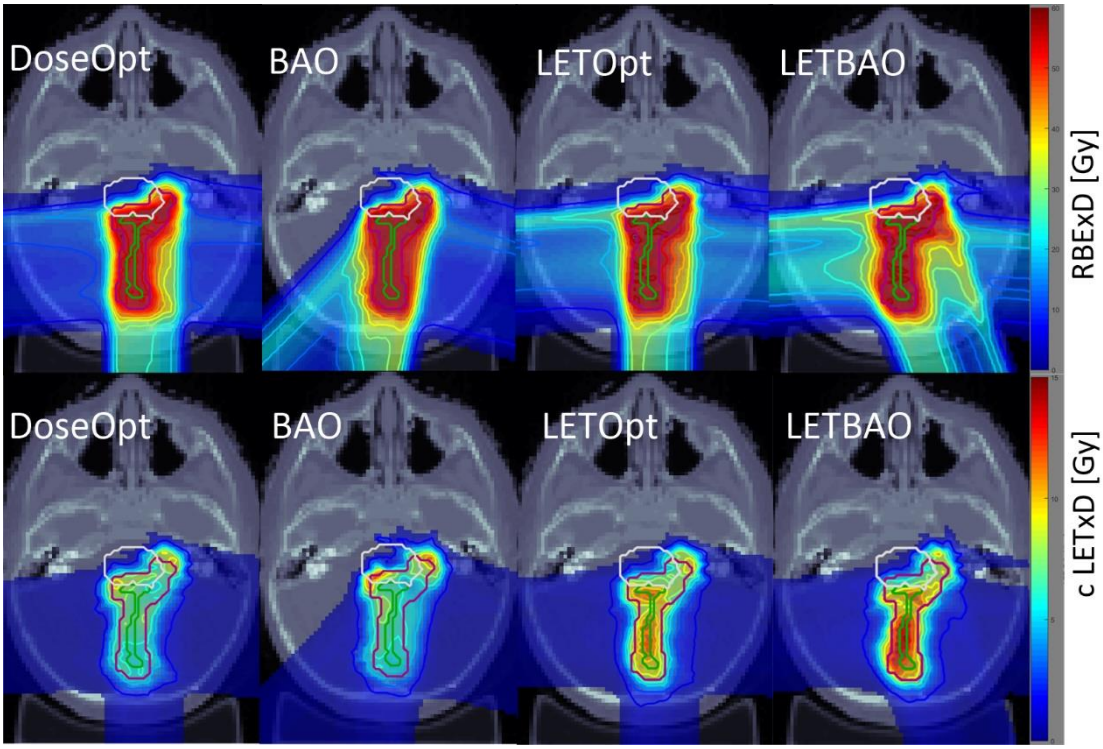

Figure 6.6: Plan comparison for the brain tumor case 1. The top two rows show the dose distributions (based on a constant RBE of 1.1). The bottom two rows show the distributions of LET-weighted dose scaled by c = 0.04 μm keV−1 (c LETxD). The CTV, PTV, and brainstem are contoured by the color green, purple and white, respectively.

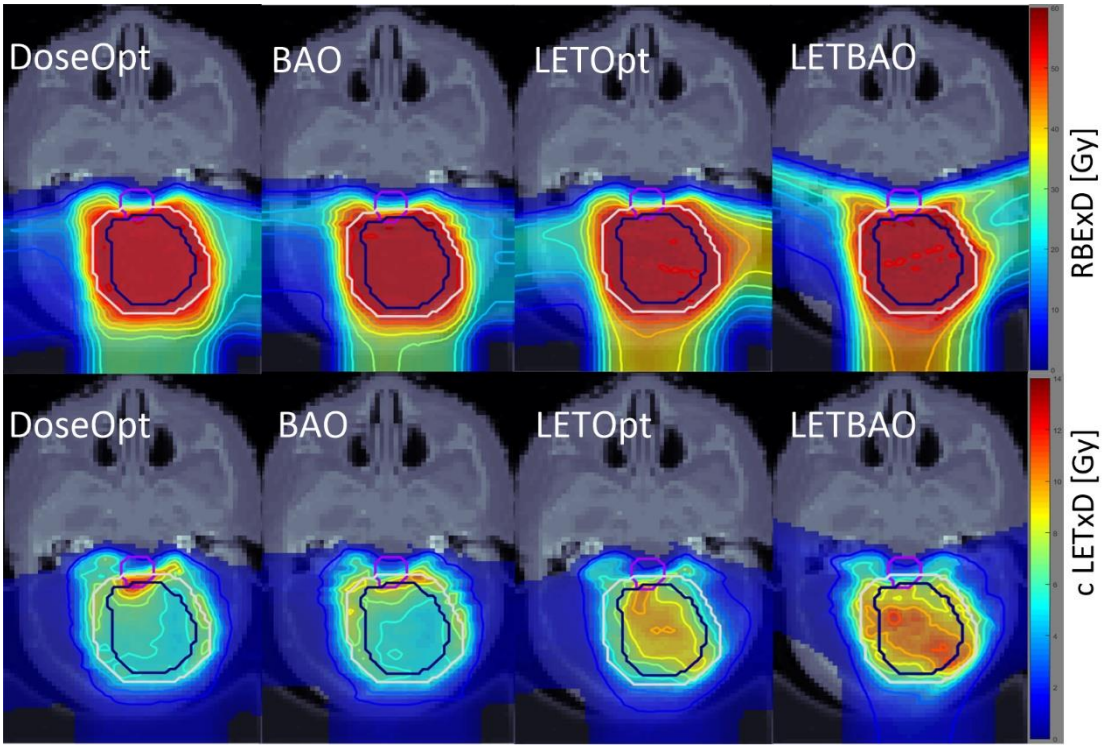

Figure 6.7: Plan comparison for the brain tumor case 2. The top two rows show the dose distributions (based on a constant RBE of 1.1). The bottom two rows show the distributions of LET-weighted dose scaled by c = 0.04 μm keV−1 (c LETxD). The CTV, PTV, and brainstem are contoured by the color blue, white and purple, respectively.

6.4 Conclusion

This study introduced a biological effect-incorporated BAO algorithm for IMPT. Compared with the clinical treatment planning methods DoseOpt and LETOpt we have used in the UT MD Anderson cancer center, our LETBAO method could achieve comparable treatment plans in terms of physical dose. More than that, we have demonstrated the LETBAO algorithm performed well in finding quality beam angles to improve the biological effect in target and spare it in the critical structure. However, future study is necessary to further validate the algorithm and understand the impact of biological effect for IMPT.

Chapter 7

Conclusions

7.1 Current Findings

The LET-incorporated method was introduced to conventional dose-based optimization. This method was able to simultaneously optimize dose and LET. No matter if we take uncertainties into consideration, this method was able to hedge against high LET in OARs and improve the low LET in the targets while maintaining adequate dose coverage and robustness.

Secondly, we presented a proof-of-concept study of biological effect-based IMPT robust optimization in order to reduce the impact of variation in protons' biological effect while limiting the degradation of the physical dose distribution from a voxel-based worst-case RO plan. By minimizing the uncertainty gap of the biological effect (approximated by the product of LET and physical dose) in each voxel, the BioRO approach provided robust distributions of biological effect to both target and critical structures. This approach does not depend on tissue parameters or variable RBE models, which are associated with large uncertainties. In addition, our three patient case studies demonstrated that BioRO can avoid elevating biological effect in critical structures.

Thirdly, we proposed and developed a distal-edge avoidance-guided optimization method to optimize IMPT plans in terms of their c LETxD distributions without degrading the physical dose distributions, which are comparable to those of LET optimization plans. We used an influence index to quantify the contribution of the

biological effect from each scanning spot on the basis of its topological relationship to different organs of interest. This method could be especially beneficial for patient cases where critical structures are adjacent to the target area. In addition, the DEAOpt approach is less complex computationally and therefore faster than the LETOpt approach.

Finally, we introduced a biological effect-incorporated BAO algorithm for IMPT. Compared with the clinical treatment planning methods DoseOpt and LETOpt we have used in the UT MD Anderson cancer center, our LETBAO method could achieve comparable treatment plans in terms of physical dose. More than that, we have demonstrated the LETBAO algorithm performed well in finding quality beam angles to improve the biological effect in target and spare it in the critical structure. However, future study is necessary to further validate the algorithm and understand the impact of biological effect for IMPT.

7.2 Future Work

7.2.1 Variable RBE optimization

In the present study, variations in tissue oxygenation and its impact on RBE were not considered. It is known that oxygen enhancement ratio (OER) decreases with increasing LET [122], [123]. However, these changes seem to be relevant for LET values higher than the maximum LET values observed in this study. Because OER is usually not considered in radiation treatment planning for photons, we have used the same strategy for protons to get comparable results [124]. However, more robust and

clinically validated biological data are needed for accurate assessment of RBE variations within the target and late-responding tissues, especially for those located in the vicinity of high-dose targets. From the methodological perspective, a robust approach that reduces the model uncertainties in the variable RBE model should be discussed. Here, we come up with a general variable RBE optimization framwork. And this framwork should be extended to avoid the model uncertainties.

The general (α/β)x ratio can be calculated by:

$$\alpha_i = \frac{\sum_j^N \alpha(LET)_{ij} D_{ij} w_j^2}{\sum_j^N D_{ij} w_j^2}, \tag{7.1}$$

and

$$\beta_i = \left(\frac{\sum_j^N \sqrt{\beta(LET)_{ij}} D_{ij} w_j^2}{\sum_j^N D_{ij} w_j^2} \right)^2. \tag{7.2}$$

Then the general variable RBE model can be formualted as:

$$\mathrm{RBE}_i = -\frac{1}{2D_i}\left(\frac{\alpha}{\beta}\right)_x + \frac{1}{D_i}\sqrt{\frac{1}{4}\left(\frac{\alpha}{\beta}\right)_x^2 + \frac{\alpha_i}{\beta_x} D_i + \frac{\beta_i}{\beta_x} {D_i}^2}. \tag{7.3}$$

The objective function of general variable RBE optimization can be written as:

$$f_R(w) = \sum_{i \in \mathrm{Target}} \lambda_T (RBE_i D_i - D_{T,prescribe})^2 + \sum_{i \in \mathrm{OARs}} \lambda_{OAR} H\big(RBE_i D_i - D_{OAR,prescribe}\big) \times (RBE_i D_i - D_{OAR,prescribe})^2. \tag{7.4}$$

The derivative of the Formulation 7.4 is as below:

$$\frac{\partial f_R(w)}{\partial w_j} = \sum_{i\in\text{Target}} \left[2\lambda_T \left(RBE_i D_i - D_{T,prescribe} \right) \times \frac{\left(\alpha(LET)_{ij} D_{ij} w_j + 2\left(\sum_j^N \sqrt{\beta(LET)_{ij}} D_{ij} w_j^2\right)\sqrt{\beta(LET)_{ij}} D_{ij} w_j\right)}{\beta_i \sqrt{\frac{1}{4}\left(\frac{\alpha}{\beta}\right)_x^2 + \frac{\alpha_i}{\beta_x} D_i + \frac{\beta_i}{\beta_x} D_i^2}} \right] + \sum_{i\in\text{OAR}} \left[2\lambda_{OAR} H\left(RBE_i D_i - D_{OAR,prescribe} \right) \times \left(RBE_i D_i - D_{OAR,prescribe} \right) \times \frac{\left(\alpha(LET)_{ij} D_{ij} w_j + 2\left(\sum_j^N \sqrt{\beta(LET)_{ij}} D_{ij} w_j^2\right)\sqrt{\beta(LET)_{ij}} D_{ij} w_j\right)}{\beta_i \sqrt{\frac{1}{4}\left(\frac{\alpha}{\beta}\right)_x^2 + \frac{\alpha_i}{\beta_x} D_i + \frac{\beta_i}{\beta_x} D_i^2}} \right]. \tag{7.5}$$

Based on the general variable RBE optimization model, how to avoid the model uncertainties (especially in (α/β)x ratio) will be explored in future work.

7.2.2 Analysis and modelling of treatment response and radiation-induced immunosuppression using machine learning techniques

Under the background of biological and physical data interpretation, there is a seen rapid development of advanced technologies. It follows the trend of data science and its related subjects such as big data, machine learning, and artificial intelligence. In future work, we plan to analyze and model the treatment response and radiation-induced immunosuppression in IMPT using machine learning techniques.

Radiation therapy is effective in treating many types of cancers. However, it can be immunosuppressive due to treatment-induced lymphocytotoxicity. Lymphocytes are highly sensitive to radiation even at low doses. Absolute lymphocyte count (ALC) has been shown to be an independent predictor of survival from cancer, and severe

radiation-induced lymphopenia (RIL) has been shown to be associated with reduced survival. Recent retrospective analyses of esophagus data have demonstrated a significant survival advantage for protons over photons. Preliminary indication is that this is likely attributable to differences in RIL between the two modalities, which, in turn may be due to differences in “dose bath” between protons and photons. Compared with photons, proton dose distributions are more “compact”. A recent study in our group suggested a strong correlation of mean body dose (MBD) with high grade ALC nadir. However, MBD is a limited surrogate. There can be large uncertainties in estimating the MBD. Moreover, MBD does not reflect the fact lymphocyte killing is not linearly proportional to dose. Such issues may affect the strength of the associations observed. For instance, a substantial subset of proton patients had low MBD, but the still developed grade 4 RIL. Thus, there is a pressing need to consider other correlates (e.g., dose-volume indices, lymphocyte killing) in order to enhance our understanding of RIL. It is essential to develop an in-depth understanding of the correlation of dose distribution patterns and dose-volume indices derived for the body as well as for organs at risk (OARs) of RIL relevance with ALC nadirs and ALCs at various time points before, during and after radiotherapy.

REFERENCES

[1] National Cancer Institute, "Cancer Trends Progress Report," no. February, 2018.

[2] A. B. Miller, B. Hoogstraten, M. Staquet, and A. Winkler, "Reporting results of cancer treatment," *Cancer*, vol. 47, no. 1, pp. 207–214, 1981.

[3] D. S. Shimm, "Perez and Brady's Principles and Practice of Radiation Oncology," *Int. J. Radiat. Oncol.*, vol. 72, no. 4, p. 1268, 2008.

[4] K. K. Ang, "Altered fractionation trials in head and neck cancer," *Semin. Radiat. Oncol.*, vol. 8, no. 4, pp. 230–236, 1998.

[5] A. J. Lomax, T. Boehringer, A. Coray, E. Egger, G. Goitein, M. Grossmann, P. Juelke, S. Lin, E. Pedroni, B. Rohrer, W. Roser, B. Rossi, B. Siegenthaler, O. Stadelmann, H. Stauble, C. Vetter, and L. Wisser, "Intensity modulated proton therapy: A clinical example," *Med. Phys.*, vol. 28, no. 3, pp. 317–324, 2001.

[6] J. Meyer, J. Bluett, R. Amos, L. Levy, S. Choi, Q. N. Nguyen, X. R. Zhu, M. Gillin, and A. Lee, "Spot scanning proton beam therapy for prostate cancer: Treatment planning technique and analysis of consequences of rotational and translational alignment errors," *Int. J. Radiat. Oncol. Biol. Phys.*, vol. 78, no. 2, pp. 428–434, 2010.

[7] T. J. Pugh, R. A. Amos, S. John Baptiste, S. Choi, Q. Nhu Nguyen, X. Ronald Zhu, M. B. Palmer, and A. K. Lee, "Multifield optimization intensity-modulated proton therapy (MFO-IMPT) for prostate cancer: Robustness

analysis through simulation of rotational and translational alignment errors," *Med. Dosim.*, vol. 38, no. 3, pp. 344–350, 2013.

[8] J. Unkelbach, T. Bortfeld, B. C. Martin, and M. Soukup, "Reducing the sensitivity of IMPT treatment plans to setup errors and range uncertainties via probabilistic treatment planning," *Med. Phys.*, vol. 36, no. 1, pp. 149–163, 2009.

[9] W. Song, J. Battista, and J. Van Dyk, "Limitations of a convolution method for modeling geometric uncertainties in radiation therapy: The radiobiological dose-per-fraction effect," *Med. Phys.*, vol. 31, no. 11, pp. 3034–3045, 2004.

[10] J. Unkelbach, T. C. Y. Chan, and T. Bortfeld, "Accounting for range uncertainties in the optimization of intensity modulated proton therapy," *Phys. Med. Biol.*, vol. 52, no. 10, pp. 2755–2773, 2007.

[11] A. Fredriksson, A. Forsgren, and B. Hårdemark, "Minimax optimization for handling range and setup uncertainties in proton therapy," *Med. Phys.*, vol. 38, no. 3, pp. 1672–1684, 2011.

[12] D. Pflugfelder, J. J. Wilkens, and U. Oelfke, "Worst case optimization: A method to account for uncertainties in the optimization of intensity modulated proton therapy," *Phys. Med. Biol.*, vol. 53, no. 6, pp. 1689–1700, 2008.

[13] International Commission on Radiation Units and Measurements, "Prescribing, recording, and reporting photon-beam IMRT," *J. ICRU*, vol. 10, no. 1, pp. 7–16, 2010.

[14] A. L. McNamara, J. Schuemann, and H. Paganetti, “A phenomenological relative biological effectiveness (RBE) model for proton therapy based on all published *in vitro* cell survival data,” *Phys. Med. Biol.*, vol. 60, no. 21, pp. 8399–8416, 2015.

[15] H. Paganetti, A. Niemierko, M. Ancukiewicz, L. E. Gerweck, M. Goitein, J. S. Loeffler, and H. D. Suit, “Relative biological effectiveness (RBE) values for proton beam therapy,” *Int. J. Radiat. Oncol. Biol. Phys.*, vol. 53, no. 2, pp. 407–421, 2002.

[16] D. Giantsoudi, C. Grassberger, D. Craft, A. Niemierko, A. Trofimov, and H. Paganetti, “Linear energy transfer-guided optimization in intensity modulated proton therapy: Feasibility study and clinical potential,” *Int. J. Radiat. Oncol. Biol. Phys.*, vol. 87, no. 1, pp. 216–222, 2013.

[17] A. Carabe-Fernandez, M. Moteabbed, N. Depauw, and H. Paganetti, “Range uncertainty in proton therapy due to variable biological effectiveness,” *Med. Phys.*, vol. 38, no. 6, p. 3639, 2011.

[18] A. F. Resch, G. Landry, F. Kamp, G. Cabal, C. Belka, J. J. Wilkens, K. Parodi, and G. Dedes, “Quantification of the uncertainties of a biological model and their impact on variable RBE proton treatment plan optimization,” *Phys. Medica*, vol. 36, pp. 91–102, 2017.

[19] H. Paganetti, “Relative biological effectiveness (RBE) values for proton beam therapy. Variations as a function of biological endpoint, dose, and linear energy transfer,” *Phys. Med. Biol.*, vol. 59, no. 22, pp. R419–R472, 2014.

[20] J. Unkelbach, P. Botas, D. Giantsoudi, B. L. Gorissen, and H. Paganetti, "Reoptimization of intensity modulated proton therapy plans based on linear energy transfer," *Int. J. Radiat. Oncol. Biol. Phys.*, vol. 96, no. 5, pp. 1097–1106, 2016.

[21] C. Grassberger, A. Trofimov, A. Lomax, and H. Paganetti, "Variations in linear energy transfer within clinical proton therapy fields and the potential for biological treatment planning," *Int. J. Radiat. Oncol. Biol. Phys.*, vol. 80, no. 5, pp. 1559–1566, 2011.

[22] L. Polster, J. Schuemann, I. Rinaldi, L. Burigo, A. L. McNamara, R. D. Stewart, A. Attili, D. J. Carlson, T. Sato, J. Ramos Méndez, B. Faddegon, J. Perl, and H. Paganetti, "Extension of TOPAS for the simulation of proton radiation effects considering molecular and cellular endpoints.," *Phys. Med. Biol.*, vol. 60, no. 13, pp. 5053–70, 2015.

[23] M. Wedenberg, B. K. Lind, and B. Hårdemark, "A model for the relative biological effectiveness of protons: The tissue specific parameter α / β of photons is a predictor for the sensitivity to LET changes," *Acta Oncol. (Madr).*, vol. 52, no. 3, pp. 580–588, 2013.

[24] A. Carabe, S. España, C. Grassberger, and H. Paganetti, "Clinical consequences of relative biological effectiveness variations in proton radiotherapy of the prostate, brain and liver," *Phys. Med. Biol.*, vol. 58, no. 7, pp. 2103–2117, 2013.

[25] J. J. Wilkens and U. Oelfke, "Analytical linear energy transfer calculations for proton therapy," *Med. Phys.*, vol. 30, no. 5, pp. 806–815, 2003.

[26] F. Marsolat, L. De Marzi, F. Pouzoulet, and A. Mazal, “Analytical linear energy transfer model including secondary particles: Calculations along the central axis of the proton pencil beam,” *Phys. Med. Biol.*, vol. 61, no. 2, pp. 740–757, 2016.

[27] M. A. Cortés-Giraldo and A. Carabe, “A critical study of different Monte Carlo scoring methods of dose average linear-energy-transfer maps calculated in voxelized geometries irradiated with clinical proton beams,” *Phys. Med. Biol.*, vol. 60, no. 7, pp. 2645–2669, 2015.

[28] W. Cao, A. Khabazian, P. P. Yepes, G. Lim, F. Poenisch, D. R. Grosshans, and R. Mohan, “Linear energy transfer incorporated intensity modulated proton therapy optimization,” *Phys. Med. Biol.*, vol. 63, no. 1, p. 15013, Dec. 2018.

[29] N. Bassler, O. Jäkel, C. S. Søndergaard, and J. B. Petersen, “Dose-and LET-painting with particle therapy,” *Acta Oncol. (Madr).*, vol. 49, no. 7, pp. 1170–1176, 2010.

[30] M. Fager, I. Toma-Dasu, M. Kirk, D. Dolney, E. S. Diffenderfer, N. Vapiwala, and A. Carabe, “Linear energy transfer painting with proton therapy: A means of reducing radiation doses with equivalent clinical effectiveness,” *Int. J. Radiat. Oncol. Biol. Phys.*, vol. 91, no. 5, pp. 1057–1064, 2015.

[31] Y. An, J. Shan, S. H. Patel, W. Wong, S. E. Schild, X. Ding, M. Bues, and W. Liu, “Robust intensity-modulated proton therapy to reduce high linear energy transfer in organs at risk,” *Med. Phys.*, pp. 1–10, 2017.

[32] W. Cao, G. Lim, X. Li, Y. Li, X. R. Zhu, and X. Zhang, “Incorporating deliverable monitor unit constraints into spot intensity optimization in intensity-modulated proton therapy treatment planning.,” *Phys. Med. Biol.*, vol. 58, no. 15, pp. 5113–25, 2013.

[33] M. Langer and J. Leong, “Optimization of beam weights under dose-volume restrictions,” *Int. J. Radiat. Oncol. Biol. Phys.*, vol. 13, no. 2, pp. 1255–1260, 1987.

[34] M. Langer, R. Brown, M. Urie, J. Leong, M. Stracher, and J. Shapiro, “Large scale optimization of beam weights under dose-volume restrictions,” *Int. J. Radiat. Oncol. Biol. Phys.*, vol. 18, no. 4, pp. 887–893, Apr. 1990.

[35] A. Niemierko, “Random search algorithm (RONSC) for optimization of radiation therapy with both physical and biological end points and constraints,” *Int. J. Radiat. Oncol. Biol. Phys.*, 1992.

[36] S. V. Spirou and C. S. Chui, “A gradient inverse planning algorithm with dose-volume constraints,” *Med. Phys.*, vol. 25, no. 3, pp. 321–333, Jun. 1998.

[37] Q. Wu, R. Mohan, A. Niemierko, and R. Schmidt-Ullrich, “Optimization of intensity-modulated radiotherapy plans based on the equivalent uniform dose.,” *Int. J. Radiat. Oncol. Biol. Phys.*, vol. 52, no. 1, pp. 224–35, Jan. 2002.

[38] I. I. Rosen, R. G. Lane, S. M. Morrill, and J. A. Belli, “Treatment plan optimization using linear programming,” *Med. Phys.*, vol. 18, no. 2, pp. 141–152, Mar. 1991.

[39] W. Cao and G. Lim, “Optimization Models for Cancer Treatment Planning,” *Wiley Encyclopedia of Operations Research and Management Science*. pp. 1–14, 14-Jan-2010.

[40] X. Wu, Y. Zhu, and L. Luo, “Linear programming based on neural networks for radiotherapy treatment planning,” *Phys. Med. Biol.*, vol. 45, no. 3, pp. 719–728, Mar. 2000.

[41] M. Langer, S. Morrill, R. Brown, O. Lee, and R. Lane, “A comparison of mixed integer programming and fast simulated annealing for optimizing beam weights in radiation therapy,” *Med. Phys.*, vol. 23, no. 6, pp. 957–964, Jun. 1996.

[42] E. K. Lee, T. Fox, and I. Crocker, “Optimization of radiosurgery treatment planning via mixed integer programming,” *Med. Phys.*, vol. 27, no. 5, pp. 995–1004, May 2000.

[43] S. M. Morrill, R. G. Lane, G. Jacobson, and I. I. Rosen, “Treatment planning optimization using constrained simulated annealing,” *Phys. Med. Biol.*, vol. 36, no. 10, pp. 1341–1361, Oct. 1991.

[44] G. A. Ezzell, “Genetic and geometric optimization of three-dimensional radiation therapy treatment planning,” *Med. Phys.*, vol. 23, no. 3, pp. 293–305, Mar. 1996.

[45] X. Wu and Y. Zhu, “A mixed-encoding genetic algorithm with beam constraint for conformal radiotherapy treatment planning,” *Med. Phys.*, vol. 27, no. 11, pp. 2508–2516, Nov. 2000.

[46] T. Bortfeld, J. Bürkelbach, R. Boesecke, and W. Schlegel, “Methods of image reconstruction from projections applied to conformation radiotherapy,” *Phys. Med. Biol.*, vol. 35, no. 10, pp. 1423–1434, Oct. 1990.

[47] X. Zhang, H. Liu, X. Wang, L. Dong, Q. Wu, and R. Mohan, “Speed and convergence properties of gradient algorithms for optimization of IMRT,” *Med. Phys.*, vol. 31, no. 5, pp. 1141–1152, Apr. 2004.

[48] G. J. Lim and W. Cao, “A two-phase method for selecting IMRT treatment beam angles: Branch-and-Prune and local neighborhood search,” *Eur. J. Oper. Res.*, vol. 217, no. 3, pp. 609–618, 2012.

[49] L. Xing, J. G. Li, S. Donaldson, Q. T. Le, and A. L. Boyer, “Optimization of importance factors in inverse planning,” *Phys. Med. Biol.*, vol. 44, no. 10, pp. 2525–2536, Oct. 1999.

[50] M. Alber, G. Meedt, F. Nüsslin, and R. Reemtsen, “On the degeneracy of the IMRT optimization problem,” *Med. Phys.*, vol. 29, no. 11, pp. 2584–2589, Oct. 2002.

[51] J. O. Deasy, “Multiple local minima in radiotherapy optimization problems with dose-volume constraints,” *Med. Phys.*, vol. 24, no. 7, pp. 1157–1161, Jul. 1997.

[52] M. Soukup, M. Söhn, D. Yan, J. Liang, and M. Alber, “Study of Robustness of IMPT and IMRT for Prostate Cancer Against Organ Movement,” *Int. J. Radiat. Oncol. Biol. Phys.*, vol. 75, no. 3, pp. 941–949, 2009.

[53] S. Webb, “The physical basis of IMRT and inverse planning,” *Br. J. Radiol.*, vol. 76, no. 910, pp. 678–689, Oct. 2003.

[54] J. Llacer, N. Agazaryan, T. D. Solberg, and C. Promberger, “Degeneracy, frequency response and filtering in IMRT optimization,” *Phys. Med. Biol.*, vol. 49, no. 13, pp. 2853–2880, 2004.

[55] F. Albertini, E. B. Hug, and A. J. Lomax, “The influence of the optimization starting conditions on the robustness of intensity-modulated proton therapy plans,” *Phys. Med. Biol.*, vol. 55, no. 10, pp. 2863–2878, May 2010.

[56] M. Chu, Y. Zinchenko, S. G. Henderson, and M. B. Sharpe, “Robust optimization for intensity modulated radiation therapy treatment planning under uncertainty,” *Phys. Med. Biol.*, vol. 50, no. 23, pp. 5463–5477, 2005.

[57] A. Ólafsson and S. J. Wright, “Efficient schemes for robust IMRT treatment planning,” *Phys. Med. Biol.*, vol. 51, no. 21, pp. 5621–5642, Nov. 2006.

[58] J. G. Li and L. Xing, “Inverse planning incorporating organ motion,” *Med. Phys.*, vol. 27, no. 7, pp. 1573–1578, Jul. 2000.

[59] T. Bortfeld, T. C. Y. Chan, A. Trofimov, and J. N. Tsitsiklis, “Robust Management of Motion Uncertainty in Intensity-Modulated Radiation Therapy,” *Oper. Res.*, vol. 56, no. 6, pp. 1461–1473, 2008.

[60] T. C. Y. Chan, T. Bortfeld, and J. N. Tsitsiklis, “A robust approach to IMRT optimization,” *Phys. Med. Biol.*, vol. 51, no. 10, pp. 2567–2583, May 2006.

[61] W. Cao, G. J. Lim, A. Lee, Y. Li, W. Liu, X. Ronald Zhu, and X. Zhang, "Uncertainty incorporated beam angle optimization for IMPT treatment planning," *Med. Phys.*, vol. 39, no. 8, pp. 5248–5256, 2012.

[62] W. Liu, Y. Li, X. Li, W. Cao, and X. Zhang, "Influence of robust optimization in intensity-modulated proton therapy with different dose delivery techniques," *Med. Phys.*, vol. 39, no. 6Part1, pp. 3089–3101, 2012.

[63] A. J. Lomax, T. Böhringer, A. Bolsi, D. Coray, F. Emert, G. Goitein, M. Jermann, S. Lin, E. Pedroni, H. Rutz, O. Stadelmann, B. Timmermann, J. Verwey, and D. C. Weber, "Treatment planning and verification of proton therapy using spot scanning: Initial experiences," *Med. Phys.*, 2004.

[64] X. R. Zhu, N. Sahoo, X. Zhang, D. Robertson, H. Li, S. Choi, A. K. Lee, and M. T. Gillin, "Intensity modulated proton therapy treatment planning using single-field optimization: The impact of monitor unit constraints on plan quality," *Med. Phys.*, vol. 37, no. 3, pp. 1210–1219, 2010.

[65] A. Smith, M. Gillin, M. Bues, X. R. Zhu, K. Suzuki, R. Mohan, S. Woo, A. Lee, R. Komaki, J. Cox, K. Hiramoto, H. Akiyama, T. Ishida, T. Sasaki, and K. Matsuda, "The M. D. Anderson proton therapy system," *Med. Phys.*, 2009.

[66] M. T. Gillin, N. Sahoo, M. Bues, G. Ciangaru, G. Sawakuchi, F. Poenisch, B. Arjomandy, C. Martin, U. Titt, K. Suzuki, A. R. Smith, and X. R. Zhu, "Commissioning of the discrete spot scanning proton beam delivery system at the University of Texas M.D. Anderson Cancer Center, Proton Therapy Center, Houston," *Med. Phys.*, 2010.

[67] J. V. Siebers, M. Lauterbach, P. J. Keall, and R. Mohan, “Incorporating multi-leaf collimator leaf sequencing into iterative IMRT optimization,” *Med. Phys.*, 2002.

[68] J. L. Bedford and S. Webb, “Constrained segment shapes in direct-aperture optimization for step-and-shoot IMRT,” *Med. Phys.*, 2006.

[69] C. Men, X. Jia, and S. B. Jiang, “GPU-based ultra-fast direct aperture optimization for online adaptive radiation therapy,” *Phys. Med. Biol.*, 2010.

[70] M. M. Coselmon, J. M. Moran, J. D. Radawski, and B. A. Fraass, “Improving IMRT delivery efficiency using intensity limits during inverse planning,” *Med. Phys.*, vol. 32, no. 5, pp. 1234–1245, 2005.

[71] S. K. Das and L. B. Marks, “Selection of coplanar or noncoplanar beams using three-dimensional optimization based on maximum beam separation and minimized nontarget irradiation,” *Int. J. Radiat. Oncol. Biol. Phys.*, vol. 38, no. 3, pp. 643–655, 1997.

[72] M. Bangert, P. Ziegenhein, and U. Oelfke, “Characterizing the combinatorial beam angle selection problem,” *Phys. Med. Biol.*, vol. 57, no. 20, pp. 6707–6723, 2012.

[73] D. Craft, “Local beam angle optimization with linear programming and gradient search,” *Phys. Med. Biol.*, vol. 52, pp. 127–135, 2007.

[74] H. Rocha, J. M. Dias, T. Ventura, B. da C. Ferreira, and M. do C. Lopes, "Beam angle optimization in IMRT: are we really optimizing what matters?," *Int. Trans. Oper. Res.*, vol. 26, no. 3, pp. 908–928, 2019.

[75] D. M. Aleman, A. Kumar, R. K. Ahuja, H. E. Romeijn, and J. F. Dempsey, "Neighborhood search approaches to beam orientation optimization in intensity modulated radiation therapy treatment planning," *J. Glob. Optim.*, vol. 42, no. 4, pp. 587–607, 2008.

[76] D. M. Aleman, H. E. Romeijn, and J. F. Dempsey, "A response surface approach to beam orientation optimization in intensity-modulated radiation therapy treatment planning," *INFORMS J. Comput.*, vol. 21, no. 1, pp. 62–76, 2009.

[77] D. Bertsimas, V. Cacchiani, D. Craft, and O. Nohadani, "A hybrid approach to beam angle optimization in intensity-modulated radiation therapy," *Comput. Oper. Res.*, vol. 40, no. 9, pp. 2187–2197, 2013.

[78] Q. Hou, J. Wang, Y. Chen, and J. M. Galvin, "Beam orientation optimization for IMRT by a hybrid method of the genetic algorithm and the simulated dynamics," *Med. Phys.*, vol. 30, no. 9, pp. 2360–2367, 2003.

[79] Y. Li, J. Yao, and D. Yao, "Automatic beam angle selection in IMRT planning using genetic algorithm," *Phys. Med. Biol.*, vol. 49, no. 10, pp. 1915–1932, 2004.

[80] D. Nazareth, S. Brunner, M. Jones, H. Malhotra, and M. Bakhtiari, "Optimization of beam angles for intensity modulated radiation therapy treatment planning using genetic algorithm on a distributed computing platform," in *Journal of Medical Physics*, 2009, vol. 34, no. 3, pp. 129–132.

[81] C. G. Rowbottom, S. Webb, and M. Oldham, "Beam-orientation customization using an artificial neural network," *Phys. Med. Biol.*, vol. 44, no. 9, pp. 2251–2262, 1999.

[82] D. Djajaputra, Q. Wu, Y. Wu, and R. Mohan, "Algorithm and performance of a clinical IMRT beam-angle optimization system," *Phys. Med. Biol.*, vol. 48, no. 19, pp. 3191–3212, 2003.

[83] G. Cabrera G., M. Ehrgott, A. J. Mason, and A. Raith, "A matheuristic approach to solve the multiobjective beam angle optimization problem in intensity-modulated radiation therapy," *Int. Trans. Oper. Res.*, vol. 25, no. 1, pp. 243–268, 2018.

[84] X. Jia, C. Men, Y. Lou, and S. Jiang, "Beam Orientation Optimization for Intensity Modulated Radiation Therapy Using Adaptive L1 Minimization," *Med. Phys.*, vol. 38, no. 6, p. 3691, 2011.

[85] W. Gu, D. O'Connor, D. Nguyen, V. Y. Yu, D. Ruan, L. Dong, and K. Sheng, "Integrated beam orientation and scanning-spot optimization in intensity-modulated proton therapy for brain and unilateral head and neck tumors," *Med. Phys.*, vol. 45, no. 4, pp. 1338–1350, 2018.

[86] H. Paganetti, “Relative biological effectiveness (RBE) values for proton beam therapy. Variations as a function of biological endpoint, dose, and linear energy transfer,” *Phys. Med. Biol.*, vol. 59, no. 22, pp. R419–R472, 2014.

[87] C. Grassberger, A. Trofimov, A. Lomax, and H. Paganetti, “Variations in linear energy transfer within clinical proton therapy fields and the potential for biological treatment planning.,” *Int. J. Radiat. Oncol. Biol. Phys.*, vol. 80, no. 5, pp. 1559–66, Aug. 2011.

[88] T. Inaniwa, N. Kanematsu, K. Noda, and T. Kamada, “Treatment planning of intensity modulated composite particle therapy with dose and linear energy transfer optimization Treatment planning of intensity modulated composite particle therapy with dose and linear energy transfer optimization,” *Phys. Med. Biol.*, vol. 62, no. 12, pp. 5180–5197, 2017.

[89] P. P. Yepes, J. G. Eley, A. Liu, D. Mirkovic, S. Randeniya, U. Titt, and R. Mohan, “Validation of a track repeating algorithm for intensity modulated proton therapy: clinical cases study,” *Phys. Med. Biol.*, vol. 61, no. 7, pp. 2633–2645, Apr. 2016.

[90] M. Steneker, A. Lomax, and U. Schneider, “Intensity modulated photon and proton therapy for the treatment of head and neck tumors,” *Radiother. Oncol.*, vol. 80, no. 2, pp. 263–267, 2006.

[91] F. Albertini, A. Bolsi, A. J. Lomax, H. P. Rutz, B. Timmerman, and G. Goitein, “Sensitivity of intensity modulated proton therapy plans to changes in patient weight,” *Radiother. Oncol.*, vol. 86, no. 2, pp. 187–194, 2008.

[92] A. J. Lomax, “Intensity modulated proton therapy and its sensitivity to treatment uncertainties 1: the potential effects of calculational uncertainties,” *Phys. Med. Biol.*, vol. 53, no. 4, pp. 1027–1042, 2008.

[93] A. J. Lomax, “Intensity modulated proton therapy and its sensitivity to treatment uncertainties 2: the potential effects of inter-fraction and inter-field motions,” *Phys. Med. Biol.*, vol. 53, no. 4, pp. 1043–1056, 2008.

[94] W. Chen, J. Unkelbach, A. Trofimov, T. Madden, H. Kooy, T. Bortfeld, and D. Craft, “Including robustness in multi-criteria optimization for intensity-modulated proton therapy,” *Phys. Med. Biol.*, vol. 57, no. 3, pp. 591–608, 2012.

[95] H. Wieser, E. Cisternas, N. Wahl, S. Ulrich, A. Stadler, H. Mescher, T. Klinge, H. Gabrys, L. Burigo, and M. Bangert, “Development of the open-source dose calculation and optimization toolkit matRad,” *Phys. Med. Biol.*, vol. 44, no. 6, pp. 2556–2568, 2017.

[96] T. Bortfeld, W. Schlegel, and B. Rhein, “Decomposition of pencil beam kernels for fast dose calculations in three-dimensional treatment planning,” *Med. Phys.*, vol. 20, no. 2, pp. 311–318, 1993.

[97] W. Liu, S. J. Frank, X. Li, Y. Li, R. X. Zhu, and R. Mohan, “PTV-based IMPT optimization incorporating planning risk volumes vs robust optimization.,” *Med. Phys.*, vol. 40, no. 2, p. 021709, 2013.

[98] U. Oelfke and T. Bortfeld, “Inverse planning for photon and proton beams,” *Med. Dosim.*, vol. 26, no. 2, pp. 113–124, Jun. 2001.

[99] M. Lowe, A. Aitkenhead, F. Albertini, A. J. Lomax, and R. I. Mackay, “A robust optimisation approach accounting for the effect of fractionation on setup uncertainties,” *Phys. Med. Biol.*, vol. 62, no. 20, pp. 1–20, 2017.

[100] D. Pflugfelder, J. J. Wilkens, S. Nill, and U. Oelfke, “A comparison of three optimization algorithms for intensity modulated radiation therapy,” *Z. Med. Phys.*, vol. 18, no. 2, pp. 111–119, Jun. 2008.

[101] E. S. Matrosov, A. M. Woods, and J. J. Harou, “Robust Decision Making and Info-Gap Decision Theory for water resource system planning,” *J. Hydrol.*, vol. 494, pp. 43–58, 2013.

[102] Y. Ben-Haim, *Info-Gap Decision Theory:Decisions Under Severe Uncertainty*. London, 2006.

[103] D. C. Liu and J. Nocedal, “On the limited memory BFGS method for large scale optimization,” *Math. Program.*, vol. 45, no. 1–3, pp. 503–528, 1989.

[104] F. A. and E. B. H. and A. J. Lomax, “Is it necessary to plan with safety margins for actively scanned proton therapy?,” *Phys. Med. Biol.*, vol. 56, no. 14, p. 4399, 2011.

[105] B. Schaffner and E. Pedroni, “The precision of proton range calculations in proton radiotherapy treatment planning: experimental verification of the relation between CT-HU and proton stopping power,” *Phys. Med. Biol.*, vol. 43, no. 6, pp. 1579–1592, Jun. 1998.

[106] a. Trofimov, J. Kang, J. Unkelbach, J. a. Adams, X. Zhang, T. Bortfeld, N. J. Liebsch, and T. F. DeLaney, "Evaluation of Dosimetric Gain and Uncertainties in Proton Therapy Delivery with Scanned Pencil Beam in Treatment of Base-of-skull and Spinal Tumors," 2010.

[107] D. Giantsoudi, J. Unkelbach, P. Botas, C. Grassberger, and H. Paganetti, "Can robust optimization for range uncertainty in proton therapy act as a surrogate for biological optimization?," *Int. J. Radiat. Oncol. Biol. Phys.*, vol. 99, no. 2, pp. S106–S107, Oct. 2017.

[108] R. Kohno, W. Cao, P. Yepes, X. Bai, F. Poenisch, D. R. Grosshans, T. Akimoto, and R. Mohan, "Biological dose comparison between a fixed RBE and a variable RBE in SFO and MFO IMPT with various multi-beams for brain cancer," *Int. J. Med. Physics, Clin. Eng. Radiat. Oncol.*, vol. 08, no. 01, pp. 32–45, 2019.

[109] G. Giovannini, T. Böhlen, G. Cabal, J. Bauer, T. Tessonnier, K. Frey, J. Debus, A. Mairani, and K. Parodi, "Variable RBE in proton therapy: comparison of different model predictions and their influence on clinical-like scenarios," *Radiat. Oncol.*, vol. 11, no. 1, p. 68, 2016.

[110] A. Carabe-Fernandez, R. G. Dale, and B. Jones, "The incorporation of the concept of minimum RBE (RBEmin) into the linear-quadratic model and the potential for improved radiobiological analysis of high-LET treatments," *Int. J. Radiat. Biol.*, vol. 83, no. 1, pp. 27–39, 2007.

[111] H. S. Wan Chan Tseung, J. Ma, C. R. Kreofsky, D. J. Ma, and C. Beltran, "Clinically applicable Monte Carlo–based biological dose optimization for the treatment of head and neck cancers withspot-scanning proton therapy," *Int. J. Radiat. Oncol. Biol. Phys.*, vol. 95, no. 5, pp. 1535–1543, 2016.

[112] E. Traneus and J. Ödén, "Introducing proton track-end objectives in intensity modulated proton therapy optimization to reduce linear energy transfer and telative biological effectiveness in critical structures," *Int. J. Radiat. Oncol. Biol. Phys.*, vol. 103, no. 3, pp. 747–757, 2019.

[113] Y. An, J. Liang, S. E. Schild, M. Bues, and W. Liu, "Robust treatment planning with conditional value at risk chance constraints in intensity-modulated proton therapy:," *Med. Phys.*, vol. 44, no. 1, pp. 28–36, 2017.

[114] X. Bai, G. Lim, H. Wieser, M. Bangert, D. Grosshans, R. Mohan, and W. Cao, "Robust optimization to reduce the impact of biological effect variation from physical uncertainties in intensity-modulated proton therapy," *Phys. Med. Biol.*, vol. 64, no. 2, p. 025004, 2019.

[115] A. J. Lomax, "Intensity modulation methods for proton radiotherapy," *Phys. Med. Biol.*, vol. 44, no. 1, pp. 185–205, 1999.

[116] T. Bortfeld, "Optimized planning using physical objectives and constraints," *Semin. Radiat. Oncol.*, vol. 9, no. 1, pp. 20–34, 1999.

[117] U. Oelfke and T. Bortfeld, "Inverse planning for photon and proton beams," *Med. Dosim.*, vol. 26, no. 2, pp. 113–124, 2001.

[118] Q. Wang, A. Johnson, P. Yepes, N. Schlegel, M. Moyers, J. Lin, L. Hong, H. Chen, J. Li, Z. Shen, M. Xu, and P. J. Taddei, "Validation of the fast dose calculator for Shanghai Proton and Heavy Ion Center," *Biomed. Phys. Eng. Express*, vol. 4, no. 6, p. 065007, 2018.

[119] A. Wächter and L. T. Biegler, *On the implementation of an interior-point filter line-search algorithm for large-scale nonlinear programming*, vol. 106, no. 1. 2006.

[120] L. A. Wolsey, *Integer Programming*. John Wiley & Sons, Inc., 1998.

[121] G. A. Ezzell, J. W. Burmeister, N. Dogan, T. J. Losasso, J. G. Mechalakos, D. Mihailidis, A. Molineu, J. R. Palta, C. R. Ramsey, B. J. Salter, J. Shi, P. Xia, N. J. Yue, and Y. Xiao, "IMRT commissioning: Multiple institution planning and dosimetry comparisons, a report from AAPM Task Group 119," *Med. Phys.*, vol. 36, no. 11, pp. 5359–5373, 2009.

[122] G. W. Barendsen, C. J. Koot, G. R. Van Kersen, D. K. Bewley, S. B. Field, and C. J. Parnell, "The effect of oxygen on impairment of the proliferative capacity of human cells in culture by ionizing radiations of different LET," *Int. J. Radiat. Biol.*, vol. 10, no. 4, pp. 317–327, 1966.

[123] L. Antonovic, A. Brahme, Y. Furusawa, and I. Toma-Dasu, "Radiobiological description of the LET dependence of the cell survival of oxic and anoxic cells irradiated by carbon ions," *J. Radiat. Res.*, vol. 54, no. 1, pp. 18–26, 2013.

[124] M. C. Frese, J. J. Wilkens, P. E. Huber, A. D. Jensen, U. Oelfke, and Z. Taheri-Kadkhoda, “Application of constant vs. variable relative biological effectiveness in treatment planning of intensity-modulated proton therapy,” *Int. J. Radiat. Oncol. Biol. Phys.*, vol. 79, no. 1, pp. 80–88, 2011.

APPENDICES

A. Comparison between RO Method and PTV-based Optimization Method

Table A.1:Parameters used for the PTV-based optimization method for a brain tumor case. Here, de and od mean deviation and over dose. TG is the target.

Structure	objective	type	penalty	dose	Bio.model	robustness	α_x	β_x
PTV	Squared-de	TG	2000	2	1.1	none	0.5	0.05
Brain	Squared-od	OAR	100	1	1.1	none	0.1	0.05
Brainstem	Squared-od	OAR	200	1.2	1.1	none	0.1	0.05
Ring	Squared-od	OAR	300	1.2	1.1	none	0.1	0.05

Table A.2: Parameters used for the RO method for a brain tumor case. Here, de and od mean deviation and over dose. TG is the target. VWWC means it is a voxel-based worst-case RO method.

Structure	objective	type	penalty	dose	Bio.model	robustness	α_x	β_x
CTV+	Squared-od	TG	500	2	1.1	VWWC	0.5	0.05
CTV-	Squared-ud	TG	1500	2	1.1	VWWC	0.5	0.05
Brain	Squared-od	OAR	100	1	1.1	VWWC	0.1	0.05
Brainstem	Squared-od	OAR	200	1.2	1.1	VWWC	0.1	0.05
Ring	Squared-od	OAR	300	1.2	1.1	VWWC	0.1	0.05

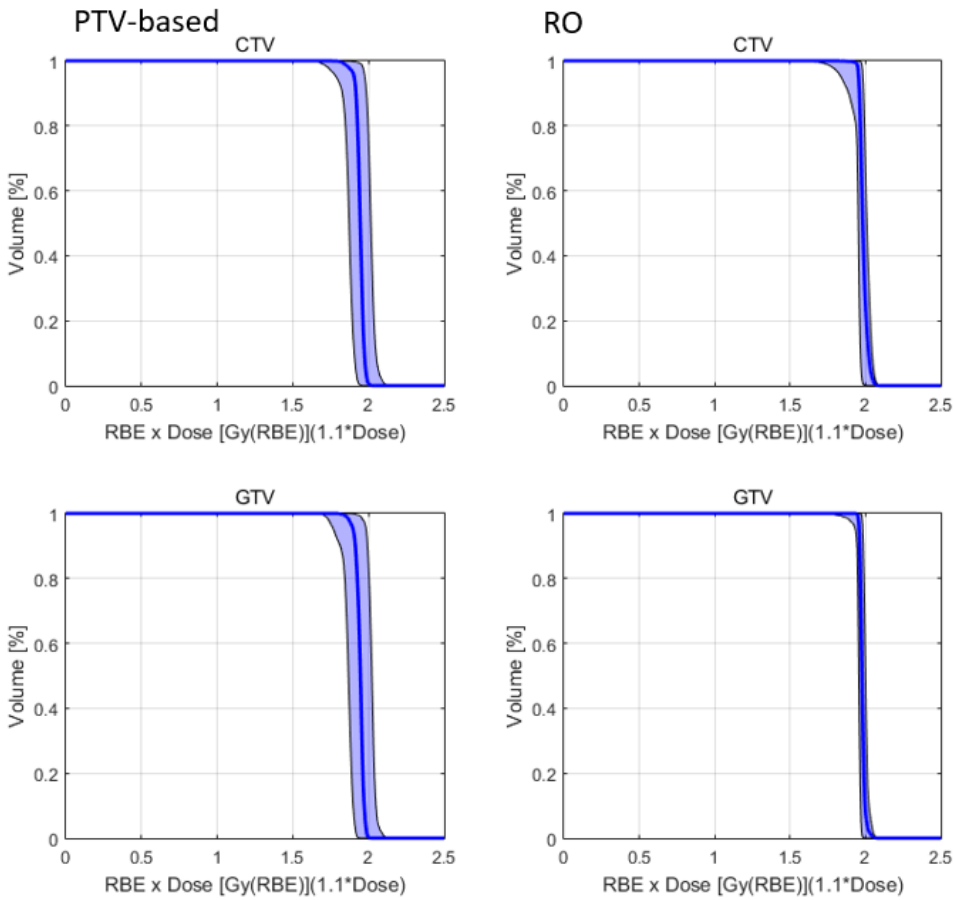

Figure A.1:Constant RBE (1.1)-weighted dose-volume histogram bands of the clinical target volume (CTV) and gross tumor volume (GTV) for the two IMPT plans in a brain tumor patient case. The bold lines indicate the nominal distributions.

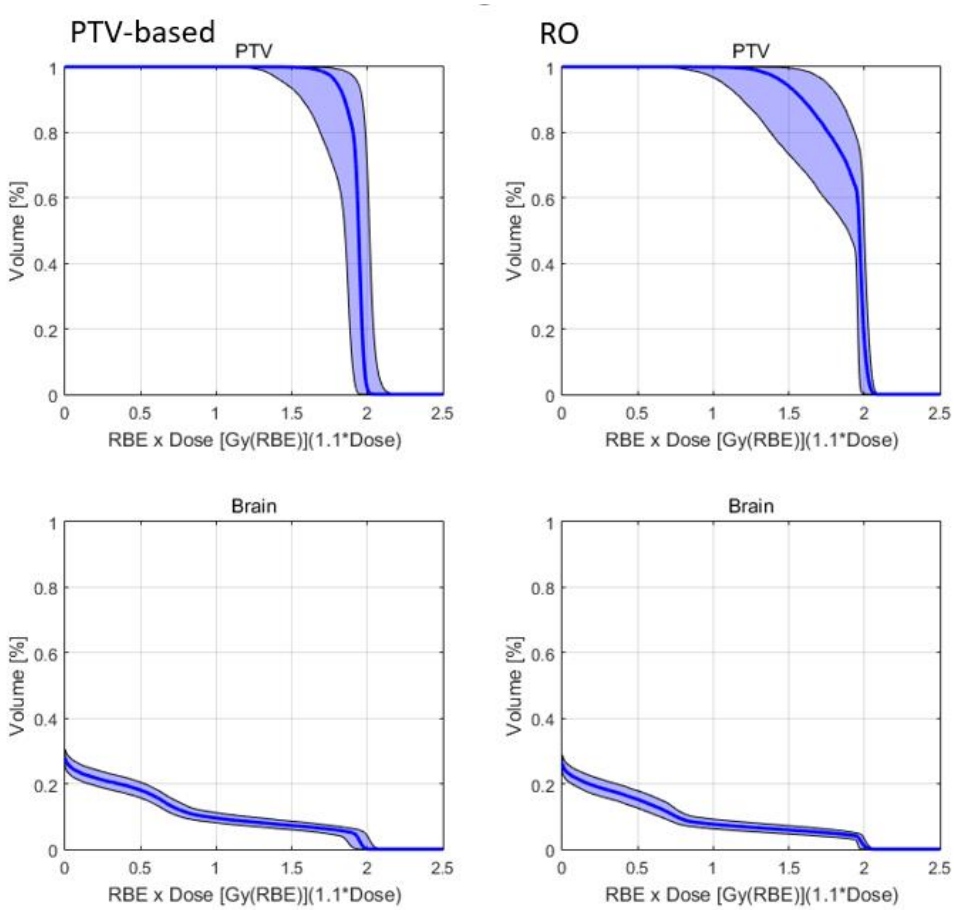

Figure A.2: Constant RBE (1.1)-weighted dose-volume histogram bands of the planning target volume (PTV) and brain for the two IMPT plans in a brain tumor patient case. The bold lines indicate the nominal distributions.

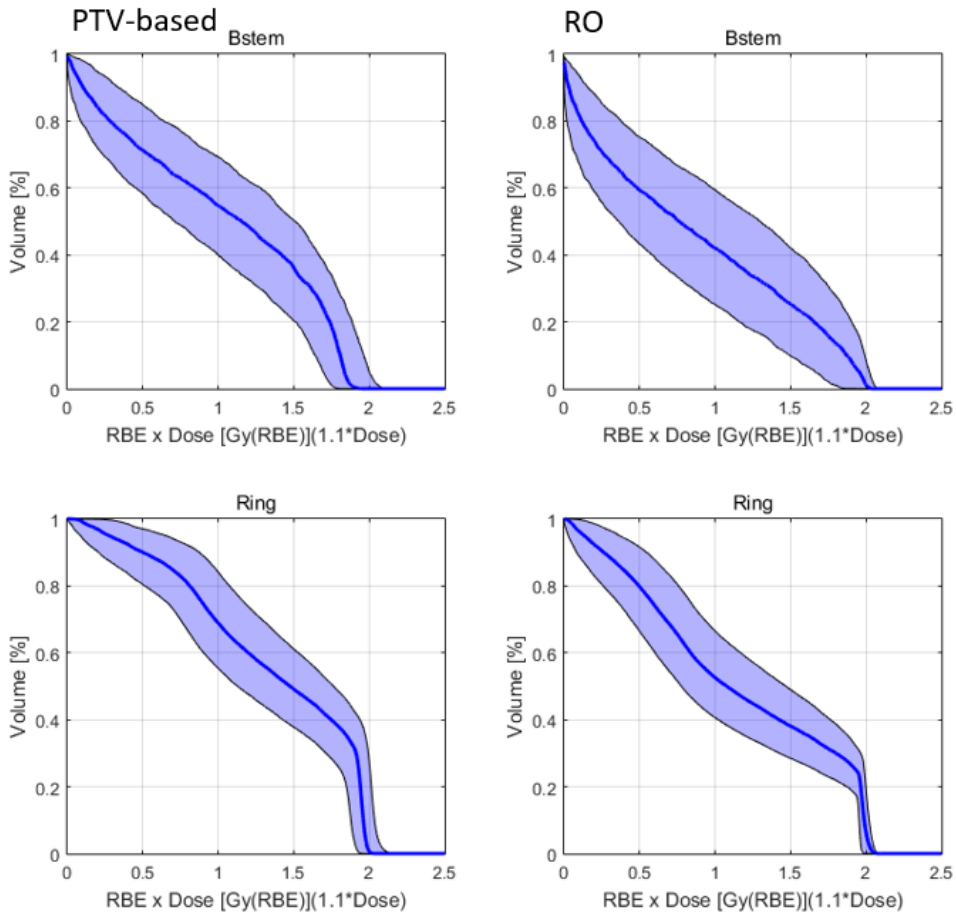

Figure A.3: Constant RBE (1.1)-weighted dose-volume histogram bands of the brainstem and ring for the two IMPT plans in a brain tumor patient case. The bold lines indicate the nominal distributions.

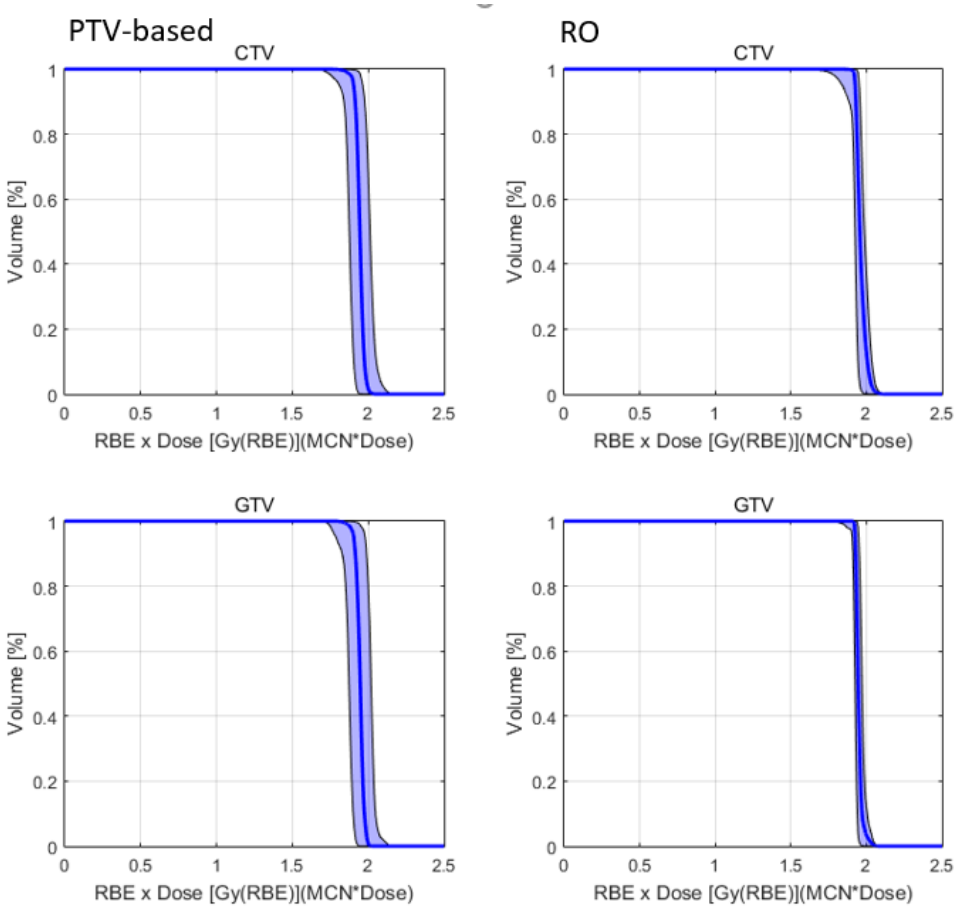

Figure A.4: Variable RBE (McNamara)-weighted dose-volume histogram bands of the clinical target volume (CTV) and gross tumor volume (GTV) for the two IMPT plans in a brain tumor patient case. The bold lines indicate the nominal distributions.

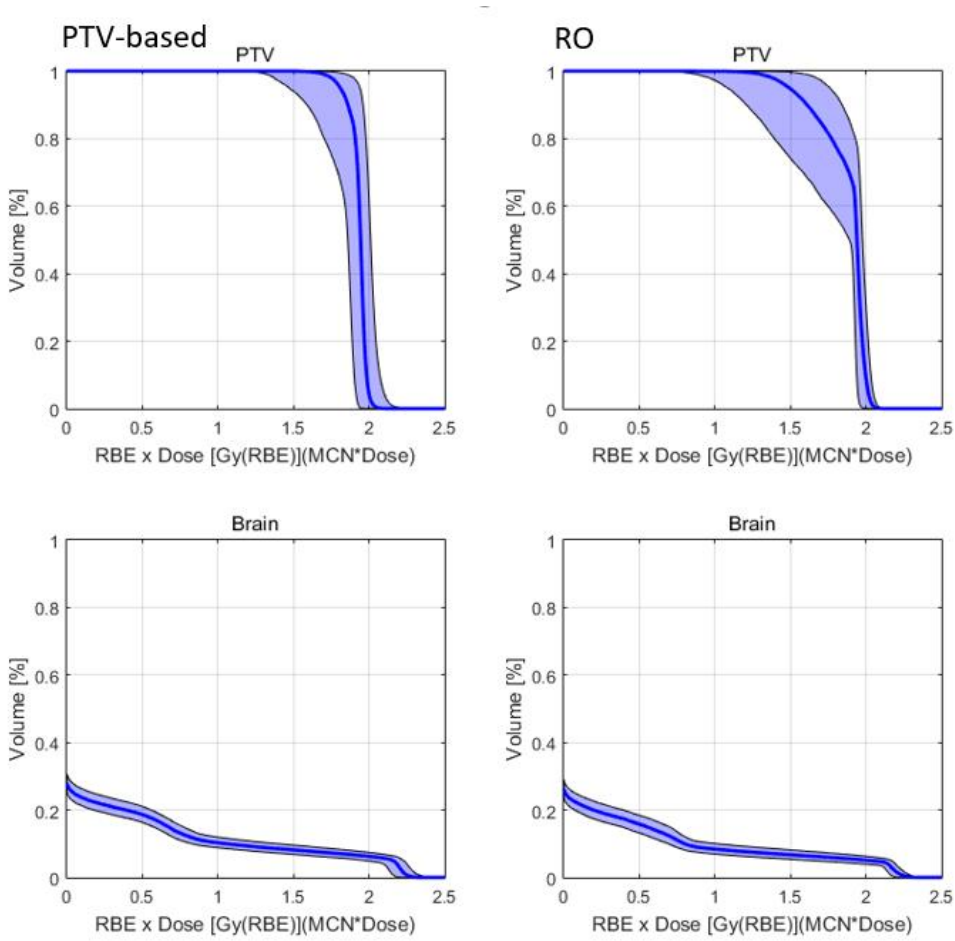

Figure A.5: Variable RBE (McNamara)-weighted dose-volume histogram bands of the planning target volume (PTV) and brain for the two IMPT plans in a brain tumor patient case. The bold lines indicate the nominal distributions.

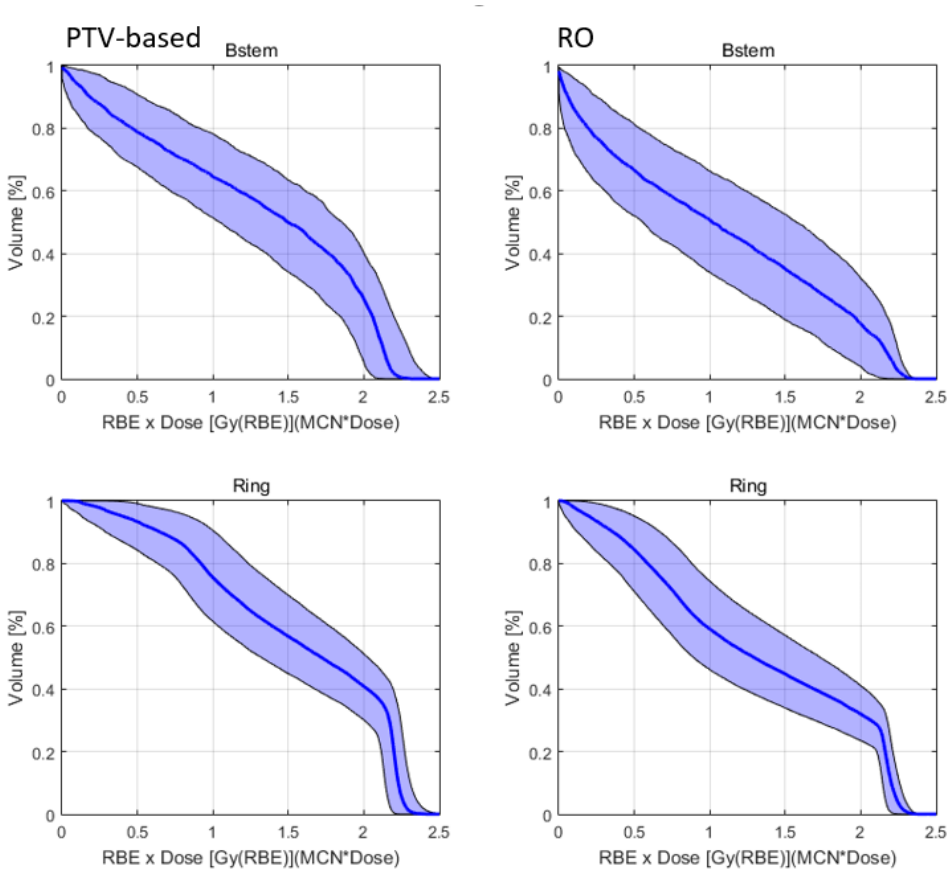

Figure A.6: Variable RBE (McNamara)-weighted dose-volume histogram bands of the brainstem and ring for the two IMPT plans in a brain tumor patient case. The bold lines indicate the nominal distributions.

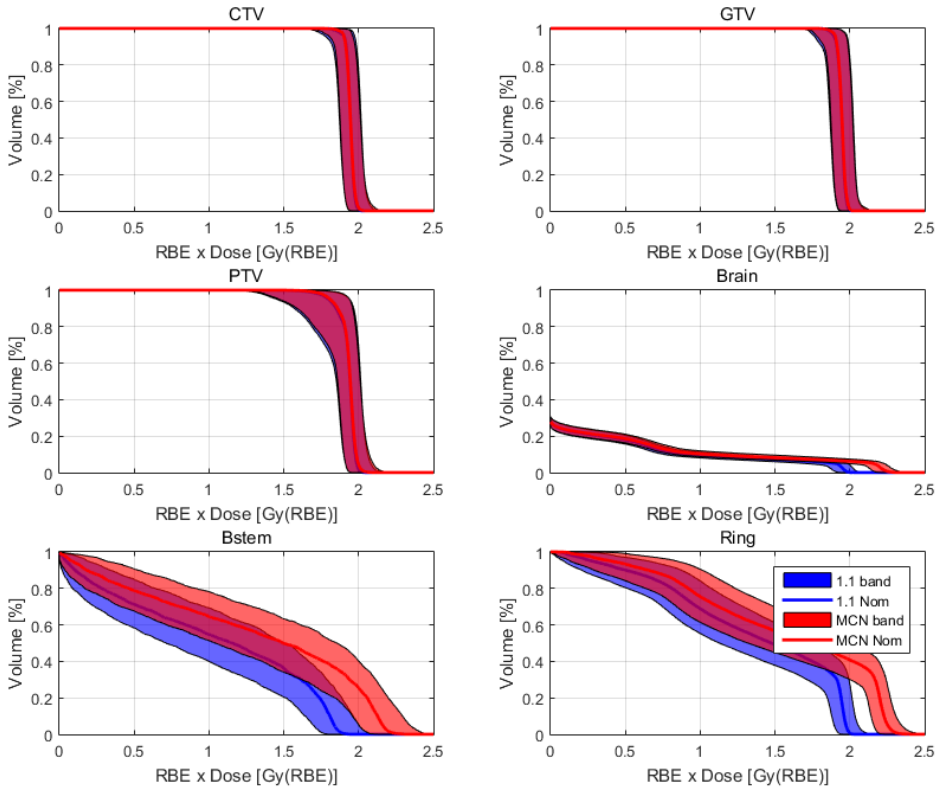

Figure A.7: RBE-weighted dose-volume histogram bands for the PTV-based optimization plan. The blud bands were based on the constant RBE (1.1) and the red bands were recalculated based on the variable RBE model (McNamara). The bold lines indicate the nominal distributions.

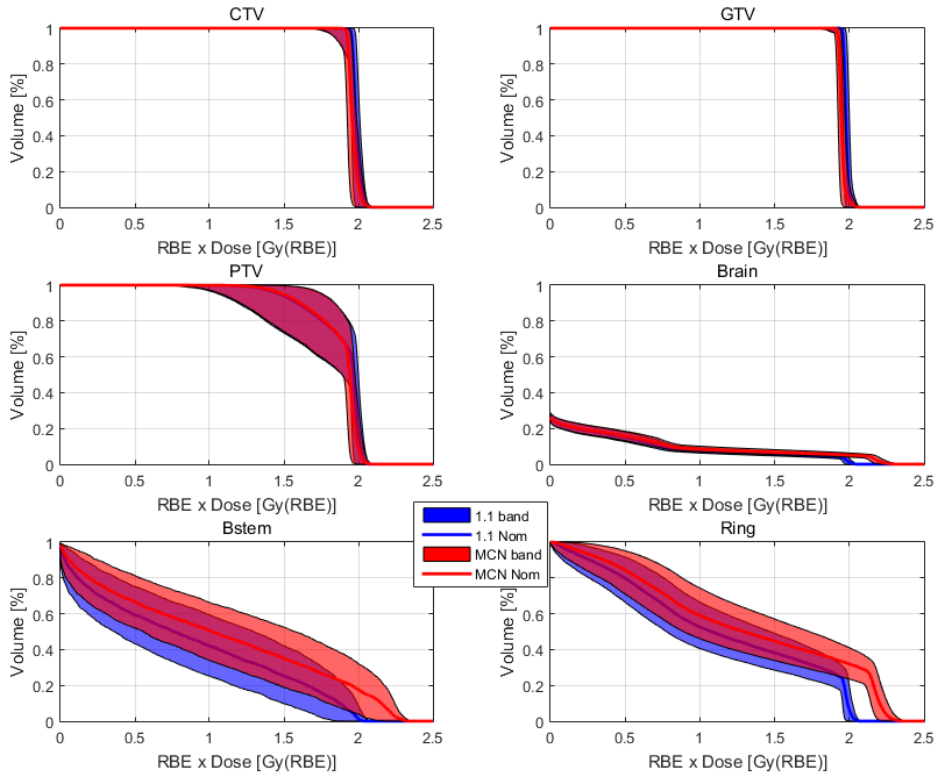

Figure A.8: RBE-weighted dose-volume histogram bands for the RO plan. The blud bands were based on the constant RBE (1.1) and the red bands were recalculated based on the variable RBE model (McNamara). The bold lines indicate the nominal distribution.

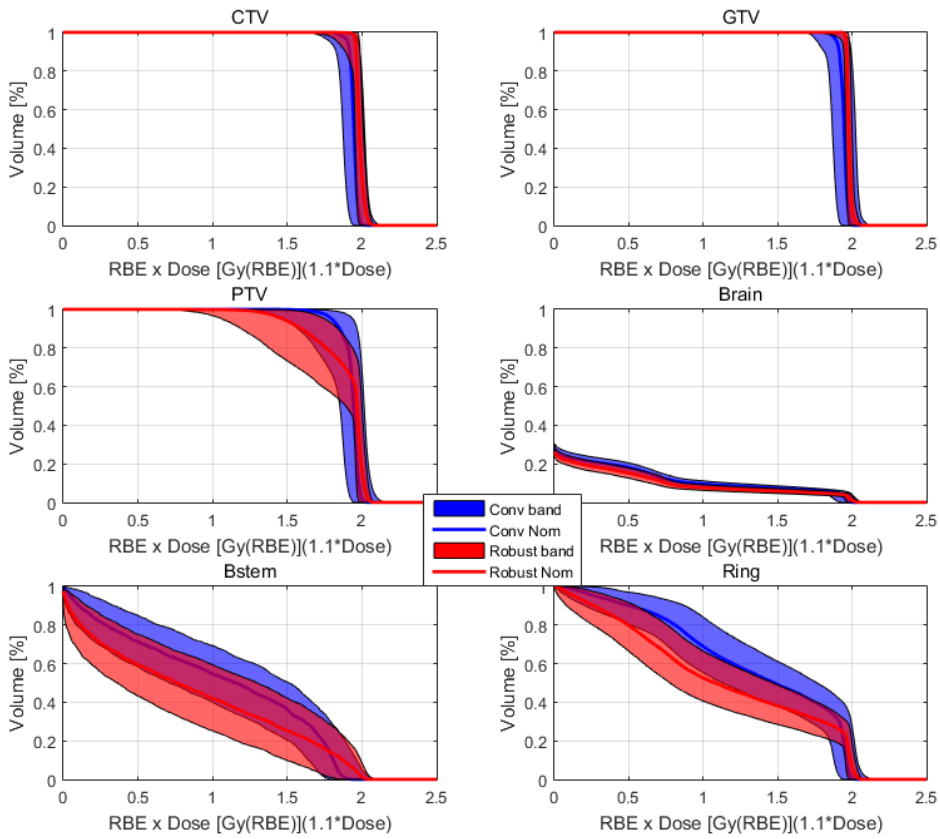

Figure A.9: Constant RBE (1.1)-weighted dose-volume histogram bands comparison of the PTV based optimization plan (blue) and RO plan (red). The bold lines indicate the nominal distribution.

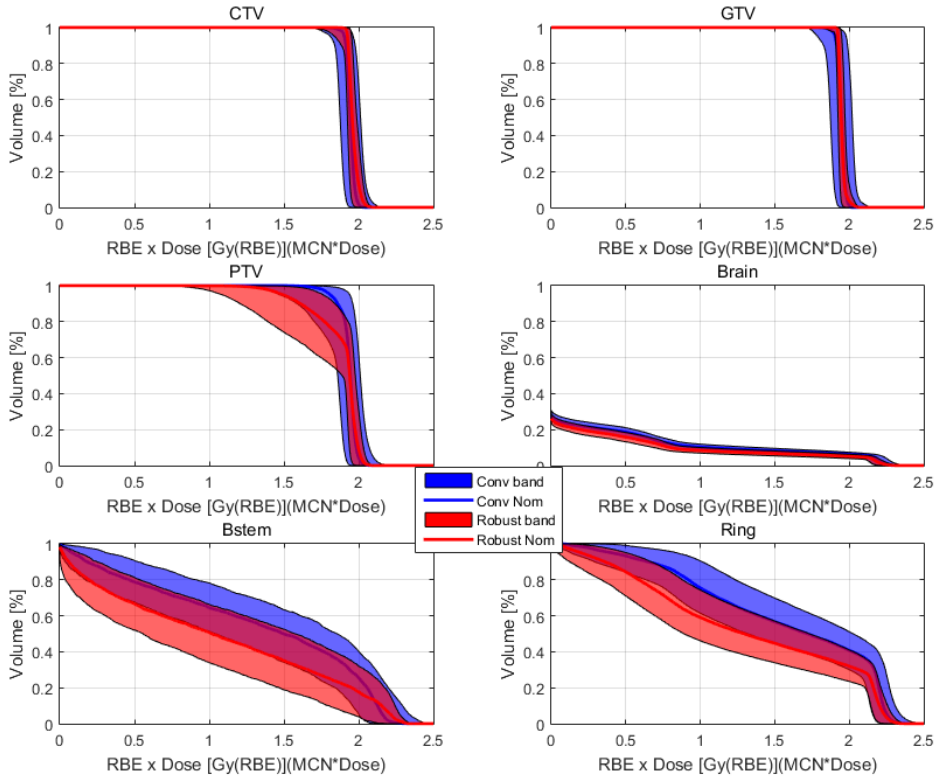

Figure A.10: Variable RBE (McNamara)-weighted dose-volume histogram bands comparison of the PTV based optimization plan (blue) and RO plan (red). The bold lines indicate the nominal distribution.

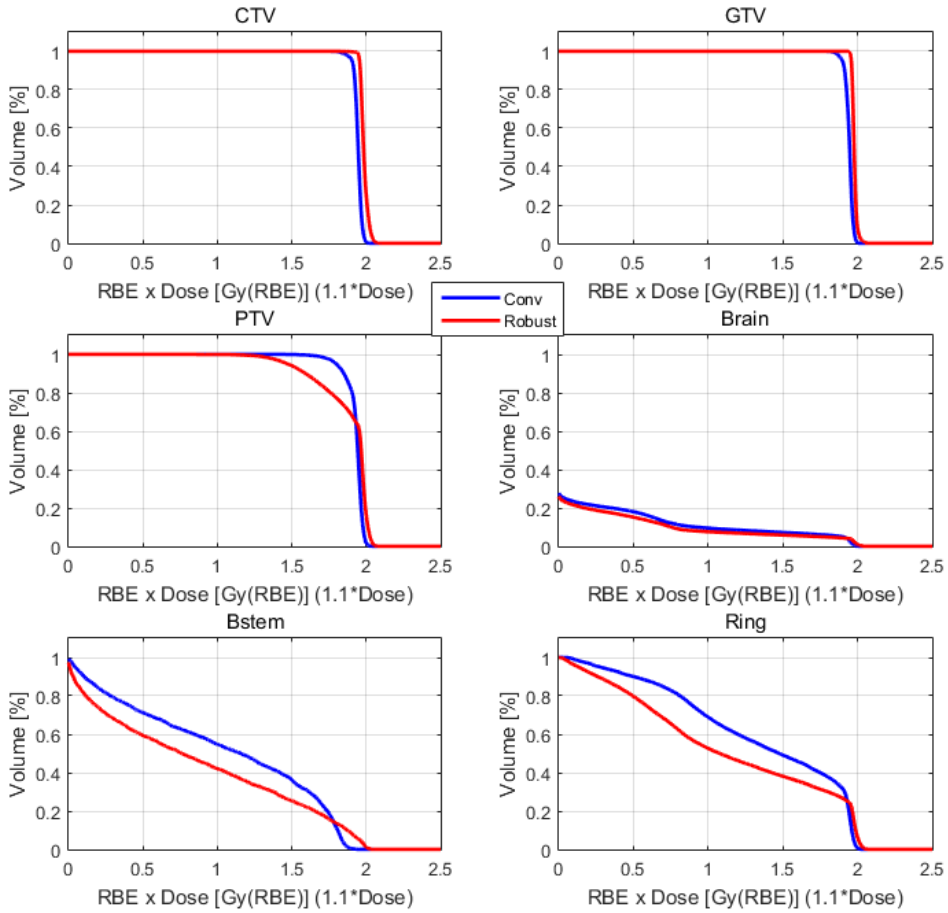

Figure A.11: Constant RBE (1.1)-weighted dose-volume histograms (nominal distribution) comparison of the PTV based optimization plan (blue) and RO plan (red).

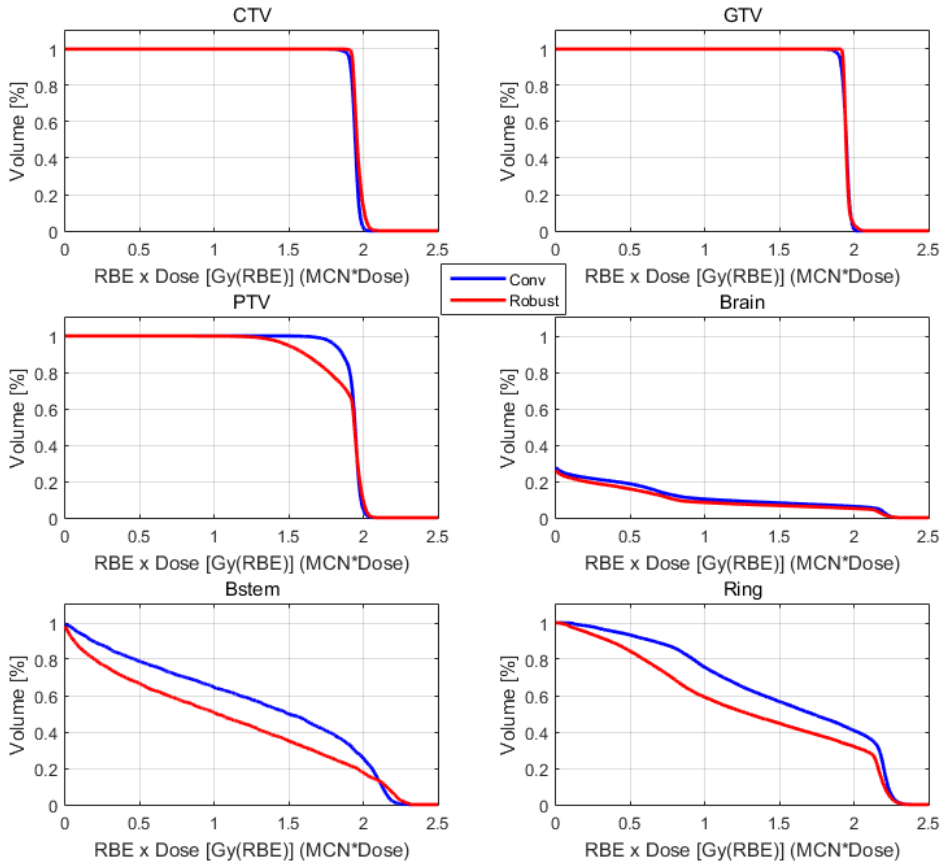

Figure A. 12: Variable RBE (McNamara)-weighted dose-volume histograms (nominal distribution) comparison of the PTV based optimization plan (blue) and RO plan (red).

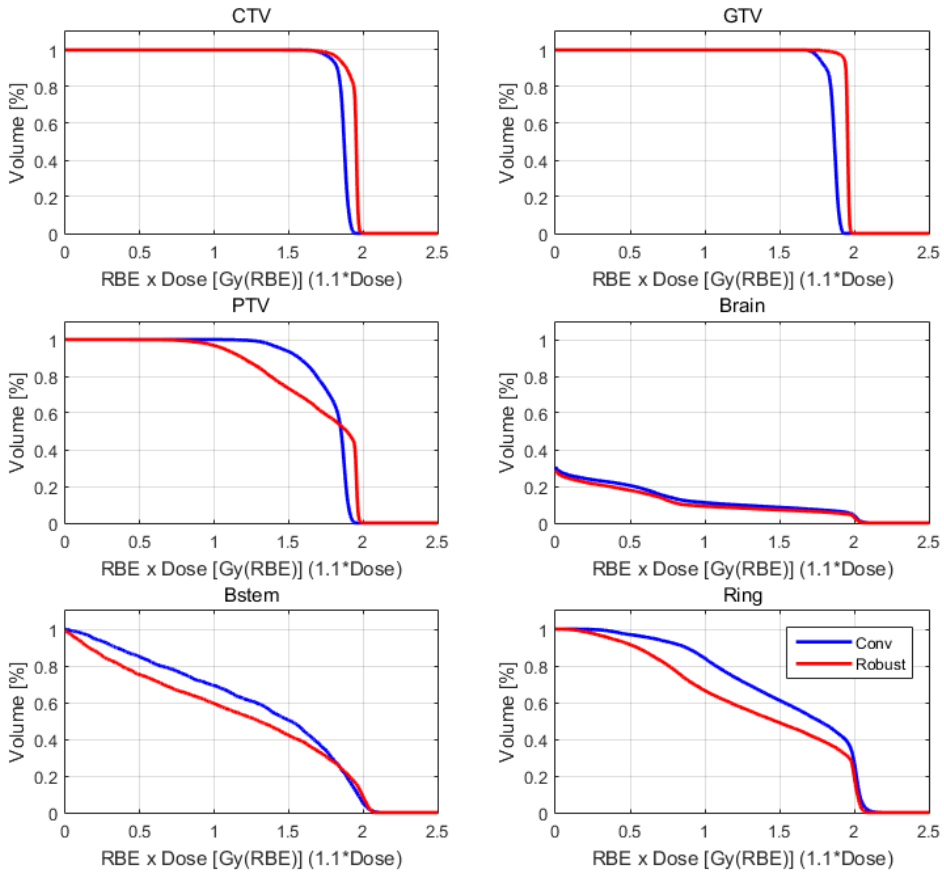

Figure A.13: Constant RBE (1.1)-weighted dose-volume histograms (worst distribution) comparison of the PTV based optimization plan (blue) and RO plan (red).

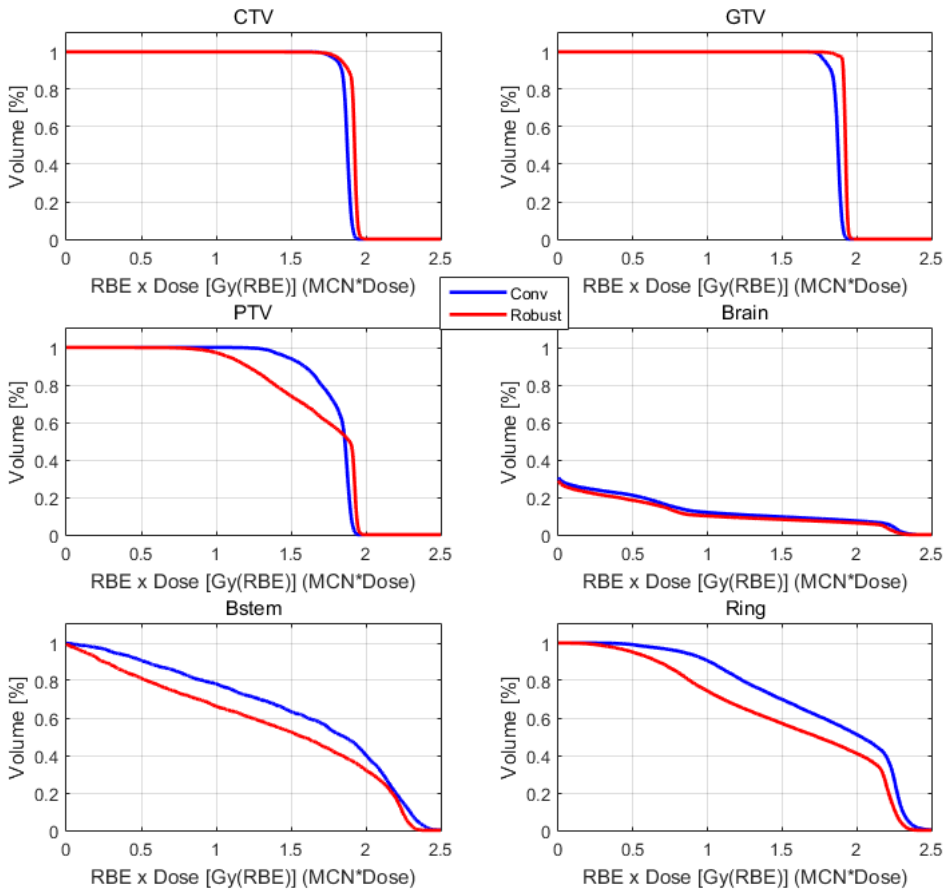

Figure A.14: Variable RBE (McNamara)-weighted dose-volume histograms (worst distribution) comparison of the PTV based optimization plan (blue) and RO plan (red).

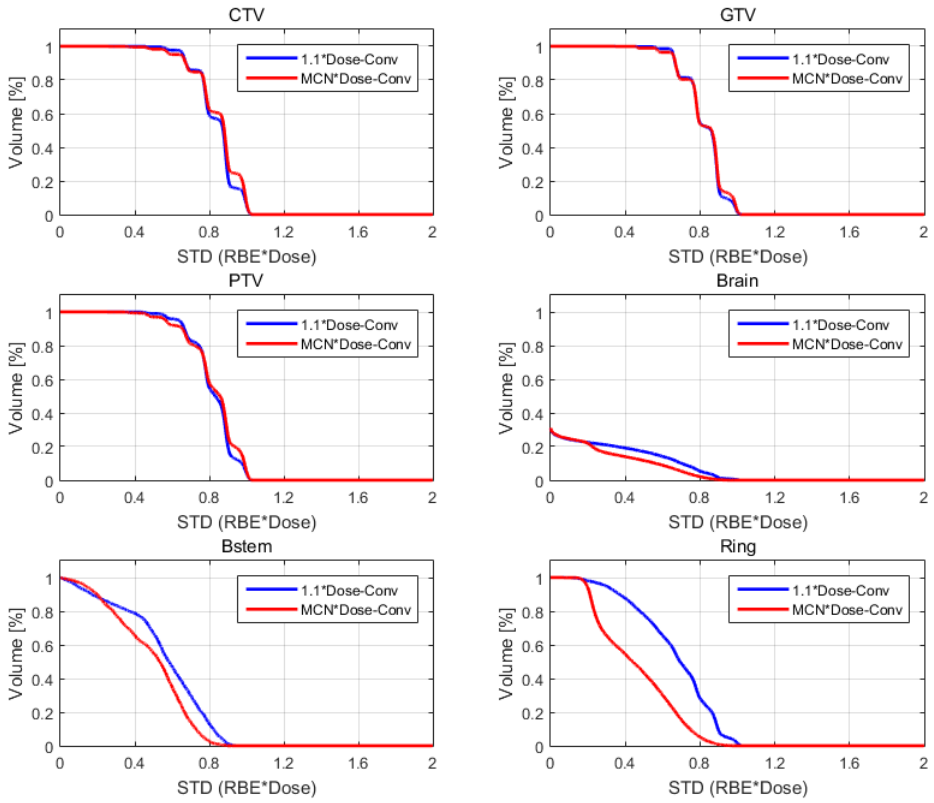

Figure A.15: Standard deviation volume histograms of the constant RBE(1.1)-weighted dose (blue) and variable RBE (McNamara)-weighted dose (red) for the PTV-based optimization plan.

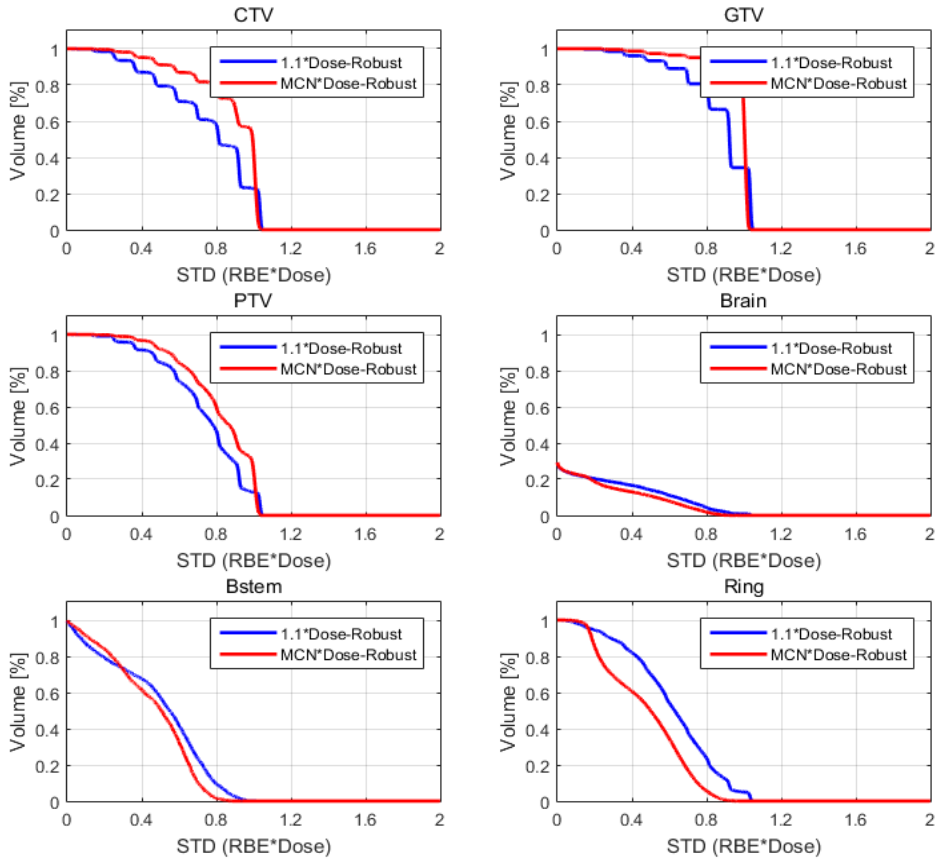

Figure A.16: Standard deviation volume histograms of the constant RBE (1.1)-weighted dose (blue) and variable RBE (McNamara)-weighted dose (red) for the RO plan.

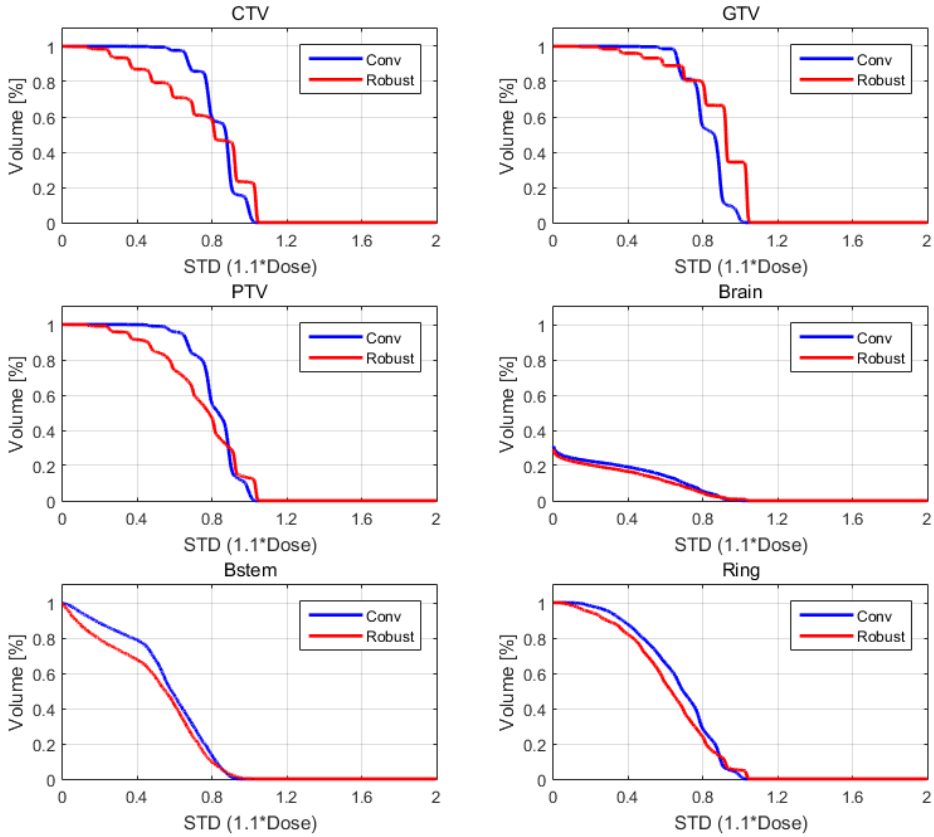

Figure A.17: Standard deviation of the constant RBE (1.1)-weighted dose volume histograms comparison of the PTV-based optimization plan (blue) and the RO plan (red).

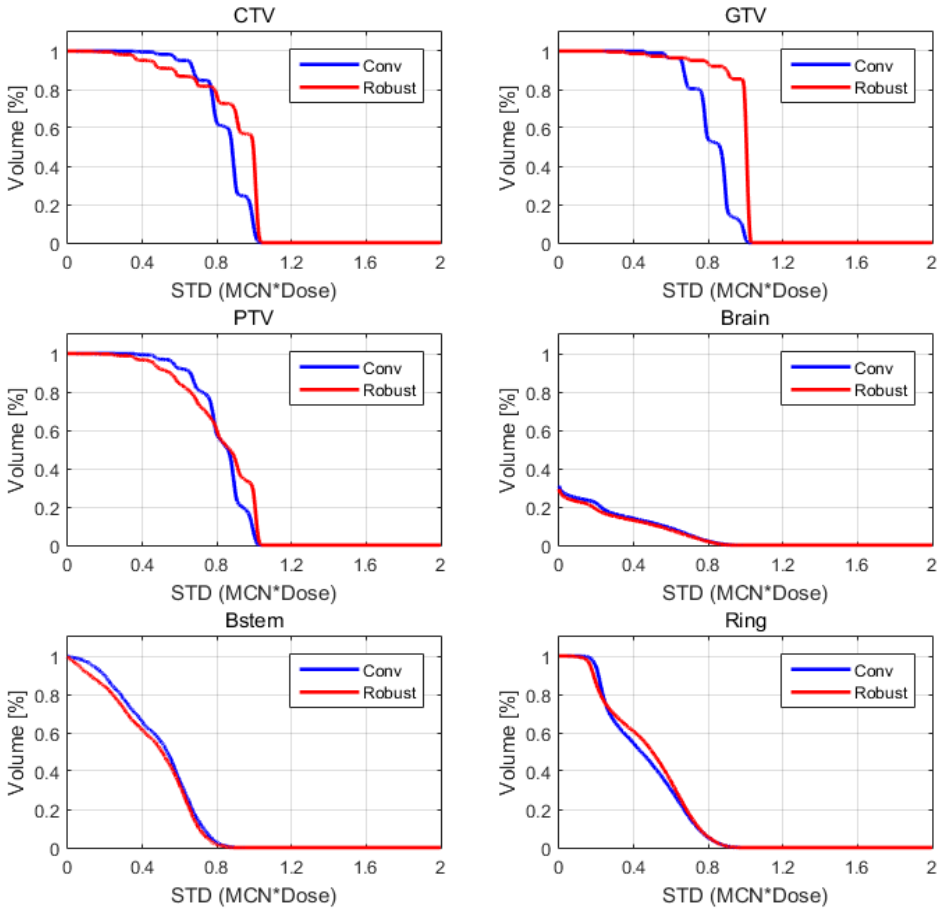

Figure A. 18: Standard deviation of the variable RBE (McNamara)-weighted dose volume histograms comparison of the PTV-based optimization plan (blue) and the RO plan (red).